Dewatering and upgrading of Loy Yang lignite using hydrothermal treatment coupled with mechanical expression

劉, 祥春

https://doi.org/10.15017/1866285

DEWATERING AND UPGRADING OF LOY YANG LIGNITE USING HYDROTHERMAL TREATMENT COUPLED WITH MECHANICAL EXPRESSION

Liu Xiangchun

2017

DEWATERING AND UPGRADING OF LOY YANG LIGNITE USING HYDROTHERMAL TREATMENT COUPLED WITH MECHANICAL EXPRESSION

by

Liu Xiangchun

A thesis submitted to the
Graduate School of Engineering
Kyushu University
Fukuoka, Japan

As partial fulfillment of the requirements for the degree of
DOCTOR OF ENGINEERING

September 2017

Contents

Abstract

The trend of the utilization of lignite is increasing because of the continuing increase in global energy demands, the decrease in high-rank coal reserves, and the wide availability of low-rank coal. However, lignite contains a high water content, which is the most important factor that limits its wide utilization. Therefore, it is necessary for lignite to dewater. On the other hand, dewatered lignite is easy to re-adsorb water. So far, dewatering and re-adsorption mechanisms of lignite are still not fully understood.

Hydrothermal treatment coupled with mechanical expression (HT–ME) is one of the most appropriate techniques. In this study, HT–ME was employed to remove water from Loy Yang (LY) lignite in order to explore dewatering and re-adsorption mechanisms, which facilitate the improvement of dewatering techniques and utilization, storage, and handling of lignite. For the HT–ME, HT stage was conducted without adding extra water and ME stage was performed at low temperature (110 ^{o}C) under atmosphere environment. To reveal dewatering and re-adsorption mechanisms, the effects of HT–ME on special physicochemical properties of the treated samples were systematically examined. Combustion performance of the HT–ME treated samples was also studied. Freeze drying (FD) technique was conducted to support and supplement HT–ME results.

The thesis consists of seven chapters. In **Chapter 1**, characteristics of lignite and previous literature related to lignite dewatering (i.e., dewatering techniques and the changes in some physicochemical properties of lignite during drying processes) were presented. Afterwards, the significances and purposes of this thesis were elucidated.

Chapter 2 focused on the changes in the hydrogen bonds (HBs) during low temperature HT process considering the forms of water in all of the samples. This can help to understand dewatering mechanism. HBs were determined using Fourier transform infrared (FT-IR) spectrum, which was obtained using diffuse reflectance infrared Fourier transform (DRIFT) method. The number of absorption bands, their peak positions, and the area of each peak in each spectrum were determined by curve-fitting analysis with the mixed Gaussian and Lorentzian function. The results showed that water was linearly and relatively easily removed at temperatures lower than 173 ℃, which was referred to as non-interfacial water. At temperatures higher than 173 ℃, dewatering slope increased, suggesting the existence of another form of water, which was relatively difficult to be removed and was named as interfacial water. Furthermore, the strength of each HB from low to high was 8.74, 14.50, 20.06, 26.36, and 32.59 kJ/mol, respectively. OH–π HBs changed apparently compared with the other four types of HBs because its strength is the weakest among these five types of HBs. The trend of the number of OH–π HBs decreased with the increase in HT temperature.

In **Chapter 3**, the changes in the gaseous, liquid, and solid products obtained from HT and HT–ME were investigated to describe the process of HT–ME dewatering, which can further help to explain dewatering and re-adsorption mechanisms. Gaseous, liquid, and solid products were characterized by gas chromatography, total organic carbon (TOC) analyzer, inductively coupled plasma atomic emission spectroscopy, high-performance liquid chromatography, and FT-IR. The results showed that volume and TOC value of wastewater increased with increasing HT temperature. Contents of monovalent cations (Na^+ and K^+) in wastewater increased significantly in temperature range 100 to 150 ℃. As to divalent cations (Mg^{2+} and Ca^{2+}), their contents increased apparently from 150 to 200 ℃ and 150 to 250 ℃, respectively. One possible explanation of this is that divalent cations are more strongly bound to carboxyl groups than monovalent cations. Volatile matter, fixed carbon, and acidic groups (i.e., phenolic hydroxyl and carboxyl groups) changed slightly below 150 ℃. Above 150 ℃, volatile matter and acidic groups decreased with increasing processing temperature and an opposite trend was observed for fixed carbon. These indicate that both HT and HT–ME upgrade LY lignite. Furthermore, water contents of HT treated samples decreased significantly by using the following ME treatment, indicating that the next ME treatment is useful for further dewatering. Combined with the results of Chapter 2, dewatering mechanism was proposed.

Chapter 4 focused on equilibrium water contents (EWCs) in samples obtained from HT and HT–ME across a range of relative humidities (RHs) to investigate the performance of EWC and its

mechanism, which can provide useful guidelines for water re-adsorption of lignite and its storage. Mesopore volume was calculated based on N_2 gas adsorption isotherm using Barrett, Joyner, and Halenda proposed method. The results showed that at RHs lower than 10%, the factor that controls EWC is water molecules–active sites interactions and one to two water molecules are associated with each carboxyl group, while in RH range 10–42%, the amount of monolayer water gains in significance and ca. two water molecules are bound to each monolayer water molecule. Within RH range 42–92%, EWC is primarily controlled by monolayer water content and mesopore volume. At RHs higher than 92%, EWC is determined by comprehensive factors such as macropores and cracks. Furthermore, EWC was generally higher than residual water content (RWC) below a RWC of ca. 5% and the opposite relationship was observed for sample with RWC above ca. 16%.

In **Chapter 5,** combustion performance of HT and HT–ME treated samples was investigated using thermogravimetric analysis to evaluate the effects of HT–ME on upgrading in combustion aspect. The relationships between various physicochemical properties (i.e., amounts of volatile matter and fixed carbon, specific surface area, and pore volume) and combustion performance were also investigated. The activation energy was calculated using the Kissinger–Akahira–Sunose method. The results showed that the ignition temperatures for samples treated using HT and HT–ME were higher than that for raw lignite and increased with increasing processing temperature, suggesting that HT and HT–ME decrease the reactivity of LY lignite. The maximum combustion rates and average activation energies of the treated samples were higher than those of raw lignite. Activation energy increased with increasing extent of conversion because combustion of volatile matter changes to char burning with the increase in extent of conversion. The activation energy for char combustion is higher than that for volatile matter.

In **Chapter 6,** LY lignite was dewatered by FD to check and supplement HT–ME results. RWC, sorption behavior, and pore size distribution were investigated. Furthermore, kerosene coating by adsorption method to study effect of covering oxygen-containing functional group on restraining water re-adsorption was also investigated. The results showed that non-interfacial and interfacial water contents determined by FD were 1.258 and 0.093 (g/g-lignite, d), which coincide quite well with those by HT method. The moisture holding capacity (MHC) of the FD treated samples was lower than that of raw lignite. This is because of their residual water contents, which determine the final water re-adsorption capacity. Moreover, adding kerosene by adsorption method decreased MHC because kerosene is coated on the surface of the lignite, which mainly covers oxygen-containing functional groups. For direct-mixing method in this study, it can decrease MHC because kerosene is coated both on the surface and in the pores of the lignite. Both of these two methods prevent water re-adsorption. The adsorption method is better than the direct-mixing method because water re-adsorption content decreased by the former is similar to that by the latter while the former consumes less kerosene.

Chapter 7 summarized the main conclusions of this thesis and provided some recommendations.

List of Figures

List of Tables

CHAPTER 1

Introduction

1.1 Research background

World energy consumption is constantly increasing with the development of the economy, and coal continues to be a very important energy source in many parts of the globe [1–6]. It is known that recoverable coal deposit around the world will last over 150 years at the current consumption rate [2]. Low-rank coal (i.e., lignite and sub-bituminous coals) accounts for approximate 45% of the word's coal reserves [7,8]. Lignite is one typical low-rank coal and is being increasing used now. At present, lignite is primarily used for electricity generation at power stations near the mines, and it is believed that lignite's utilization in other aspects will increase in the future because of the rapid increase in high-rank coal consumption and lignite's own advantages over high-rank coal, such as abundance, easy access, low cost, and low sulfur content [1,2].

However, lignite contains a high percentage of water, which is responsible for low thermal efficiency, high power consumption, high transportation and storage costs, increased CO_2 emission, and great spontaneous combustion risk. Currently, the amount of CO_2/MWh produced by burning lignite is one third higher than burning black coals and a relative decrease of 30% in CO_2/MWh can be achieved by using lignite with moisture content decreased from 60% to 40% [9–14]. During combustion process, 20–25% of heat from lignite combustion is wasted in dewatering [7,15].These cause serious application problems and inhibit lignite's wide utilization [1,2]. The continued improvement in living standards and increasing world population demand cheaper energy with less

environmental impacts, particularly reduced emissions of CO_2 and other air pollutions [1]. Therefore, dewatering of lignite is a necessary process to increase lignite's economic efficiency and wide spread applications in industry in an environmentally friendly and efficient manner.

1.2 Overview of lignite

1.2.1 Distribution of lignite

Lignite is moderately available. **Fig. 1.1** shows lignite resources and reserves worldwide as of 2015, by region. As seen, lignite resource of North American is the highest, followed by Asia and Commonwealth of Independent States (CIS). Germany, USA, China, Indonesia, Turkey, Australia, and India produce a large amount of lignite [16].

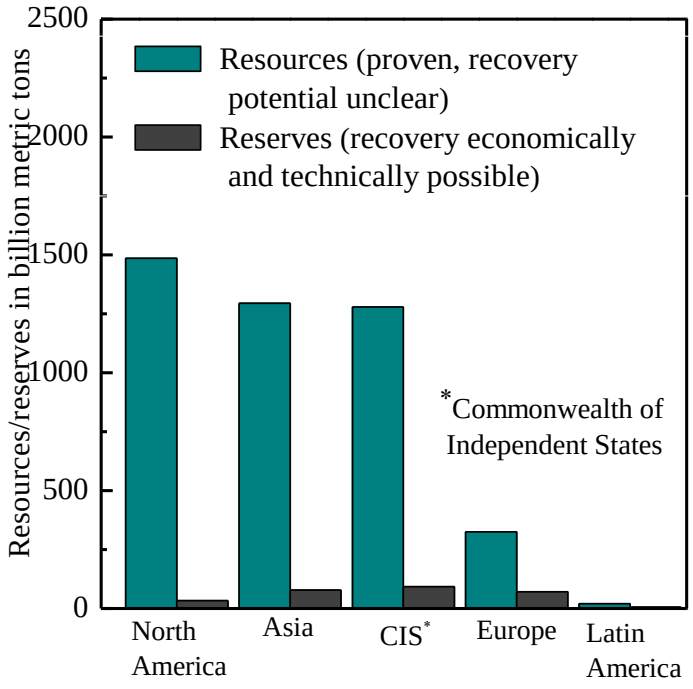

Fig. 1.1 Lignite resources and reserves worldwide as of 2015, by region (in billion metric tons) [17]

1.2.2 Characteristics of lignite

Lignite is brownish-black and is located relatively near the surface, which eliminates the risk of CH_4 or CO buildup. Lignite contains a high water content (ca. 30–65 wt.% on an as-received basis), a low level of fixed carbon (25–35 wt.% on an as-received basis), and a low level of sulfur. Its ash content varies up to 50 wt.%. Lignite's volatile matter content is high (> ca. 32 wt.% on an as-received basis) and it produces high levels of air pollution emissions. Calorific value of lignite approximately ranges from 10 to 20 MJ/kg on a dry ash-free basis [16,18–23]. Compared with high-rank coal, lignite contains much higher oxygen content, which main is in the form of oxygen-containing functional groups. The main oxygen-containing functional groups in lignite are phenolic hydroxyl groups, followed by carboxyl and carbonyl groups. There are also low contents of methoxyl groups and ring oxygen in lignite [19]. On the other hand, lignite is highly porous. **Fig. 1.2** shows pore structure in lignite. Generally, there are two types of pores in lignite, i.e., open and closed pores. Note that for lignite, open pores have a more effect than closed pores and pore structure consists mainly of macro- and mesopores. The number of micropores in lignite can be negligible [24].

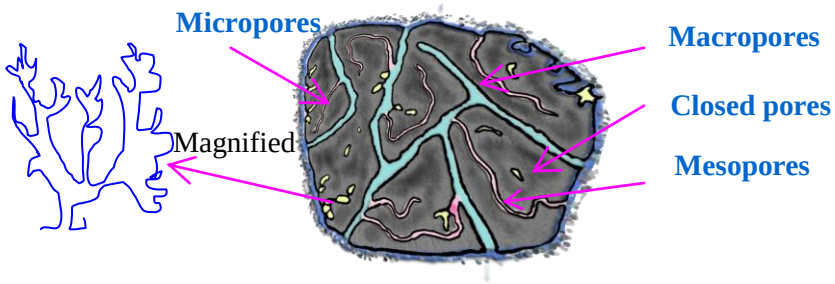

Fig. 1.2 Pore structure in lignite

The first explicit model of lignite was published in 1976 by Wender (**Fig. 1.3**) [25], which is useful as an aid to memory and a basis for prediction in a preliminary way. This model captures lots of essential features of lignite structure. For instance, it consists of several single aromatic rings linked and cross-linked by aliphatic side chains. The oxygen is in a variety of types, such as carboxylic acid, phenol, alcohol, furan, and ketone. This model also incorporates an aryl-methoxy group and some C_3-aliphatic side chains [26]. The modes of lignite have been developed by many researchers based on the products of pyrolysis, liquefaction, and extraction with the use of modern analysis instruments, e.g., nuclear magnetic resource spectroscopy (NMR), Fourier transform infrared spectroscopy (FT-IR), X-ray photoelectron spectroscopy (XPS), high performance liquid chromatography (HPLC), gas chromatography-mass spectrometer (GC-MS), and computational chemistry [26–29].

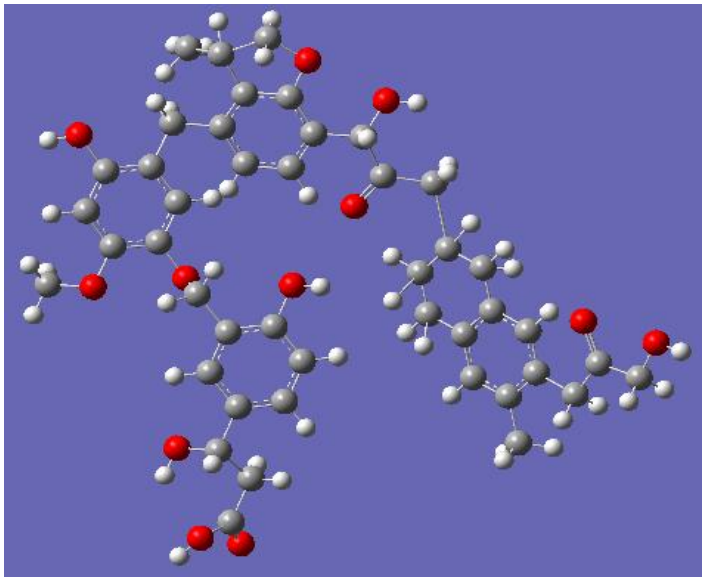

Fig. 1.3 The molecular representation of lignite proposed by Wender (Wender's model) [25]

1.3 Water in lignite

1.3.1 Water–lignite interaction

Lignite contains abundant oxygen-containing functional groups resulting in a hydrophilic character, which is the main reason for its high water content. On the other hand, lignite is porous leading to the easy transport of water, action of capillaries, and large volume for retaining water, which is also an important reason why lignite contains a high amount of water content [1,2]. The oxygen-containing functional groups and pores of lignite result in the interaction of moisture with lignite. Water–lignite interactions can be classified as the following: hydrogen interaction, Van der Waals force, capillary force, and chemical interaction.

Water molecules interact with the surface of lignite by hydrogen bonds with oxygen-containing functional groups. Schafer [30] studied the effects of carboxyl and phenolic hydroxyl groups on water content and stated that water content depends primarily on the carboxyl groups and, to a lesser extent, on the phenolic hydroxyl groups. Further research [31] showed that water adsorption is assumed to occur on the active adsorption sites, and carboxyl groups are the main preferential active adsorption sites on the surface of lignite when compared with the other functional groups. Furthermore, Van der Waals force is between coal chemical structure and water molecules. Water existed in capillaries of coal contains capillary force. Huang et al. [32] studied the desorption energy of water in two kinds of Chinese lignite and found that physical desorption energy [Eq. (1)], which is inversely proportional to the distance between the molecule of lignite species in the surface and water molecule over the surface, accounts for about 39.0% and capillary desorption energy [Eq. (2)], which is inversely proportional to capillary radius, only takes ca. 0.2%, which can be ignorable for thermal drying.

$$Q_2 = A\left[\frac{2}{5}\left(\frac{\sigma}{z}\right)^{10} - \left(\frac{\sigma}{z}\right)^{4} - \left(\frac{\sigma^4}{3\nabla\,(0.61\nabla+z)^3}\right)\right] \quad (1)$$

where Q_2 is physical desorption energy; $A = 2\pi\rho_s\varepsilon\sigma^2\nabla$ and ρ_s is the solid number density (the number of the solid molecules per unit of volume); ε is the minimum potential energy; ∇ is the distance between lattice planes; z is the vertical distance between the surface of the solid and the water molecule; σ is the critical distance when Q_2 decreases to zero.

$$Q_3 = (2\kappa/\delta)\cdot\upsilon_1 \quad (2)$$

where Q_3 is capillary desorption energy; κ is the surface tension of water (0.0756 N/m); δ is the radius of capillary; υ_1 is the density of water (1g/cm^3).

Crystal water, which is very difficult to be removed by traditional thermal drying techniques, involves chemical interactions between water and metal salts and its content is very low [32].

1.3.2 Forms of water in lignite

Many fundamental studies have investigated the types of water in lignite and there is still a need to clarify this. It is generally accepted that water retained in lignite can be divided into two major types (i.e., freezable and non-freezable water) on the basis of the characteristic phase transaction, which includes congelation and fusion. Freezable water is in the larger pores and exists in a free phase; non-freezable water is either adsorbed on the internal surface or is in the smaller pores and exists in a bound phase [2].

Early research [33] used the specific heat capacities measured by differential scanning calorimetry (DSC) of coal samples and the apparent specific heat capacities of water in coal samples compared to that of pure water to classify the forms of water in lignite, as

shown in **Fig. 1.4**. Water content of an as-received Wyodak coal is 37 g/100g–dry coal. Samples with various water contents were prepared from Wyodak coal by allowing it to lose water slowly. Only samples with a larger amount of water exhibit small sharp peaks at 273 K, meaning that a phase transition, where ice formed by bulk water melts, occurs, (**Fig. 1.4**). This suggests that a small fraction of water in the coal resembles bulk water. Furthermore, largely round peaks of these samples are also observed at 260 K, suggesting this fraction of freezable water does not behave as perfect pure water.

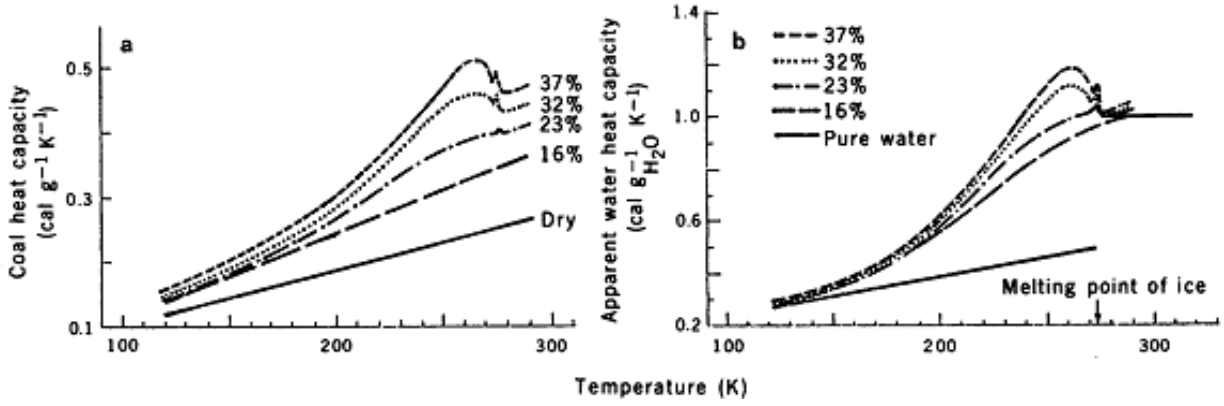

Fig. 1.4 (a) The specific heat capacity of samples of Wyodak coal containing the indicated amounts of naturally occurring water (percent defined as the grams of water per 100 g of dried coal). (b) The apparent specific heat capacity of the water in the Wyodak coal samples of (a) compared to that of pure water [33]

Allardice et al. [34] plotted the heat of sorption of moisture on Yallourn lignite as a function of moisture content (**Fig. 1.5**). As seen, the isosteric heat of desorption is approximately equal to the heat of water evaporation at moisture contents down to ca. 60 g/100g–dry coal, indicating that the water being desorbed in this region is not bound to the lignite in any way but is water from the spaces between the coal particles or in large pores with diameter greater than 10^{-5} cm [35]. In the region between 60 and ca. 15

g–water/100g–dry coal, the heat of desorption increases gradually, which can be attributed to desorption of water from progressively smaller capillaries or pores. Below water contents of 15 g/100g–dry coal, the heat of desorption increases steeply. This is because of desorption of multilayer and then monolayer moisture which is gradually more strongly bound to the surface with decreasing moisture content. It is not economical to remove the last two layers of water due to the steeply increased energy.

Allardice et al. [36] stated that weakly associated water can be removed by isothermal evacuation and more strongly associated water can be removed only by increasing temperature. The release of the latter may be associated with the thermal decomposition of functional groups.

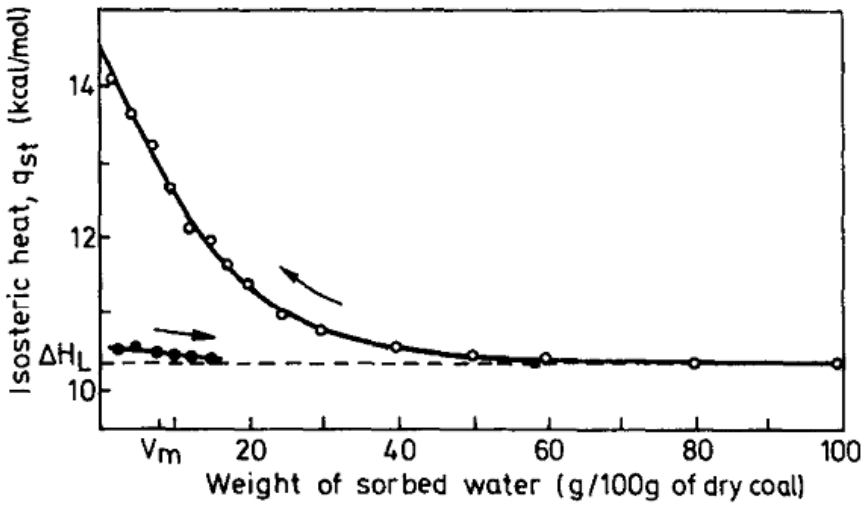

Fig. 1.5 Heat of sorption of water on brown coal as a function of moisture content [34]

Norinaga et al. [37] applied DSC and proton NMR (^{1}H-NMR) techniques to quantify different types of water in eight coals ranging from lignite to bituminous. The transition of liquid-water-to-solid-ice is accompanied by evolution of latent heat, which can be detected by DSC, as well as by a decrease in molecular mobility, which can be detected

by ^{1}H-NMR. DSC technique cannot directly measure non-freezable water, which is calculated by the difference. Tahmasebi et al. [38] suggested that the reason why non-freezable water cannot be detected in DSC thermograms is the very small amount of heat generated during the phase transition of this type of water and Sheng et al. [39] theorized that water becomes non-freezable when the molecular cluster is too small; specifically, when the number of water molecules involved in the water molecular cluster is less than a critical value of around 10. As to ^{1}H-NMR technique, it can measure non-freezable water directly. They classified water into three types: free water that is identical with bulk water, bound water that freezes at a lower temperature than free water, and non-freezable water that never freezes in the present temperature range. Compared with previous studies, Norinaga et al. [37] divided freezable water into free and bound water and determined the amounts of free, bound, and non-freezable water from their respective congelation characteristics. Shown in **Fig. 1.6** are DSC thermograms of coal samples and pure water. For Yallourn, Loy Yang (LY), and Morwell lignites, their water contents are 57.5, 56.7, and 55.5 wt% on an as-received basis, respectively. All of them have a large sharp peak at 258 K, which is similar to that of pure water, suggesting that a large fraction of water in these coals resembles bulk water. In addition, a small round peak at 226 K is also observed for these three lignites. The authors determined the quantity of heat as a function of water content and obtained the congelation heat values of 333 J/g for free water and 188 J/g for bound water using DSC technique. The congelation of free and bound water in ^{1}H-NMR is the conversion of slowly decaying components into a Gaussian one at 263 to 273 K and 213 to 263 K, respectively. For Yallourn lignite, the contents of free, bound, and non-freezable water determined by DSC method are 52%,

26%, and 22%, respectively. ^{1}H-NMR result shows that free and bound water contents are 56% and 25%, respectively. As to non-freezable water, it still has some mobility and thus gives exponential decays even at 213 K. In summary, the amount of freezable water (i.e., free and bound water) determined by DSC coincides quite well with ^{1}H-NMR result.

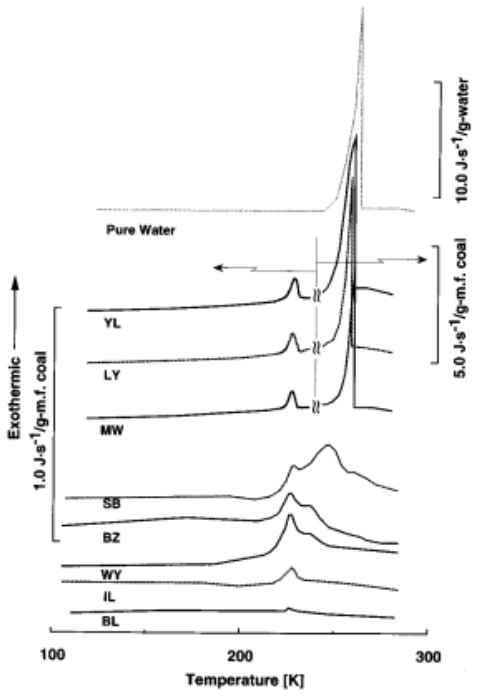

Fig. 1.6 DSC thermograms of the coal samples and pure water [37]

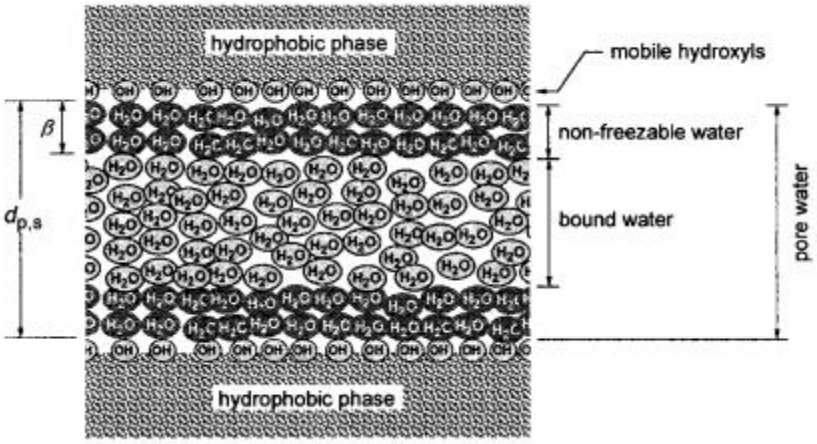

Fig. 1.7 Model of slit-like pores of moistened coal: The mobile coal protons are identical with those of hydroxyl groups. All of the hydroxyl groups are solvated by pore water on pore surface [40]

Hayashi et al. [40] proposed a slit-like model for pores that are filled with water (**Fig. 1.7**). They aimed to estimate the size of pores in moist coals on the basis of the NMR relaxation characteristics of water adsorbed in the pores as the molecular probe and concluded: (1) Pores filled with water are slit-like rather than cylindrical in shape; (2) The dimensions of pores for the raw Yallourn and Beulah Zap are about 3 and 2 nm, respectively; and (3) The pore dimension decreases with the content of pore water roughly in a linear manner.

More detailed classification of water in coals was reported by Karr [41]: (1) Interior adsorption water which is contained in micropores and microcapillaries; (2) Surface adsorption water which forms a layer of water molecules adjacent to coal molecules but only on the particle surface; (3) Capillary water that is held in capillaries; (4) Interparticle water that is held in small crevices formed between coal particles; and (5) Adhesion water which forms a layer or film around the surface of individual or agglomerated particles.

1.3.3 Adsorption and desorption processes of water in lignite

With regard to the process of water adsorption in lignite, it includes four steps. First, water molecules are bound to the surface of lignite by hydrogen bonds with active adsorption sites, which main are oxygen-containing functional groups. This part of water is monolayer water. Afterward, with increasing adsorbed water content, water molecules are associated with monolayer molecules, which play the role of the secondary adsorption sites. This phenomenon includes the formation of water clusters. As the adsorbed water increases further, more water is filled in pores and capillary condensation in narrow pores occurs, causing the growth of water clusters. Finally, the increased adsorbed water is in

the form of free water contained in the places such as spaces between the lignite particles, macropores, and cracks [42–44].

Water desorbs in order of increasing bond strength. Water without any interaction with lignite (free water) is first removed, followed by weakly adsorbed water (bound water). Water strongly adsorbed at active adsorption sites on the surface of lignite (non-freezable water) is the last desorbed [34,45].

1.4 Drying techniques for lignite

Lignite's high water content makes drying a necessary component of upgrading or utilization process and results in a large number of drying techniques being developed and some of these techniques have been widely used. However, a major breakthrough on reducing drying cost is still a great challenge [4,46–50]. Drying techniques for lignite are in general grouped into evaporative drying techniques [e.g., microwave irradiation (MI) dewatering, thermal drying, and freeze drying (FD)] and non-evaporative dewatering methods [including hydrothermal treatment (HT), mechanical thermal expression (MTE) dewatering, solvent dewatering, and so on] [1,51–53]. During evaporation drying process, the moisture is mainly removed as water vapor from lignite. As to non-evaporative dewatering, the removed water from lignite is in the form of liquid. Therefore, the latent heat of vaporization is saved. More explanations for some typical and relatively new dewatering techniques are given in **Sections 1.4.1 and 1.4.2**. In this thesis, HT coupled with mechanical expression (HT–ME) was used for lignite dewatering. HT stage was conducted without adding extra water and ME stage was performed at low temperature (110 ^{o}C) under atmosphere environment. FD was used to examine non-interfacial and interfacial water contents obtained by HT. Furthermore, for HT and HT–ME, pores,

residual water content, and oxygen-containing functional groups change simultaneously. With regard to FD, it has a little influence on oxygen-containing functional groups and its effect on pore volumes is not clear. Oxygen-containing functional groups covered by kerosene were used to investigate effects of oxygen-containing functional groups on water re-adsorption. We hope our studies of these two drying methods can improve and broaden lignite dewatering techniques.

1.4.1 Evaporative dewatering

Thermal drying, where energy such as hot gases is either directly or indirectly applied to lignite at atmosphere pressure, is considered as the most commercialized technique for industry except for the high energy consumption.

MI drying is employed as an alternative to conventional convective and conductive heating. MI utilizes electromagnetic energy, which is derived from electrical energy with a conversion efficiency less than 85%, to generate thermal energy [54–56]. It is widely used in various fields (e.g., food industry, agricultural industry, and light industry) and plays an indispensable role among all drying techniques because MI offers some unique advantages, such as rapid and selective heating, energy transfer (instead of heat transfer), penetrating deep into sample, and enhancing water loss [57,58]. Additionally, there is a growing interest of MI applied in coal processing, including improvements of liquefaction and slurryability [59,60], enhancement of grindability [54], and desulphurization [61]. Microwave is an expensive drying technique and there are also a substantial fire risk and entrainment of fine particles out of reactor because of rapid drying.

FD is another alternative dehydration technique, which is widespread and plays an indispensable role among various drying techniques [62–64]. In general, the operation process of FD dewatering includes the following: (1) preparation of the material, (2) freezing step during which water in the material becomes frozen by low temperatures, (3) ice sublimation phase that is the transition directly from ice to vapor at temperatures and pressures below the triple point of water, and (4) ultimate storage of the FD treated materials [64–66]. For more than 65 years, FD was almost exclusively applied within the biological and pharmaceutical industries as a batch type operation. It has gradually shifted from batch to semi-continuous and even purely continuous operations with its utilization in the food industry, which faces large production demands. This significantly increases productivity [64]. In addition, FD can produce high-quality dried products, which are suitable for long-term storage and long-distance transportation [64,67]. This can solve the primary problem of lignite; it is mostly used at power stations located at or near a mine because of its high water content. The major issue of FD is that it is an expensive dewatering technique because of vacuum and refrigeration units. Further modifications are required to make it more profitable. Researchers have proposed several pathways to solve this challenging issue, for instance, atmospheric pressure lyophilization [66] and FD combined with microwave heating [63].

1.4.2 Non-evaporative dewatering

Non-evaporative techniques with drying medium of either steam (Fleissner process [68]) or hot water (Evans and Siemon [69]) have been proposed. Non-evaporative techniques were suggested as far back as that Fleissner patented a semi-continuous drying technique using saturated steam in 1927 [68]. Studies have directly focused on

hydrothermally treating low-rank coal since 1983 [70]. HT is an effective dewatering process, in which lignite is treated with water or steam at temperatures around 150–350 °C with autogenously saturated pressures [71]. In addition, HT can upgrade the lignite toward a more mature coal by removing soluble organic and inorganic compounds from lignite and changing the chemical structure of lignite, thus decrease inorganic and CO_2 emission contents of HT solid products. Simultaneously, the resultant wastewater is contained with undesirable organic and inorganic compounds, thus requiring extensive treatment. Continuous works to improve HT are generally toward three aspects: (1) the effects of process conditions of HT on the physicochemical properties of solid products; (2) assessments and improvements of wastewater quality produced from HT; (3) the effects of HT process conditions on gaseous products. According to Favas and Jackson [72], a temperature of 320 °C applying slurry with a dry lignite/water ratio of 1:3 is optimum condition. Under the condition, solid products of relatively low porosity without too much pollution in wastewater and without the generation of excessive pressure can be obtained.

The original mechanical compression of 16 MPa at both ambient temperature and 100 °C experiments were conducted in the 1940s by Dulhunty, who attempted to recreate the coalification process to study coal rank metamorphism [73–77]. A more efficient technique called MTE has been developed since 1996 at University of Dortmund [78]. A 25 t/h demonstration plant was built at the Niederauβem power station of RWE in Germany and came into operation in 2001 [78]. MTE combinedly uses mechanical and thermal dewatering methods, which offers the possibility of rapid dewatering even under moderate process conditions. Generally, the temperatures and pressures of MTE are

approximate 150–210 °C and lower than 12 MPa, respectively [79,80]. The utilization of the subsequent mechanical expression with heating during MTE is very significant to improve dewatering technique because of its advantages. It leads to a highly consolidated solid product with the collapse of pores and the ruin of colloidal structure, which can reduce the content of re-adsorbed water and the reactivity of solid product [79,80]. Moreover, the pressured product is easily handled and transported with reducing environment contamination. Note that a purely mechanical expression dewatering is not suitable for technical application because high pressure should be maintained for at least 20 min [1]. Many further detailed researches have been conducted mainly in Australia, Japan, China, and Germany, which are generally toward three aspects: (1) the effects of process conditions of MTE on the physicochemical properties; (2) assessments and improvements of the wastewater quality produced from MTE; and (3) the effects of MTE process conditions on gaseous products.

1.5 Changes in lignite structure during dewatering

This thesis focused on effects of HT–ME on some physicochemical properties (e.g., forms of water, hydrogen bonds, pore structure, specific surface area, proximate and ultimate analyses, oxygen-containing functional groups, water re-adsorption capacity, organic and inorganic matters in wastewater, and combustion performance) of lignite. This provides valuable information for the improvement of lignite dewatering techniques and the utilization, storage, and handling of the treated samples. Although some indirect studies of the above described physicochemical properties have been published, there is no direct and systematical investigation of this. Related literature is reviewed as follows.

1.5.1 Changes in pore structure

Many researchers reported that lignite has a gel-like structure that swells and shrinks in response to water uptake and loss [81,82]. Lignite shows a marked desorption/re-adsorption hysteresis, that is, the re-adsorption isotherm following a lower trajectory over the full relative pressure range. This implies the irreversible loss of moisture. A capillary condensation hysteresis (high-pressure hysteresis) is usually confined to relative pressures over approximate 0.5. The low-pressure hysteresis persisted to relative pressures below 0.1 can be explained by the irreversible collapse of the pore structure of lignite during dewatering process [34]. Mraw et al. [83] also suggested that the significant difference between water desorption and re-adsorption isotherms of lignite can be attributed to the changes in lignite structure during drying process, such that there are relatively few small- and medium-size water clusters present in the re-adsorbed water. This is presumable because of the pore collapse in the gel-like structure of the raw lignite. More detailed analysis of the collapse of the pore structure was given by Evans [45]. He investigated the drying behavior of Yallourn lignite with a water content of 200 g/100 g–dry lignite. Samples were dried by placing them in desiccators with a range of different relative humidities. The results showed that the water in large pores (free water) is first removed by evaporation, followed by that in the larger capillaries, but collapse of the coal structure is relatively small because of the ordered arrangement and structural rigidity of the coalified vegetable macrostructure. However, when the water content drops to ca. 40 g/100 g–dry lignite, the shrinkage forces caused by empting small capillaries are large enough to result in their complete collapse. As the multilayer water is removed, hydrogen bonds cause the gel structure to collapse and distort, leading to more intensive shrinkage.

The maximum shrinkage, which occurs at a water content of 16 g/100 g–dry lignite, corresponds to two water layers surrounding each micelle. When the monolayer water is removed, stronger hydrogen bonds between water molecules and active adsorption sites cause inter-micellar linkages to be remade, possibly direct linkages from certain active adsorption sites to others. In many cases no linkage will be possible, and the relaxation of the structure corresponds to the shrinkage drops.

Norinaga et al. [84] examined effects of the extent of pre-drying on the porous structure of water-swollen coal using NMR technique. Irreversible decreases in the total volume of pores (V_p) filled with water and pores filled with freezable water take place when the pre-drying removes non-freezable water. However, pores filled with non-freezable water are almost independent of the extent of the pre-drying. The changes in the pore size distribution of Yallourn coal clearly demonstrate that the irreversible decrease in V_p can be explained by the irreversible shrinkage of pores with radii of ca. 2 nm, which are abundant in the raw coal.

A fixed-bed reactor was used by Yang et al. [85] to remove water from an Inner Mongolia lignite. Total volume, surface area, and porosity of the treated samples obtained at temperatures lower than 60 °C increase obviously relative to those of raw lignite and then gradually decrease with increasing temperature and are similar to raw sample at 120 °C. At low temperatures, the shrinkage forces caused by removal of the water adsorbed on the surface of lignite lead to collapse of the pore structure and the disintegration of the macropores, resulting in an increase in mesopores and a larger surface area. With increasing temperature, the stronger shrinkage forces lead to the disintegration of the mesopores and a decrease in surface area is observed.

Investigation on changes in pore size distribution of LY lignite treated by MTE shows that total pore volume decreases with increasing MTE temperature and pressure because of the progressive collapse of macropores. This is associated with a little increase in mesopore volume because macropores are compressed, decrease in diameter, and become mesopores [86]. Note that MTE process has a little effect on micropores. Extended study was undertaken by Bergians et al. [80] to investigate effects of MTE on the compressibility and pore size distribution of three low-rank lignites sourced from Australia, Greece, and Germany. The MTE produces a low porosity sample, which undergoes further shrinkage upon oven drying at 105 °C. An increase in experimental temperature (higher than ca. 85 °C) results in an increase in mesopore volume, which is attributed to a hardening of the coal structure, leading to pore volume retention and a consequent decrease in percent shrinkage on oven drying. Both of the macro- and mesopore volumes decrease with increasing MTE pressure. Furthermore, the compressibility values derived from mercury extrusion data show that the MTE process has a slight effect on the network strength of the skeletal network structure of all of these three lignites. Effects of acid treatment on pore size distribution of the MTE products were studied by Vogt et al. [79]. The results show that effects of acid treatment on pore size distribution and shrinkage are not very significant for any of the coals. Only in the case of the most severe MTE condition (200 °C) on BM coal, an apparent increase in the mesopore volume can be observed compared with the water case, which may be because pores of mesopore dimensions were closed by discrete mineral particles in water, but dissolved by the acid.

1.5.2 Changes in functional groups

The changes in functional groups are predominant in the formation and/or destruction of the oxygen-containing polar functional groups primarily including carboxyl and hydroxyl groups, which will lead to a decrease in oxygen content and moisture-holding capacity. Consequently, reactivity of lignite decreases. In other words, the tendency of spontaneous combustion decreases. Oxygen is removed in forms of water, CO_2, and CO generated by decomposition of oxygen-containing functional groups during heating process [2]. In addition, the changes in functional groups also contain aliphatic carbon and aromatic carbon group changes.

Two Morwell lignites were thermally dewatered at temperatures ranging from 150 to 300 °C [87]. Phenolic groups start to break down at 150 °C, and the breakdown is significant above 200 °C. Alcoholic groups are stable to 200 °C, but break down thereafter. The main product of decomposition of both these groups is probably water. Free-carboxylic acid groups are stable up to 150 °C, but then decompose markedly. A small but steady breakdown of carboxylate groups from 20 to 200 °C is observed, with increased breakdown above 200 °C. CO_2 is generated because of the decomposition of both these groups. Carbonyl groups are stable below 150 °C, but decompose at higher temperatures, possibly resulting in the formation of CO and CO_2.

Various methods have subsequently been used to investigate the changes in oxygen-containing functional groups, such as FT-IR, XPS, GC–MS, and NMR. From FT-IR spectra, a gradual decrease in the relative intensity of the broad band between 3700 and 3100 cm^{-1}, which is hydroxyl groups, is observed because of the removal of water and the decomposition of hydroxyl-functionalized carbohydrates. A band between 3000 and 2800

cm^{-1} corresponds to aliphatic carbon groups, showing no obvious change. The relative intensity of stretching vibration of carboxyl groups at 1760−1680 cm^{-1} gradually decreases with increasing experimental temperature. The peaks of aromatic carbon at 1603 cm^{-1} of the treated samples are a little sharper relative to that of raw lignite, suggesting the upgrading of lignite [88]. Similar results were reported by others [89,90].

GC−MS was used by Blazsó et al. [91] to analyze effects of HT on pyrolysis of Mersebury lignite. The results show that less CO_2 and CO are produced at 350−500 °C from the treated samples than those from raw lignite because of the partial elimination of the carboxyl groups by HT. CO_2 could be formed from various carboxyl groups of different parts of the organic matter at pyrolysis temperatures 350−500 °C and it is produced from the carbonates of mineral matter at higher temperatures. CO could be the product of the thermal decomposition reaction of carbonyl groups, aryl ethers or heterocyclic oxygen-containing organic molecular segments. The yield of hexane and alkanes above C_{20} increases by HT, suggesting that the attachment of the long alkyl chains to the network of lignite may become looser or less because of HT. The amount of alkyl benzenes formed under pyrolysis is little affected by HT.

As to XPS results, The C1s peak is deconvolved. The relative abundance of C−O, which is closely related to hydroxyl groups, decreases from 22.35% in raw sample to 9.79% in sample treated by HT at 300 °C. The relative abundance of O−C=O, which is closely related to carboxyl groups, declines from 4.11% in raw sample to 1.26% in sample treated by HT at 300 °C [88]. Han et al. [92] examined both C1s and O1s peaks and similar results were concluded.

^{13}C cross-polarization/total suppression of spinning sidebands NMR spectroscopy was used to characterize the changes in functional groups of XiMeng lignite treated by HT [93]. The alkyl carbon signal of sample treated at 320 °C reduces by 80.1% whereas that of aromatic carbons increases by 22.2% relative to those of raw lignite. These may be attributed to desorption of volatile aliphatic hydrocarbons and polymerization of aromatic groups and/or hydrocarbons. The intensities of O–alk groups from 50 to 90 ppm, which are assigned to aliphatic hydroxyl, methoxyl, and ethers groups, initially increase and subsequently decrease as HT temperature increases, likely because lignite is oxidized by a small amount of residual oxygen trapped in pores at temperatures lower than 250 °C. As the temperature further increases, oxidation decreases and hydrogen bonded hydroxyl groups tends to be destroyed or broken during HT process. The intensities of carboxyl and carbonyl groups consistently decrease with increasing temperature, indicating a partial decomposition of the unstable carboxyl and carbonyl groups due to the deep HT modification. The relative intensities of phenolic hydroxyl groups only slightly decrease because of their high bonding energy and stable chemical property. Similar results were reported by Liu et al [94].

1.5.3 Changes in water re-adsorption content

Valuable works on water re-adsorption behavior of lignite have been presented. These studies show that many factors, e.g., oxygen-containing functional groups, pore volume, relative humidity, and residual water content, affect water re-adsorption [1,2,95–98].

The relationship between water re-adsorption content and residual water content was reported by many researchers. For LY lignite treated by HT and MTE [44], below a threshold residual water level (ca. 5 to 16%), its water re-adsorption content is higher

than its residual water content. This trend is generally observed. The opposite relationship is found for samples with residual water content higher than 16%. However, for samples within the threshold, water re-adsorption content can be either higher or lower than residual water content depending on relative humidity. The study of Hulston et al. [86] on samples with residual water contents higher than ca.16% showed that the water re-adsorption contents at RH=96% are slightly lower than the residual water content in the residual water content range of about 16–44%. Above a residual water content of 44%, the water re-adsorption contents at RH=96% are substantially lower than the residual water contents. Similar results have also been reported by Vogt et al [79]. Superficially, if the residual water content of a sample is higher than that of another sample, its water re-adsorption content shows a general trend of higher than other sample [44]. Essentially, water re-adsorption content is mainly determined by oxygen-containing functional groups and pores. These two factors determine water–lignite interaction. Pores also provide volume for retaining water. Samples with low residual water contents usually are treated under severe conditions, meaning much more pore volume and oxygen-containing functional groups decrease. Therefore, relatively low water re-adsorption contents are observed. Samples with high water contents are dewatered under relatively mild conditions, suggesting slight changes in pore volume and, especially, in oxygen-containing functional groups. Consequently, relatively high water re-adsorption water contents are obtained.

On the other hand, relative humidity of the environment where samples are put should also be considered since increased relative humidity means increased water vapor in external environment, which provides more water source for the re-adsorption, and

difference between the water vapor in external environment controlled by relative humidity and the residual water content determines the level of diffusion adsorption or desorption force. Water re-adsorption content results from the competitive or synergistic effects between water–lignite interactions and diffusion forces (i.e., diffusion adsorption or desorption force). In addition, value of the threshold residual water content is determined by dewatering conditions and physicochemical properties of lignite sample.

1.5.4 Changes in other aspects

Wastewater is generated during lignite dewatering process, which is acidic and contains dissolved organic and inorganic compounds. As to evaporative dewatering techniques, wastewater is removed in the form of steam. After condensation, liquid water can be collected. For non-evaporative techniques, liquid wastewater can be collected directly. Because lignite contains a high water content, a substantial water resource is produced during dewatering process [99]. For instance, in the Latrobe Valley, 66 million tonnes–lignite/year is mined, which is equal to ca. 40 Giga-litres of water generated. Short-term plants for a 150 tonne−raw lignite/hour plant followed by a 100 tonne−raw lignite/hour plant may yield 60 mega-litres of water and 400 Giga-litres of water per year, respectively [100].

Knowledge of the composition of the wastewater is meaningful for determining appropriate future management strategies and assessing its potential for reuse. The concentrations and types of contaminations in wastewater are related to properties of lignite used and experimental conditions. Total organic carbon and biochemical oxygen demand are generally employed as guidelines for wastewater, which increase with increasing experimental temperature [100]. This implies that more and more dissolved

organic matter is removed from lignite. Major organic compounds existed in wastewater produced by HT are glucose, xylose, glyceraldehydes, acetic acid, and levulinic acid [101]. The HT process at high temperatures gives phenolic compounds in the effluent [71].

Other parameters to assess water quality are concentration and type of inorganic matter. The temperature where divalent cations (Ca^{2+} and Mg^{2+}) are greatly removed into wastewater is higher than that of monovalent cations (Na^{+} and K^{+}). One possible explanation is that most divalent cations are more strongly bound to carboxyl groups than monovalent cations [101]. Moreover, Fe, Al, and Zn cations can also be detected in wastewater [102–107]. In general, wastewater contains organic and inorganic compounds at levels that exceed those recommended for the identified reuse or disposals options. Therefore, remediation of wastewater is necessary. Researchers have proposed several methods to solve this issue such as using lignite itself as a filter bed adsorbent, anaerobic digestion in combination with ozonation and/or coagulation, and gasification [102–105].

In general, calorific values of the dewatered samples increase compared with that of raw sample. The decrease in volatile matter content, the increase in fix carbon content, and the changes in physicochemical properties of the dewatered samples decrease self-ignition of lignite [90,108–112].

1.6 Objectives and outline of this thesis

1.6.1 Objectives

Despite lignite's advantages, its utilization is largely confined to electricity generation at power stations located at or near a mine up to the present. Lignite contains a high water content, which is the most important factor that limits its wide utilization. In summary,

currently, there is no commercial drying process, which can economically produce a dried product. This product can satisfy the demands of storage, handing, transportation, environment, and utilization. Furthermore, so far dewatering and re-adsorption mechanism of lignite are still not completely understood. HT–ME was employed for lignite dewatering in this study. HT stage was conducted without adding extra water and ME stage was performed at low temperature (110 ^{o}C) under atmosphere environment. To check non-interfacial and interfacial water contents, a comparison of these two types of water determined by HT and FD was made. In addition, for HT and HT–ME, pores, residual water content, and oxygen-containing functional groups change simultaneously. However, FD has a slight effect on oxygen-containing functional groups and effect of FD on pore volumes is not clearly. Oxygen-containing functional groups covered by kerosene were used to investigate effects of oxygen-containing functional groups on water re-adsorption of FD treated samples. We hope our studies of these two drying methods can improve and broaden lignite dewatering techniques.

The changes in the hydrogen bonds of the different types of water in lignite as a function of temperature during the dewatering process are not completely understood. The understanding of this can provide useful engineering design guidelines for the targeted control of lignite dewatering technologies and help to understand dewatering mechanism. In **Chapter 2**, we investigated the changes in the hydrogen bonds during low temperature dewatering of lignite considering the types of water in lignite.

Conventionally, HT and HT–ME are carried out by adding extra water or steam to ignite before or during treatment process. However, this will increase the volume of wastewater and energy requirement. Furthermore, conventional HT–ME consists of two

successive stages: HT (stage 1) and then mechanical expression at the same temperature of HT process with autogenously saturated pressure (Stage 2). To our knowledge, there are no researches that were conducted to investigate stage 1 and HT–ME products separately. Furthermore, we wanted to explore stage 2 under more moderate conditions. In **Chapter 3**, stage 1 was conducted by without adding extra water, and stage 2 was performed at low temperature (110 ^{o}C) under atmosphere environment. We aimed to separately investigate stage 1 and HT–ME products. Of particular interest was the microscopic description of the process of HT–ME considering the types of water in lignite.

Although some studies on the performance of equilibrium water content of lignite have been published, there is little detailed analysis of the phenomenon. Systematical investigation of this can provide useful guidelines for the targeted control of the water re-adsorption of lignite and its storage. We detailedly reported the influence of carboxyl groups, monolayer water content, mesopore volume, and residual water content on the equilibrium water contents at various relative humidities in **Chapter 4**. Of particular interest was the analysis of the changes in the mechanism with increasing relative humidity.

TG analysis was used to investigate changes in the combustion performances of samples treated using HT and HT–ME with changes in the physicochemical properties, namely, the specific surface area, pore volume, and the amounts of volatile matter and fixed carbon (**Chapter 5**).

FD method was used to support and supplement HT–ME results, namely, it can confirm non-interfacial and interfacial water contents determined by HT and investigate

effects of residual water content and oxygen-containing functional groups on water re-adsorption separately (**Chapter 6**).

1.6.2 Outline

There thesis is divided into 7 chapters.

Background information about lignite is presented in **Chapter 1**, including characteristics of lignite, dewatering techniques, and the changes in lignite structure during dewatering. The objectives of this thesis are then specified.

Chapter 2 describes the changes in hydrogen bands during low temperature dewatering. FT-IR was used to determine the changes in the number of the different types of hydrogen bands. The number of absorption bands, their peak positions, and the area of each peak were determined by curve-fitting analysis with Gaussian and Lorentzian functions.

In **Chapter 3**, the changes in the gaseous, liquid, and solid products obtained from HT and HT−ME were investigated. Gaseous, liquid, and solid products were characterized by multiple techniques. Furthermore, a microscopic description of the changes was presented.

Chapter 4 detailedly discusses effects of the changes in carboxyl groups, monolayer water content, pore volume, and residual water content during HT and HT−ME processes on equilibrium water content at various relative humidities.

Chapter 5 examines effects of HT and HT−ME on combustion performance of LY lignite considering various physicochemical properties, i.e., the amounts of volatile matter and fixed carbon, specific surface area, and pore volume. The activation energy was also calculated using the Kissinger−Akahira−Sunose method.

In **Chapter 6**, FD was used to remove water from LY lignite. Effects of FD on residual water content, re-adsorption or desorption behavior, and pore size distributions were investigated. Furthermore, coating with different amounts of kerosene by direct-mixing or adsorption methods to restrain water re-adsorption was also discussed.

Chapter 7 summarizes the main conclusions and some recommendations are made for further research.

References

[1] C.Z. Li, Advances in the Science of Victorian Brown Coal, Elsevier, Amsterdam, 2004.

[2] J.L. Yu, A. Tahmasebi, Y.N. Han, F.K. Yin, X.C. Li, A review on water in low rank coals: The existence, interaction with coal structure and effects on coal utilization, Fuel Process. Technol. 106 (2013) 9–20.

[3] T. Thielemann, S. Schmidt, J. P. Gerling, Lignite and hard coal: Energy suppliers for world needs until the year 2100−an outlook, Int. J. Coal Geol. 72 (2007) 1–14.

[4] V.P. Singh, B.D. Singh, A. Singh, M.P. Singh, R.P. Mathews, S. Dutta, V.A. Mendhe, S. Mahesh, S. Mishra, Depositional palaeoenvironment and economic potential of Khadsaliya lignite deposits (Saurashtra Basin), western India: Based on petrographic, palynofacies and geochemical characteristics, Int. J. Coal Geol. 171 (2017) 223–242.

[5] D. Mitrović, N. Đoković, D. Životić, A. Bechtel, A. Šajnović, K. Stojanović, Petrographical and organic geochemical study of the Kovin lignite deposit, Serbia, Int. J. Coal Geol. 168 (2016) 80–107.

[6] A.T. Stock, R. Littke, A. Lücke, L. Zieger, T. Thielemann, Miocene depositional environment and climate in Western Europe: The lignite deposits of the Lower Rhine Basin, Int. J. Coal Geol 157 (2016) 2–18.

[7] M. Karthikeyan, W. Zhonghua, A.S. Mujumdar, Low-rank coal drying technologies–Current status and new developments, Dry. Technol. 27 (2009) 403–415.

[8] A. Tahmasebi, J.L. Yu, Y.N. Han, F.K. Yin, S. Bhattacharya, D. Stokie, Study of chemical

structure changes of Chinese lignite upon drying in superheated steam, microwave, and hot air, Energy Fuels 26 (2012) 3651–3660.

[9] D.J. Allardice, L.M. Clemow, G. Favas, W.R. Jackson, M. Marshall, R. Sakurovs, The characterisation of different forms of water in low rank coals and some hydrothermally dried products, Fuel 82 (2003) 661–667.

[10] G. Domazetis, P. Barilla, B.D. James, R. Glaisher, Treatments of low rank coals for improved power generation and reduction in greenhouse gas emissions, Fuel Process. Technol. 89 (2008) 68–76.

[11] X.C. Liu, T. Hirajima, M. Nonaka, K. Sasaki, Investigation of the changes in hydrogen bonds during low-temperature pyrolysis of lignite by diffuse reflectance FT-IR combined with forms of water, Ind. Eng. Chem. Res. 54 (2015) 8971–8978.

[12] X.C. Liu, T. Hirajima, M. Nonaka, T.M. Anggoro, K. Sasaki, Use of FTIR combined with forms of water to study the changes in hydrogen bonds during low-temperature heating of lignite, Dry. Technol. 34 (2016) 185–193.

[13] R.K. Dwari, K.H. Rao, Dry beneficiation of coal–a review, Min. Process. Extr. Metall. Rev. 28 (2007) 177–234.

[14] Z.H. Rao, Y.M. Zhao, C.L. Huang, C.L. Duan, J.F. He, Recent developments in drying and dewatering for low rank coals, Prog. Energ. Combust. 46 (2015) 1–11.

[15] M. Karthikeyan, J.V.M. Kuma, C.S. Hoe, D.L.Y. Ngo, Factors affecting quality of dried low-rank coals, Dry. Technol. 25 (2007) 1601–1611.

[16] https://www.thebalance.com/what-is-lignite-1182547

[17] https://en.statista.com/statistics/534556/lignite-resources-and-reserves-worldwide/

[18] https://en.wikipedia.org/wiki/Lignitehttps://en.wikipedia.org/wiki/Lignite

[19] S.Q. Zhang, Coal Chemistry, China University of Mining and Technology Press, Xuzhou, 2004.

[20] J.A. Ferguson, M.W. Rowe, Calorific value of lignites from proximate analysis, Thermochim. Acta 107 (1986) 291–298.

[21] K.L. Smith, L.D. Smoot, Characteristics of commonly-used US coals-towards a set of standard researchcoals, Prog. Energ. Combust. 16 (1990) 1–53.

[22] S. Küçükbayrak, E. Kadioğlu, Effect of pyrolysis on the proximate and ultimate analysis of lignite, Thermochim. Acta 155 (1989) 1–6.

[23] D.F. Umar, H. Usui, B. Daulay, Change of combustion characteristics of Indonesian low rank coal due to upgraded brown coal process, Fuel Process. Technol. 87 (2006) 1007–1011.

[24] Mahidin, Y. Ogaki, H. Usui, O. Okuma, The advantages of vacuum-treatment in the thermal upgrading of low-rank coals on the improvement of dewatering and devolatilization, Fuel Process. Technol. (84) 2003 147–160.

[25] I. Wender, Catalytic synthesis of chemicals from coal, Catal. Rev. Sci. Eng. 14 (1976) 97–129.

[26] J.P. Mathews, A.L. Chaffee, The molecular representations of coal–a review, Fuel 96 (2012) 1–14.

[27] C.X. Pan, X.Y. Wei, H.F. Shui, Z.C. Wang, J. Gao, C. Wei, X.Z. Cao, Z.M. Zong, Investigation on the macromolecular network structure of Xianfeng lignite by a new two-step depolymerization, Fuel 109 (2013) 49–53.

[28] L.J. Yan, Y.H. Bai, R.F. Zhao, F. Li, K.C. Xie, Correlation between coal structure and release of the two organic compounds during pyrolysis, Fuel 145 (2015)12–17.

[29] F. Yang, Y.C. Hou, W.Z. Wu, M.G. Niu, S.H. Ren, Q. Wang, A new insight into the structure of Huolinhe lignite based on the yields of benzene carboxylic acids, Fuel 189 (2017) 408–418.

[30] H.N.S. Schafer, Factors affecting the equilibrium moisture contents of low-rank coals, Fuel 51 (1972) 4–9.

[31] J. Nishino, Adsorption of water vapor and carbon dioxide at carboxylic functional groups on the surface of coal, Fuel 80 (2001) 757−764.

[32] Q.X. Huang, G.S. Zhou, B. Yu, S.K. Wang, Y. Chi, J.H. Yan, Quantitative model for predicting the desorption energy of water contained in lignite, Fuel 157 (2015) 202–207.

[33] S.C. Mraw, D.F. Naas-O'Rourke, Water in coal pores: low-temperature heat capacity behavior of the moisture in Wyodak coal, Science 205 (1979) 901–902.

[34] D.J. Allardice, D.G. Evans, The-brown coal/water system. Part 2. Water sorption isotherms on bed-moist Yallourn brown coal, Fuel 50 (1971) 236−253.

[35] J.S. Yu, Coal Chemistry, Metallurgical Industry Press, Beijing, 2006.

[36] D.J. Allardice, D.G. Evans, The brown–coal/water system. Part 1. The effect of temperature on the evolution of water from brown coal, Fuel 50 (1971) 201–210.

[37] K. Norinaga, H. Kumagai, J. Hayashi, T. Chiba, Classification of water sorbed in coal on the basis of congelation characteristics, Energy Fuels 12 (1998) 574–579.

[38] A. Tahmasebi, J.L. Yu, H.X. Su, Y.N. Han, J. Lucas, H.L. Zheng, T. Wall, A differential scanning calorimetric (DSC) study on the characteristics and behavior of water in low-rank coals, Fuel 135 (2014) 243–252.

[39] P. Sheng, R.W. Cohen, J.R.J. Schrieffer, Melting transition of small molecular clusters, Phys. C: Solid State Phys.14 (1981) 565–569.

[40] J.I. Hayashi, K. Norinaga, N. Kudo, T. Chiba, Estimation of size and shape of pores in moist coal utilizing sorbed water as a molecular probe, Energy Fuels 15 (2001) 903–909.

[41] J.C. Karr, Analytical Methods for Coal and Coal Products, Academic Press, London, 1978.

[42] D. Charrière, P. Behra, Water sorption on coals, J. Colloid Interf. Sci. 344 (2010) 460–467.

[43] T. Shigehisa, T. Inoue, H. Kumagai, Water adsorption and desorption of upgraded brown coal. Part 1: Isotherms of adsorption and desorption, Energy Fuels 28 (2014) 4986−4992.

[44] X.C. Liu, T. Hirajima, M. Nonaka, K. Sasaki, Effect of hydrothermal treatment coupled with mechanical compression on equilibrium water content of Loy Yang lignite and mechanism, Mater. Trans. 57 (2016) 935–942.

[45] D.G. Evans, The brown-coal/water system: Part 4. Shrinkage on drying, Fuel 52 (1973) 186−190.

[46] X.L. Shang, C.D. Si, J.J. Wu, Z.Y. Miao, Y.X. Zhang, Y. Wang, B.B. Wang, K. Hou, Comparison of drying methods on physical and chemical properties of Shengli lignite, Dry. Technol. 34 (2016) 454–461.

[47] M.D. Erić, M.B. Stakić, M.J. Banjac, Fluid bed drying as upgrading technology for feasible treatment of Kolubara lignite, Thermal Science 20 (2016) 167–181.

[48] X.X. Jing, Y.L. Yang, Z.Q. Li, X. Liu, L.P. Chang, W.R. Bao, Physical and chemical structure changes of Huolinhe lignite during thermal treatment and its effect on moisture re-adsorption, International Journal of Oil, Gas and Coal Technology 11 (2016) 397–410.

[49] H. Osman, S.V. Jangam, J.D. Lease, A.S. Mujumdar, Drying of low-rank coal (LRC)–A review of recent patents and innovations, Dry. Technol. 29 (2011) 1763–1783.

[50] S.V. Jangam, M. Karthikeyan, A.S. Mujumdar, A critical assessment of industrial coal drying technologies: Role of energy, emissions, risk and sustainability, Dry. Technol. 29 (2011) 395–407.

[51] H. Kanda, H. Makino, Energy-efficient coal dewatering using liquefied dimethyl ether, Fuel 89 (2010) 2104–2109.

[52] K. Miura, K. Mae, R. Ashida, T. Tamura, T. Ihara, Dewatering of coal through solvent extraction, Fuel 81 (2002) 1417–1422.

[53] Y. Iwai, Y. Koujina, Y. Arai, I. Watanabe, I. Mochida, K. Sakanishi, Low temperature drying of low rank coal by supercritical carbon dioxide with methanol as entrainer, J. Supercrit. Fluids 23 (2002) 251–255.

[54] B.K. Sahoo, S. De, B.C. Meikap, Improvement of grinding characteristics of Indian coal by microwave pre-treatment, Fuel Process. Technol. 92 (2011) 1920–1928.

[55] P.L. Jones, A.T. Rowley, Diaelectric dryers. In Industrial Drying of Foods, C.G.J. Baker, Ed. Springer, The Netherlands, 1997.

[56] M. Zhang, J. Tang, A.S. Mujumdar, S. Wang, Trends in microwave-related drying of fruits and vegetables, Trends Food Sci. Technol. 17 (2006) 524–534.

[57] P. Rattanadecho, N. Makul, Microwave-assisted drying: A review of the state-of-the-art, Dry. Technol. 34 (2016) 1–38.

[58] J. Cheng, F. Zhou, X. Wang, J.Z. Liu, Z.H. Wang, J.H. Zhou, K.F. Cen, Physicochemical properties of wastewater produced from the microwave upgrading process of Indonesian lignite, Fuel 158 (2015) 435–442.

[59] E.H. Şimşek, A. Karaduman, A. Olcay, Liquefaction of Turkish coals in tetralin with microwaves, Fuel Process. Technol. 73 (2001) 111–125.

[60] J. Cheng, J.H. Zhou, Y.C. Li, J.Z. Liu, K.F. Cen, Improvement of coal water slurry property through coal physicochemical modifications by microwave irradiation and thermal heat, Energy Fuels 22 (2008) 2422–2428.

[61] J.I. Hayashi, K. Kusakabe, S. Morooka, The role of microwave irradiation in coal desulphurization with molten caustics, Fuel 69 (1997) 739–742.

[62] J.I. Lombraña, M.C. Villarán, Interaction of kinetic and quality aspects during freeze drying in an adsorbent medium, Ind. Eng. Chem. Res. 35 (1996) 1967–1975.

[63] W. Wang, G.H. Chen, Freeze drying with dielectric-material assisted microwave heating, AIChE J. 53 (2007) 3077–3088.

[64] L. Rey, J.C. May, Freeze Drying/Lyophilization of Pharmaceutical and Biological Products, third ed., Informa Healthcare, London, 2010.

[65] L.J.J. Hansen, R. Daoussi, C. Vervaet, J.P. Remon, T.R.M. Beer, Freeze-drying of live virus vaccines: A review, Vaccine 33 (2015) 5507–5519.

[66] L.A. Segura, C.A. Oyarzún, Experimental evidence of mass transfer mechanisms during freeze-drying in a capillary porous medium, Int. J. Refrig. 35 (2012) 2102–2119.

[67] G. Broeckx, D. Vandenheuvel, I.J.J. Claes, S. Lebeer, F. Kiekensa, Drying techniques of probiotic bacteria as an important step towards the development of novel pharmabiotics, Int. J. Pharmaceut. 505 (2016) 303–318.

[68] H. Fleissner, Method of drying coal and the like, U.S. Patent US1632829, 1927.

[69] D.G. Evans, S.R. Siemon, Dewatering brown coal before combustion, J. Inst. Fuel 43 (1970) 413–419.

[70] M. Liu, J.J. Yan, B.F. Bai, D.T. Chong, X.K. Guo, F. Xiao, Theoretical study and case analysis for a predried lignite-fired power system, Dry. Technol. 29 (2011) 1219–1229.

[71] T. Nakajima, H. Hasegawa, H. Takanashi, A. Ohki, Ecotoxicity of effluents from hydrothermal treatment process for low-rank coal, Fuel 104 (2013) 36–40.

[72] G. Favas, W.R. Jackson, Hydrothermal dewatering of lower rank coals. 1. Effects of process conditions on the properties of dried product, Fuel 82 (2003) 53–57.

[73] J.A. Dulhunty, Physical changes accompanying drying of some Australian lignites, J. Proc. Royal. Soc. New South Wales 80 (1946) 22–27.

[74] J.A. Dulhunty, Some effects of compression on the physical properties of low rank coal, J. Proc. Royal. Soc. New South Wales 82 (1948) 265–271.

[75] J.A. Dulhunty, High-pressure equipment for experimental research on coal metamorphism, Aust. J. Sci. 16 (1954) 236–238.

[76] J.A. Dulhunty, Experiments in physical metamorphism of brown coals, Fuel 39 (1960) 155–162.

[77] R.A. Wheeler, A.F.A. Hoadley, S.A. Clayton, Modelling the mechanical thermal expression behaviour of lignite, Fuel 88 (2009) 1741–1751.

[78] C. Bergins, Kinetics and mechanism during mechanical/thermal dewatering of lignite, Fuel 82 (2003) 355–364.

[79] C. Vogt, T. Wild, C. Bergins, K. Strauß, J. Hulston, A.L. Chaffee, Mechanical/thermal dewatering of lignite. Part 4: Physico–chemical properties and pore structure during an acid treatment within the MTE process, Fuel 93 (2012) 433–442.

[80] C. Bergins, J. Hulston, K. Strauss, A.L. Chaffee, Mechanical/thermal dewatering of lignite. Part 3: Physical properties and pore structure of MTE product coals, Fuel 86 (2007) 3–16.

[81] D.G. Evans, Effects of colloidal structure on physical measurements on coals, Fuel 52 (1973) 155–156.

[82] G.D. Bongers, W.R. Jackson, F. Woskoboenko, Pressurised steam drying of Australian low-rank coals. Part 2. Shrinkage and physical properties of steam dried coals, preparation of dried coals with very high porosity, Fuel Process. Technol. 64 (2000) 13–23.

[83] S.C. Mraw, D.F. O'rourke, Water in coal pores: The enthalpy of fusion reflects pore size distribution, J. Colloid Interface Sci. 89 (1982) 268–271.

[84] K. Norinaga, J.I. Hayashi, N. Kudo, T. Chiba, Evaluation of effect of predrying on the porous structure of water-swollen coal based on the freezing property of pore condensed water, Energy Fuels 13 (1999) 1058–1066.

[85] Y.L. Yang, X.X. Jing, Z.Q. Li, X. Liu, Y.L. Zhang, L.P. Chang, Effect of drying conditions on moisture re-adsorption performance of dewatered lignite, Dry. Technol. 31 (2013) 1430–1437.

[86] J. Hulston, G. Favas, A.L. Chaffee, Physico-chemical properties of Loy Yang lignite dewatered by mechanical thermal expression, Fuel 84 (2005) 1940–1948.

[87] J.B. Murray, D.G. Evanst, The brown/water system: Part 3. Thermal dewatering of brown coal, Fuel 51 (1972) 290–296.

[88] Y.X. Zhang, J.J. Wu, Y. Wang, Z.Y. Miao, C.D. Si, X.L. Shang, N. Zhang, Effect of hydrothermal dewatering on physico-chemical structure and surface properties of Shengli Lignite, Fuel 164 (2016) 128–133.

[89] A. Tahmasebi, J. Yu, Y. Han, X. Li, A study of chemical structure changes of Chinese lignite duringfluidized-bed drying in nitrogen and air, Fuel Process. Technol. 101 (2012) 85–93.

[90] M. Sakaguchi, K. Laursen, H. Nakagawa, K. Miura, Hydrothermal upgrading of Loy Yang Brown coal–effect of upgrading conditions on the characteristics of the products, Fuel Process. Technol. 89 (2008) 391–396.

[91] M. Blazsó, E. Jakab, A. Vargha, T. Székely, H. Zoebel, H. Klare, G, Keil, The effect of hydrothermal treatment on a Merseburg lignite, Fuel 65 (1986) 337–341.

[92] Y.N. Han, Z.Q. Bai, J.J. Liao, J. Bai, X. Dai, X. Li, J.L. Xu, W. Li, Effects of phenolic hydroxyl and carboxyl groups on the concentration of different forms of water in brown coal and their dewatering energy, Fuel Process. Technol. 154 (2016) 7–18.

[93] J.H.Wu, J.Z. Liu, X. Zhang, Z.H. Wang, J.H. Zhou, K.F. Cen, Chemical and structural changes in XiMeng lignite and its carbon migration during hydrothermal dewatering, Fuel 148 (2015) 139–144.

[94] J.Z. Liu, J.H. Wu, J.F. Zhu, Z.H. Wang, J.H. Zhou, K.F. Cen, Removal of oxygen functional groups in lignite by hydrothermal dewatering: An experimental and DFT study, Fuel 178 (2016) 85–92.

[95] J.H. Wu, J. Wang, J.Z. Liu, Y.M. Yang, J. Cheng, Z.H. Wang, J.H. Zhou, K.F. Cen, Moisture removal mechanism of low-rank coal by hydrothermal dewatering: Physicochemical property analysis and DFT calculation, Fuel 187 (2017) 242–249.

[96] C.F. You, H.M. Wang, K. Zhang, Moisture adsorption properties of dried lignite, Energy Fuels 27 (2013) 177–182.

[97] C.B. Man, Y.H. Liu, X. Zhu, D.F. Che, Moisture readsorption peformance of air-dried and hydrothermally dewatered lignite, Energy Fuels 28 (2014) 5023−5030.

[98] Y.L. Zhang, X.X. Jing, K.G. Jing, L.P. Chang, W.R. Bao, Study on the pore structure and oxygen-containing functional groups devoting to the hydrophilic force of dewatered lignite, Appl. Surf. Sci. 324 (2015) 90–98.

[99] X.Q. Han, J.J. Yan, S. Karellas, M. Liu, E. Kakaras, F. Xiao, Water extraction from high moisture lignite by means of efficient integration of waste heat and water recovery technologies with flue gas pre-drying system, Appl. Therma. Eng. 110 (2017) 442–456.

[100] C.J. Butler, A.M. Green, A.L. Chaffee, Assessment of the water quality produced from mechanical thermal expression processing of three Latrobe Valley lignites, Fuel 85 (2006) 1364–1370.

[101] X.C. Liu, T. Hirajima, M. Nonaka, K. Sasaki, Hydrothermal treatment coupled with mechanical expression for Loy Yang lignite dewatering and the microscopic description of the process, Dry. Technol. 34 (2016) 1471–1483.

[102] Y. Artanto, E. McDonnell, T.V. Verheyen, S. Adeloju, A.L Chaffee, The remediation of MTE water by combined anaerobic digestion and chemical treatment, Fuel 88 (2009) 1786–1792.

[103] C.J. Butler, A.M. Green, A.L. Chaffee, Remediation of mechanical thermal expression product waters using raw Latrobe Valley brown coals as adsorbents, Fuel 86 (2007) 1130–1138.

[104] C.J. Butler, A.M. Green, A.L. Chaffee, MTE water remediation using Loy Yang brown coal as a filter bed adsorbent, Fuel 87 (2008) 894–904.

[105] H. Nakagawa, A. Namba, M. Bohlmann, K. Miura, Hydrothermal dewatering of brown coal and catalytic hydrothermal gasification of the organic compounds dissolving in the water using a novel Ni/carbon catalyst, Fuel 83 (2004) 719–725.

[106] J.J. Liao, Y. Fei, M. Marshall, A.L. Chaffee, L.P. Chang, Hydrothermal dewatering of a Chinese lignite and properties of the solid products, Fuel 180 (2016) 473–480.

[107] Y.L. Artanto, A.L. Chaffee, Dewatering Low rank coals by mechanical thermal expression (MTE) and its influence on organic carbon and inorganic removal, Coal Prep. 25 (2005) 251–267.

[108] J.M. Fu, J. Wang, Enhanced slurryability and rheological behaviors of two low-rank coals by thermal and hydrothermal pretreatments, Powder technol. 266 (2014) 183–190.

[109] G. Favas, W.R. Jackson, Hydrothermal dewatering of lower rank coals. 2. Effects of coal characteristics for a range of Australian and international coals, Fuel 82 (2003) 59–69.

[110] Q.Q. He, H. Yeasmin, Z.Y. Miao, K.J. Wan, S.M. Huang, A. Hoadley, Y. Qi, A.L. Chaffee, A comparison of acid treatment in the dewatering of Chinese and Australian lignites by mechanical thermal expression at high temperatures, Fuel Process. Technol. 144 (2016) 282–289.

[111] X.C. Liu, T. Hirajima, M. Nonaka, K. Sasaki, Effects of hydrothermal treatment coupled with mechanical expression on combustion performance of Loy Yang lignite, J. Therm. Anal. Calorim. 126 (2016) 1925–1935.

[112] D.F. Umar, H. Usui, B. Daulay, Effects of processing temperature of hot water drying on the properties and combustion characteristics of an Indonesian low rank coal, Coal Prep. 25 (2005) 313–322.

CHAPTER 2

Investigation of the changes in hydrogen bonds during low temperature hydrothermal treatment of Loy Yang lignite process by diffuse reflectance FT-IR combined with forms of water

2.1 Introduction

Lignite is being increasingly used and has some advantages over high-rank coal [1–5]. However, lignite is also characterized by a higher percentage of water, which inhibits its economic benefits and competitiveness in electricity production, combustion, gasification, and so on. Therefore, the removal of water from lignite is an important process to increase its widespread application in industry. Although numerous technologies for lignite drying already exist, it is often challenging to find one that is cost-effective in all aspects [8,9].

Many fundamental studies have investigated the types of water in lignite, and provide theoretical guidelines for the economic efficiency of dewatering technologies. The techniques used to investigate the forms of water in lignite include proton nuclear magnetic resonance spectroscopy (^{1}H-NMR), X-ray diffraction (XRD), and differential scanning calorimetry (DSC) [10–13]. It is accepted that water in lignite exists as freezable (including free and bound water) and non-freezable water. More detailed classification of the types of water in lignite, including free water, bound water, non-freezable water, crystal water, and closed pore water, has been proposed by several research groups [14–16].

It is well known that the hydrogen bands (HBs) in coal have a significant effect on its properties (e.g., swelling and reactivity), chemical structure, and utilization. The most important types of HBs are formed by hydroxyls groups of water molecules and the various oxygen-containing functional groups in lignite [17]. Therefore, it is extremely important to study the HBs in lignite for its effective utilization and to better understand its structure [18].

Cannon et al. [19,20] first applied infrared spectrometry to coal research and discovered the existence of HBs in coal. Various methods have subsequently been used to determine the HBs in coal, including solvent swelling and extraction, Fourier transform infrared (FT-IR) spectroscopy, ^{1}H-NMR, and DSC [18–24]. Solvent swelling and extraction, and FT-IR techniques are the most widely used methods. The significance of HBs in coals was recognized as far back as the experiments and analyses of solvent swelling and extraction of coal. Painter et al. [22] pointed out that interpretation of the swelling of coal based on solubility or Flory–Huggins parameters, which are only applicable to systems with weak London dispersion forces, are inadequate because relatively strong directional interactions (e.g., HBs) also exist in coal. Since the pioneering work, the solvent swelling and extraction method has been used to estimate the HB strengths in coals, and the changes in HBs have also been used to explain the mechanism of coal swelling [3]. Compared with the solvent swelling and extraction method, the FT-IR technique has its own unique advantages, and the occurrence, type, and strength distribution of HBs in coal can be examined [23]. Miura et al. [24] attempted to quantitatively estimate the number of various HBs using the diffuse reflectance infrared Fourier transform (DRIFT) technique. They reported that the HBs in coal range

from 10 to 70 kJ/mol in strength, and the number of relatively weak HBs in lignite significantly decrease below 150 ℃. Based on the literature, the main types of HBs formed by hydroxyls groups in lignite are summarized in **Table 2.1** [22,25–28].

Fundamental studies of the forms of water in lignite and the changes in the HBs during dewatering are important. It can provide useful engineering design guidelines for the targeted control of lignite dewatering technologies and help to explain dewatering mechanism. However, the changes in the HBs of the different types of water in lignite as a function of temperature during the dewatering process are not completely understood. In this chapter, the changes in the HBs during low temperature hydrothermal treatment of lignite process were investigated considering the forms of water.

Table 2.1 Main types of HBs formed by hydroxyl groups in lignite [22,25–28]

Peak center (cm^{-1})	Assignment
3611	Free OH groups [22]
3516	OH–π HBs [22]
3400	Self-associated *n*-mers (*n*>3) [22]
3300	OH–ether O HBs [22]
3200	Tightly bound cyclic OH tetramers [22]
2800–3100	OH–N (acid/base structures) [22]
-	HBs between non-freezable water molecules and oxygen-containing functional groups [25–28]
-	HBs within non-freezable clusters [25–28]
-	HBs within bound water clusters [25–28]
-	HBs between bound water clusters and active sites on the surface of the capillary of lignite [25–28]
-	Free water molecule HBs [25–28]

2.2 Experimental

2.2.1 Sample

An Australian lignite (Loy Yang, LY) was used as the coal sample. The lignite sample was ground to pass through an 840-μm sieve for the experiments. The proximate and ultimate analyses are shown in **Table 2.2**.

Table 2.2 Proximate and ultimate analyses of raw lignite

Lignite	Proximate analysis (wt %)						Ultimate analysis (wt %, daf)				
	M_{ar}	M_{ad}	MHC	A_d	V_{daf}	FC_{daf}	C	H	N	S	O*(diff.)
LY	57.47	9.29	36.02	0.74	51.3	48.7	64.8	4.9	0.6	0.3	29.4

ar – as received basis; ad – air dry basis; MHC – moisture holding capacity; daf – dry ash free basis; d – dry basis.

2.2.2 Hydrothermal treatment

About 6 g raw lignite was placed in a steel filter (ϕ = 60 μm), and three of the steel filters were fixed in the middle of the cylinder of a 0.5 L batch-type reactor equipped with an automatic temperature controller (MA22, Taiatsu techno, Japan). Fig. **2.1** shows the schematic of hydrothermal treatments (HT) batch-type reactor. N_2 gas was flushed through the sealed system to remove air. The reactor was then pressurized with N_2 gas to 1.5 MPa at room temperature to make sure that hydrothermal condition that the pressure in the reactor should be at least a litter higher than saturated steam pressure can be maintained. **Fig. 2.2** shows saturated steam pressure curve and temperature and pressure relationship during the experiments. The results revealed that hydrothermal condition can be maintained. A series of HTs were performed at different temperatures (50, 100, 150,

200, and 250 ℃) for 40 min at an average heating rate of ca. 5 ℃/min. Samples were collected after the reactor was cooled to room temperature.

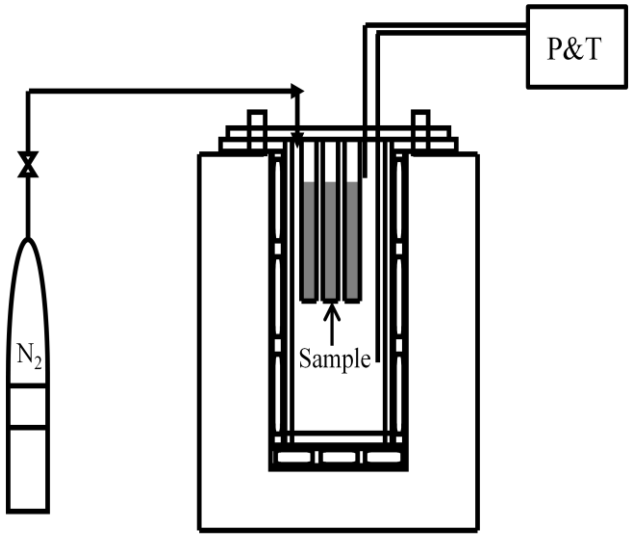

Fig. 2.1 Schematic of HT batch-type reactor

The residual water contents of all of the samples was measured by the fractional mass release observed during heating in an oven (WFO-50, Eyela, Japan) at 105 ℃, when pyrolysis generally does not occur, for 6 h. In brief, samples (m_{li} of raw lignite, weight of raw lignite, and m_{li} of treated samples, weight of heat treated lignite) were separately placed in weighing bottles (m_1, mass of the weighing bottle, lid, and sample). Then, the open weighing bottles were placed in the oven at 105 ℃. After 6 h, the weighing bottles were taken out, cooled in a desiccator, and weighed with lids (m_i). The residual water content was calculated using

$$\text{Residual water content (\%)} = [(m_1 - m_i)/m_{li}] \times 100\%. \quad (1)$$

The residual water content on dry basis (d) was calculated using

$$\text{Residual water content (g/g-lignite, d)} =$$

$$\{\text{residual water content (\%)}/[100 - \text{residual water content (\%)}]\} \times 100\%. \quad (2)$$

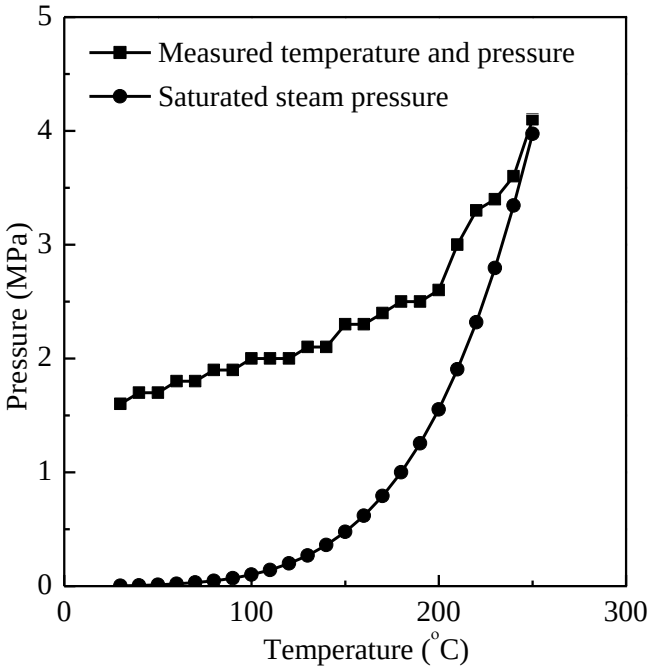

Fig.2.2 Saturated steam pressure curve and measured temperature and pressure relationship

2.2.3 FT-IR analysis

The FT-IR spectra (400–4000 cm^{-1}) were recorded with the DRIFT technique using a FT-IR spectrometer (JASCO 670 Plus, Japan). About 0.5 mg finely ground samples were used. The number of absorption bands, their peak positions, and the area of each peak were determined by the curve fitting program PeakFit v4.12 with the mixed Gaussian and Lorentzian function [29–31], and the second derivative method was used for curve resolving [31]. Furthermore, enhanced version of Levenburg-Marquardt non-linear minimization algorithm was employed by PeakFit v4.12.

The strength distributions of HBs were determined according to the literature [22,24]. Briefly, the amount of OH for the *j*th peak, $(n_{OH})_j$, was estimated by Beer's law:

$$(n_{OH})_j = (A_j)'/\{\alpha_0[1 + 0.0147(\Delta\nu_{OH})_j]\} \text{ (mol-OH/kg)}, \quad (3)$$

where α_0 and $(A_j)'$ are the absorption coefficients of the stretching vibration of free OH and the integrated area of the *j*th peak, respectively. $(\Delta\nu_{OH})_j$ is the OH wavenumber shift from the wavenumber of free OH (3611 cm^{-1}).

The normalized amount of OH, $(n_{OHn})_j$, was obtained by

$$(n_{OHn})_j = (n_{OH})_j/[(n_{OH})_1]_{raw}, \quad (4)$$

where $[(n_{OH})_1]_{raw}$ is the amount of OH of the first peak of raw lignite.

The strength of the *j*th HB, $(-\Delta H)_j$, was calculated by

$$(-\Delta H)_j = 0.067(\Delta\nu_{OH})_j + 2.64 \text{ (kJ/mol)} \quad (5)$$

The integrated area of the *j*th peak of lignite treated at different temperatures, $[(A_j)_t]'$, was obtained by

$$[(A_j)_t]' = (A_j)_t\,[(A_6)_{raw}/(A_6)_t], \quad (6)$$

where $(A_j)_t$ is the original integrated area of the *j*th peak obtained by curve-fitting analysis of the FT-IR spectra at different temperatures (**Table 2.3**). $(A_6)_t$ is the original integrated area of aromatic hydrogen atoms treated at different temperatures. $(A_6)_{raw}$ is the original integrated area of the aromatic hydrogen atoms of raw lignite. The integrated area of aromatic hydrogen atoms was chosen because the structure of aromatic hydrocarbons is difficult to decompose or form below 300 ℃ under N_2 conditions, which means that the integrated area of aromatic hydrogen atoms should only slightly change [24]. The average HB strength was calculated as

$$(-\Delta H)_{av} = [\sum_j (n_{OHn})_j\,(-\Delta H)_j]/\sum_j (n_{OHn})_j, \quad (7)$$

where j = 1–5.

Table 2.3 Results of the curve-fitted spectra of the 2800–3560 cm^{-1} region for LY lignite treated at 50 ℃

Peak center (cm^{-1})	Assignment	Symbol	Original integrated area $[(A_j)_t]$	Integrated area $\{[(A_j)_t]'$
3611	Free OH groups	-	-	-
3520	OH–π HBs	1	37.16	37.26
3434	Self-associated *n*-mers (*n*>3)	2	8.07	8.09
3351	OH–ether O HBs	3	20.43	20.48
3257	Tightly bound cyclic OH tetramers	4	10.22	10.24
3164	OH–N (acid/base structures)	5	5.63	5.65
3030	Aromatic hydrogen atoms	6	7.40	7.42
2993, 2960, 2920	Aliphatic hydrogen atoms	-	-	-

2.2.4 Carboxyl groups analysis

The number of carboxyl groups was measured by an improved barium exchange technique [32] to investigate the changes in pyrolysis water from the decomposition reaction of carboxyl groups (Detailed experimental process is presented in **Section 3.2.4**). The experiment was repeated three times.

2.3 Results and discussion

2.3.1 Forms of water in lignite

Fig. 2.3 shows the effect of temperature on the residual water content of lignite. **Fig. 2.3(a)** shows that the residual water content linearly decreased with increasing temperature in the range 50–150 ℃, which indicates that a single type of water was released in this temperature range. We refer to this type of water as non-interfacial water,

which is non-bound and weakly bound to lignite. Above 150 ℃, the slope decreases as the temperature increases, indicating that another form of water was released, which is relatively difficult to be removed because it is strongly bound to the surface of lignite. It is named as interfacial water. The water removed in the temperature range 150–200 ℃ included non-interfacial and interfacial water. To determine the amounts of non-interfacial and interfacial water, the two lines in the temperature ranges 50–150 ℃ and 200–250 ℃ were extended (dashed lines in **Fig. 2.3**), which meet at point A in **Fig. 2.3**. Point A is the border between these two types of water. From point A [**Fig. 2.3(b)**], the non-interfacial and interfacial water contents of in raw lignite were 1.255 and 0.096 (g/g-lignite, d), respectively. Furthermore, it is generally accepted that water in lignite exists in the forms of freezable and non-freezable water depending on the strength of the water–lignite interactions [10–13]. The relative difficulty of removing the two types of water is in the order non-freezable water > freezable water. These suggest that the water removed in the temperature ranges 50–150 ℃ and 200–250 ℃ were similar to freezable and non-freezable water, respectively. Above 200 ℃, an increase in temperature resulted in only a slight decrease in the water content, which means that it is not energy efficient to remove the remaining water by HT.

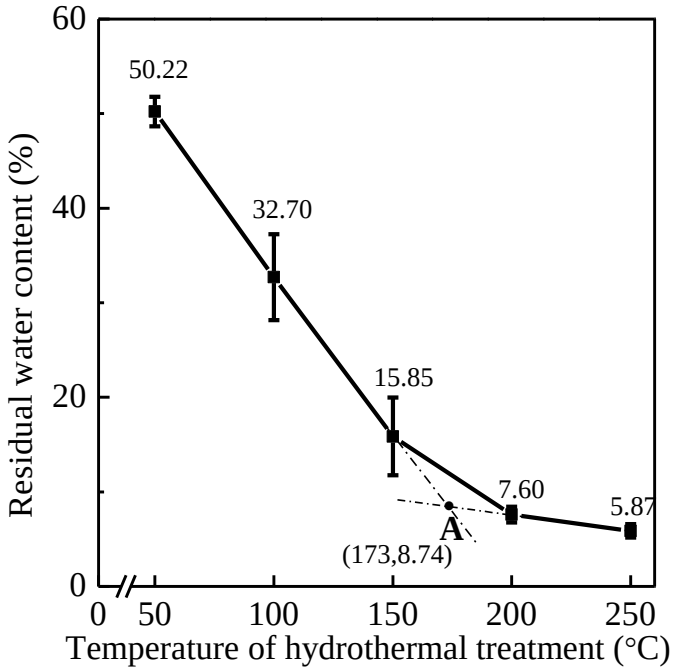

Fig. 2.3 Effect of temperature on residual water contents (%) of treated samples

Table 2.4 Concentrations of carboxyl groups of all of the samples (mmol/g, d)

Sample	–COOH	Sample	–COOH
Raw	1.74±0.10	150 ℃	1.54±0.11
50 ℃	1.63±0.26	200 ℃	1.45±0.05
100 ℃	2.00±0.16	250 ℃	0.78±0.10

The number of carboxyl groups was presented in **Table 2.4**. From **Table 2.4**, when the temperature reached 250 ℃, there was a significant decrease in the concentration of carboxyl groups, which suggests that pyrolysis water, produced from decomposition [Eq.(8)] [24], started to be apparently released at 200 ℃.

$$2\text{–COOH} \rightarrow \text{–COOCO–} + H_2O \quad (8)$$

2.3.2. Effect of temperature on HBs

2.3.2.1 FT-IR Spectroscopy

Fig. 2.4(a) shows the DRIFT spectra of all of the samples treated at a range of temperatures. Enlargements of the spectra in the range 2800–3650 cm^{-1} are shown in **Fig. 2.4(b)**. To accurately investigate the changes in the strength distributions of the HBs, the spectra in this region were divided into 10 peaks by a curve-fitting method, and the results are consistent with the results reported in the literature [22,24]. An example of the method is given in **Fig. 2.5**. It should be mentioned that the peak positions proposed by Miura et al. [24] are slightly different from those proposed by Painter et al [22] (**Table 2.1**). The assignment, symbols, and integrated areas of the ten peaks in this study are summarized in **Table 2.3**. Typical representative HBs 1–5 are shown in **Fig. 2.6**.

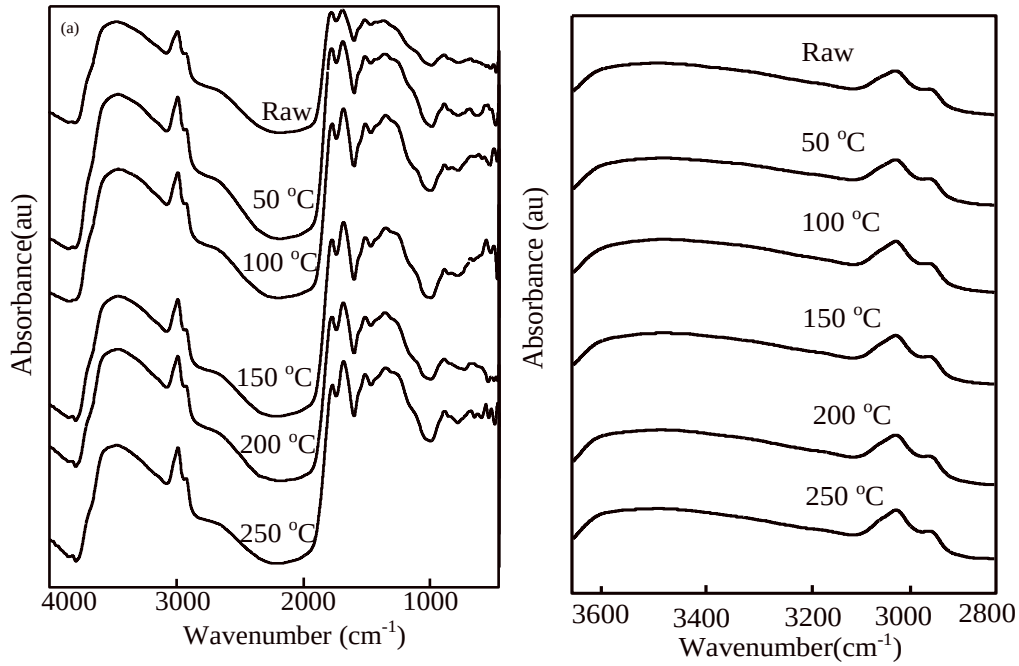

Fig. 2.4 (a) FT-IR spectra of all of the samples treated at a range of temperatures. (b) FT-IR spectra of all of the samples in the range 2800–3650 cm^{-1}

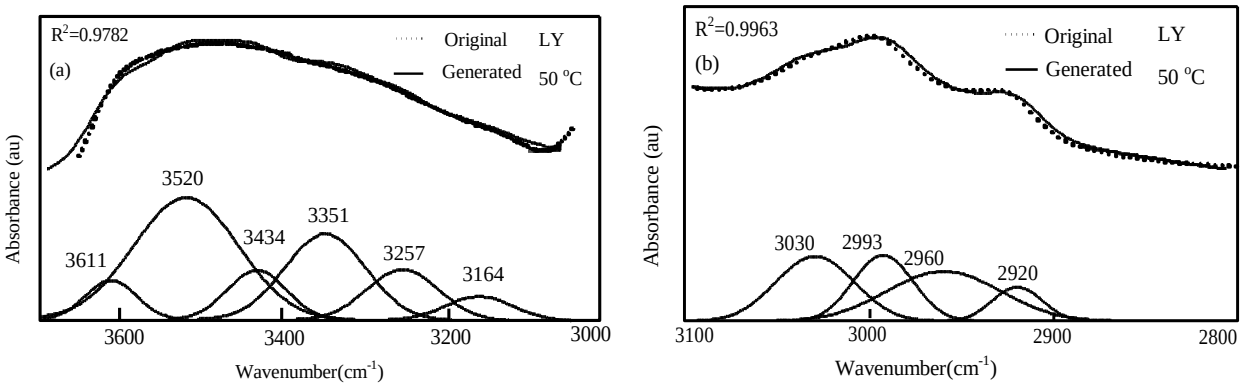

Fig. 2.5 Curve-fitted spectra of the 3050–3650 cm^{-1} and 2800–3100 cm^{-1} regions for LY treated at 50 ℃

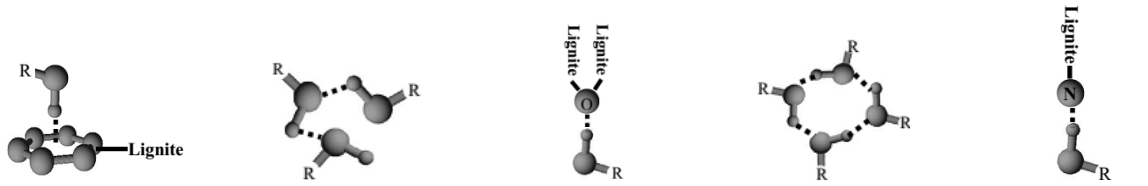

(1) OH–π HBs (2) Self–associated *n*-mers (3) OH–ether O HBs (4) Tightly bound cyclic OH tetramers (5) OH–N HBs

Fig. 2.6 Typical representative HBs 1 to 5.  represents the OH group that exists in the form of a free OH group in lignite and water, and R represents lignite or H in water

2.3.2.2. Changes in the HBs

The changes in the amount of OH of the *j*th peak, $(n_{OHn})_j$, with temperature are shown in **Fig. 2.7**. The $-\Delta H$ value represents the strength of the HB: $(-\Delta H)_1$ = 8.74 kJ/mol, $(-\Delta H)_2$ = 14.50 kJ/mol, $(-\Delta H)_3$ = 20.06 kJ/mol, $(-\Delta H)_4$ = 26.36 kJ/mol, and $(-\Delta H)_5$ = 32.59 kJ/mol. The results show that $(n_{OHn})_j$ changed with temperature.

In **Fig. 2.7**, the trend of the changes in the bars corresponding to HBs 1 and 3 is the same. They were both lower at 50 to 100 ℃ than bars corresponding to the raw lignite. Based on the literature [24–28], the HBs 1 and 3 include OH of water molecules–lignite interactions and OH of lignite–lignite interactions. HBs 1 and 3 showed relatively low

strength, 8.74 kJ/mol and 20.06 kJ/mol, respectively, and they decreased within this low temperature range, indicating the decrease in OH of water molecules–lignite interaction. In addition, bound water is retained by molecular interactions with the porous system of the lignite [3,12], suggesting that bound water includes OH of water molecules–lignite interactions and interactions between OH of water molecules. Therefore, the decrease in the number of HBs 1 and 3 in the temperature range indicates that the removal of bound water took place and bound water was a constituent of non-interfacial water. HB 2 is also a relatively weak HB, 14.50 kJ/mol, and formed by OH of water molecules–lignite interactions, OH of lignite–lignite interactions, and interactions between OH of water molecules. The removal of free water (free water is the other part of non-interfacial water. It has no specific interactions with the lignite matrix and only includes interactions between OH of water molecules) led to the decrease in the number of interactions between OH of water molecules. Therefore, the bar corresponding to HB 2 for the sample treated at 50 ℃ is lower than that for raw lignite. Furthermore, the number of water molecules in the water cluster decreases because of fractional removal of free water with increasing temperature. Norinaga et al [10]. reported that coal can shrink in response to the loss of water, and this behavior might then lead to the transition of one type of water to another type within the coal matrix. The transition of one type of water to another type of water because of the increase in its cluster size has also been reported [33]. Based on the above analyses, the decrease in the free water molecules in the cluster might then lead to transition of the remaining free water to bound water and increase the number of OH of water molecules–lignite interactions. Consequently, the normalized amount of HB 2 in the sample treated at 100 ℃ increased relative to the sample treated at 50 ℃ (**Fig. 2.7**).

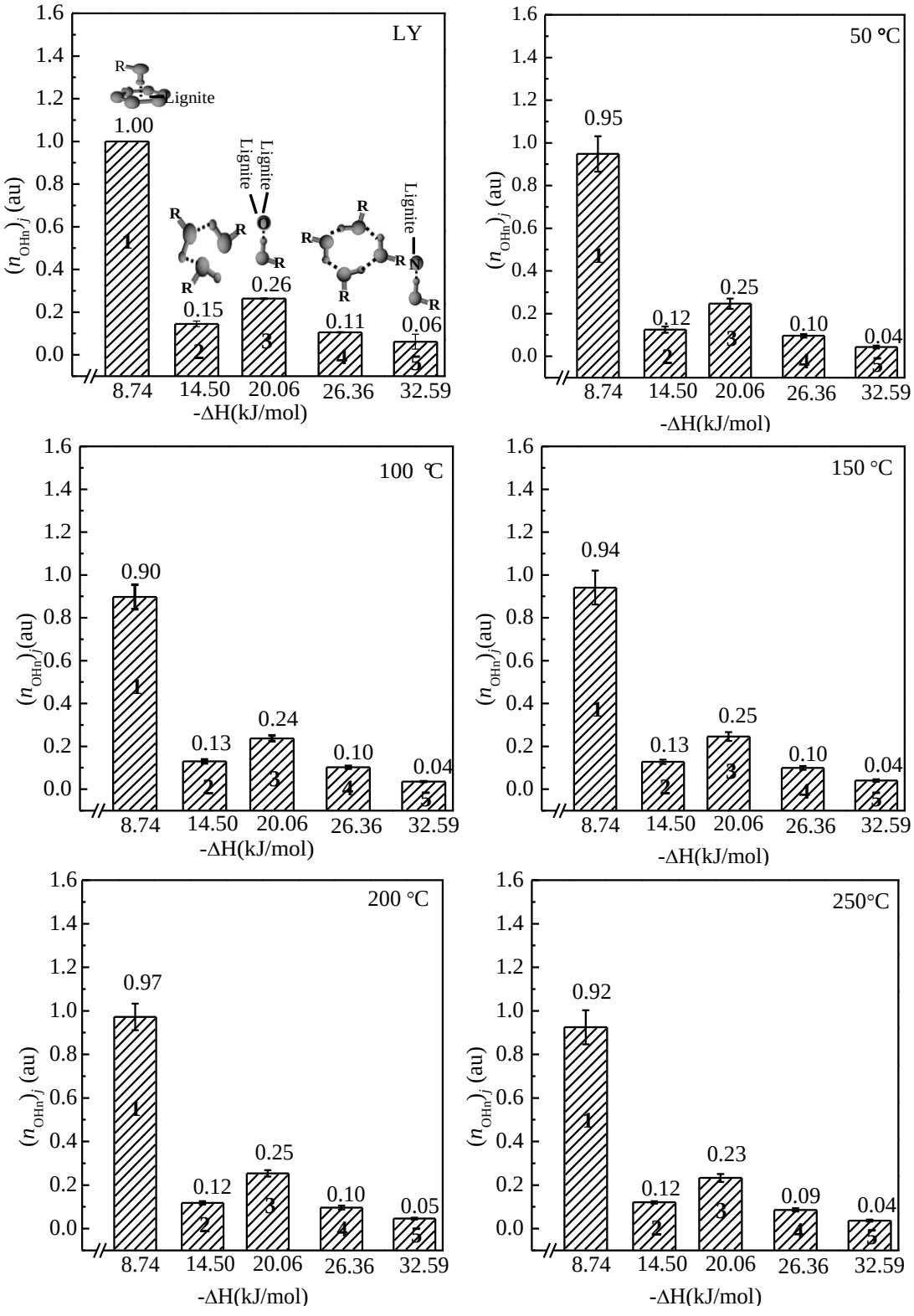

Fig. 2.7 Change of $(n_{OHn})_j$ with temperature for LY lignite

With an increase of the temperature from 100 to 200 ℃, the number of HBs 1 and 3 increased. Interfacial water is difficult to be removed because it is likely to be condensed in micropores and/or bind to carboxyl groups on the surface of lignite via specific interactions such as HBs, which means that interfacial water includes OH of water molecules–lignite interactions and interactions between OH of water molecules. In summary, the increase in the number of HBs 1 and 3 is directly related to the competition between the transition of bound water to interfacial water, which increases the number of OH–lignite interactions, and the desorption of bound and interfacial water, which decreases the number of OH–lignite interactions. HB 2 showed a general trend of decreasing with increasing temperature. When bound water transformed to interfacial water, the amount of HB 2 between OH of water decreased because the size of bound water cluster is larger than that of interfacial water cluster. However, the amount of HB 2 between OH of water molecules and OH of carboxyl groups on the surface of lignite increased because interfacial-water–lignite interactions are the strongest of all of the forms of water. Furthermore, the removal of interfacial water led to a decrease in the number of OH–OH interactions. The changes in the amount of HB 2 can be attributed to the competition of the above factors.

In the temperature range 200–250 ℃, the main type of removed water was interfacial water (**Fig. 2.3**). There was also a significant decrease in the concentration of carboxyl groups (**Table 2.4**). Tahmasebi et al. [34,35] suggested that a decrease in the concentration of oxygen-containing functional groups results in a lower strength of HBs between water molecules and active sites on the coal structure. This leads to a decrease in OH–lignite interactions. The amounts of HB 2 in LY treated at 200 and 250 ℃ were the

same, which suggests that increasing the temperature from 200 to 250 ℃ had little effect on the number of OH–OH interactions.

Fig. 2.8 shows the change in the average HB strength, $(-\Delta H)_{av}$, with temperature, which is around 13 kJ/mol for all of the samples. Therefore, temperature has little effect on the $(-\Delta H)_{av}$ value. This agrees with the observations of Miura et al [24], who reported that the $(-\Delta H)_{av}$ values for high-rank coals decreased between 230 and 270 ℃ associated with a glass transition, but it did not change for low-rank coal. The $(-\Delta H)_{av}$ values for low-rank coal are 20 to 24 kJ/mol, which are significantly higher than those reported in this study. The $(-\Delta H)_{av}$ values estimated here and those in the literature [24] are in the range of typical HBs strength, whose values vary between ca. 8.4 and 63 kJ/mol [36,37].

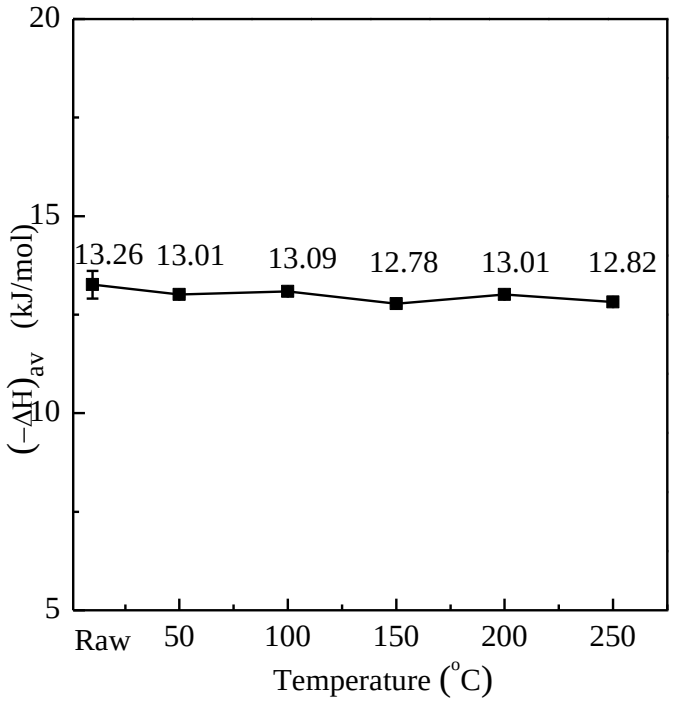

Fig. 2.8 Change of the average strength of hydrogen bonds, $(-\Delta H)_{av}$, with temperature for LY lignite

It should also be noted that only the number of the relatively weak HBs 1, 2, and 3 changed, and there was little change in the number of relatively strong HBs 4 and 5. This is in agreement with the types of water in lignite, among which interfacial-water–lignite-matrix interactions are the strongest.

2.3.2.3. Microscopic changes in the HBs during low-temperature dewatering

When lignite is heated at low temperatures ($T \leq 100$ ℃), the main removed water is non-interfacial water. The number of OH–lignite interactions (HBs 1 and 3) containing OH of water–lignite interactions and OH of lignite–lignite interactions decrease in this temperature range. This can be attributed to the removal of bound water, a constituent of non-interfacial water. The size of the bound water cluster is smaller than that of the free water cluster. Therefore, bound water clusters can be condensed in capillaries with diameters less than several microns [38], which means that there are interactions between bound water clusters and lignite. Free water has no specific interactions with lignite. Consequently, the number of HBs 1 and 3 decrease in these conditions. This can be attributed to the breaking of bound-water-cluster–lignite HBs. Furthermore, the number of OH–OH interactions (HB 2), that is, interactions between OH groups of water molecules, interactions between OH groups of water molecules and OH groups of lignite, and interactions between OH groups of lignite, first decreases and then increases. First, the removal of free water leads to a decrease in the number of interactions between water molecules. Then, the HBs broken between free water molecules decreases the number of water molecules in the free water cluster, thereby inducing the transition of free water to bound water, which includes bound-water-molecule HBs. Consequently, the amount of HB 2 increases. At medium temperatures ($100 < T \leq 200$ ℃), the main released water is bound and interfacial water. The interactions between interfacial water clusters and

carboxyl groups on the surface of lignite are the strongest among the all types of water. The number of OH–lignite interactions (HBs 1 and 3) increase. An explanation for this behavior could be the competition between the transition of bound water to interfacial water, and the desorption of bound and interfacial water. Furthermore, the number of OH–OH interactions (HB 2) decreases. The dewatering leads to a decrease in the number of OH–OH interactions of water molecules. Because interactions between interfacial water clusters and carboxyl groups on the surface of lignite are the strongest, the interactions between the OH groups of carboxyl groups and the OH groups of water molecules increase when bound water transforms to interfacial water. The removal of bound and interfacial water leads to a decrease in the number of OH–OH interactions. Changes in HB 2 can be attributed to the comprehensive effect of the above factors. At higher temperatures ($200 < T \leq 250$ ℃), the main removed water is interfacial water, and the number of carboxyl groups drastically decreases because of lignite pyrolysis. OH–lignite interactions (HBs 1 and 3) decreased as a result of the removal of interfacial water and pyrolysis of carboxyl groups. The amounts of HB 2 in LY treated at 200 and 250 ℃ were the same. Changes in this temperature range were the removal of interfacial water and the decomposition of carboxyl groups, which lead to the decrease in the number of interactions between OH of water molecules and interactions between OH of carboxyl groups, respectively. However, decomposition reaction in this temperature range leads to the formation of new oxygen-containing functional groups [39], which may increase the number of OH–OH interactions. The result of HB 2 in this temperature range can be attributed the comprehensive effects of the above two.

2.4 Conclusions

In this study, pyrolysis water produced from decomposition of carboxyl groups, which started to be drastically released at 200 ℃. The non-interfacial and interfacial water contents of the total water weight in raw lignite were 1.255 and 0.096 (g/g-lignite, d), respectively.

The changes in the number of relatively weak HBs can be understood in terms of the removal of the different types of water and decomposition of carboxyl groups. At low temperatures ($T \leq 100$ ℃), the main removed water was non-interfacial water, including free and bound water. The number of OH–lignite interactions decreased in this temperature range. This can be attributed to the breaking of bound-water-cluster–lignite HBs. Furthermore, the removal of free water induces a decrease in the number of OH–OH interactions. Then, the breaking of HBs between free water molecules decreases the number of water molecules in the free water cluster, thereby inducing the transition of free water to bound water. Consequently, the amount of HB 2 increased. At medium temperatures ($100 < T \leq 200$ ℃), the main released water was bound and interfacial water. The change in the number of OH–lignite and OH–OH interactions was the result of the competition between the transition of bound water to interfacial water and the desorption of bound and interfacial water. At higher temperatures ($200 < T \leq 250$ ℃), the main removed water was interfacial water. The decrease in OH–lignite interactions is because of the removal of interfacial water and decomposition of carboxyl groups.

References

[1] C. Öner, Ş. Altun, Flue gas emissions from the burning of asphaltite and lignite in a rotating head combustor with secondary air delivery, Energy Fuels 28 (2014) 4511–4516.

[2] J.M. Beér, Combustion technology developments in power generation in response to environmental challenges, Prog. Energy Combust. Sci. 26 (2000) 301–327.

[3] C.Z. Li, Advances in the Science of Victorian Brown Coal, Elsevier, Amsterdam, 2004.

[4] X.J. Yang, C. Zhang, P. Tan, T. Yang, Q.Y. Fang, G. Chen, Properties of upgraded Shengli lignite and its behavior for gasification, Energy Fuels 28 (2014) 264–274.

[5] M. Liu, J.J. Yan, B.F. Bai, D.T. Chong, X.K. Guo, F. Xiao, Theoretical study and case analysis for a predried lignite-fired power system, Dry. Technol. 29 (2011) 1219–1229.

[6] K. Zhang, C.F. You, Effect of upgraded lignite product water content on the propensity for spontaneous ignition, Energy Fuels 27 (2013) 20–26.

[7] C.B. Man, Y.H. Liu, X. Zhu, D.F. Che, Moisture readsorption performance of air-dried and hydrothermally dewatered lignite, Energy Fuels *28* (2014) 5023–5030.

[8] M. Karthikeyan, Z.H. Wu, A.S. Mujumdar, Low-rank coal drying technologies—Current status and new developments, Dry. Technol. 27 (2009) 403–415.

[9] H. Osman, S.V. Jangam, J.D. Lease, A.S. Mujumdar, Drying of low-rank coal (LRC)—A review of recent patents and innovations, Dry. Technol. 29 (2011) 1763–1783.

[10] K. Norinaga, H. Kumagai, J. Hayashi, T. Chiba, Classification of water sorbed in coal on the basis of congelation characteristics, Energy Fuels 12 (1998) 574–579.

[11] Y. Fei, A.L. Chaffee, M. Marshall, W.R. Jackson, Lignite-water interactions studied by phase transition-differential scanning calorimetry, Fuel 84 (2005) 1557–1562.

[12] J.L. Yu, A. Tahmasebi, Y.N. Han, F.K. Yin, X.C. Li, A review on water in low rank coals: The existence, interaction with coal structure and effects on coal utilization, Fuel Process. Technol. 106 (2013) 9–20.

[13] A. Tahmasebi, J.L. Yu, H.X. Su, Y.N. Han, J. Lucas, H.L. Zheng, T. Wall, A differential scanning calorimetric (DSC) study on the characteristics and behavior of water in low-rank coals, Fuel 135 (2014) 243–252.

[14] C. Karr, Analytical Methods for Coal and Coal Products, Academic Press, New York, 1978.

[15] M.L. Roux, Q.P. Campbell, An investigation into an improved method of fine coal dewatering, Miner. Eng. 16 (2003) 999–1003.

[16] X.C. Liu, Forms of Water in Shengli Lignite and Effect of Metal Ions on Its Water Absorption Capacity, Master thesis, China University of Mining & Technology, Xuzhou, 2014.

[17] C. Chen, J.S. Gao, Y.J. Yan, Observation of the type of hydrogen bonds in coal by FTIR, Energy Fuels 12 (1998) 446–449.

[18] D.T. Li, W. Li, B.Q. Li, A new hydrogen bond in coal, Energy Fuels 17 (2003) 791–793.

[19] C.G. Cannon, Infra-red spectra of coals and coal products, Nature 171 (1953) 308.

[20] C.G. Cannon, G.B. Sutherland, The Infra-red absorption spectra of coals and coal extracts, Trans. Faraday Soc. 41 (1945) 279–288.

[21] S.R. Taylor, N.C. Li, Nature of hydrogen bonding in coal-derived asphaltenes, Fuel 57 (1978) 117–121.

[22] P.C. Painter, M. Sobkowiak, J. Youtcheff, FT-i.r. study of hydrogen bonding in coal, Fuel 66 (1987) 973–978.

[23] W. Li, Z.Q. Bai, J. Bai, Z.X. Guo, Decomposition kinetics of hydrogen bonds in coal by a new method of in-situ diffuse reflectance FT-IR, J. Fuel Chem. Technol. 39 (2011) 321–327.

[24] K. Miura, K. Mae, W. Li, T. Kusakawa, F. Morozumi, A. Kumano, Estimation of hydrogen bond distribution in coal through the analysis of oh stretching bands in diffuse reflectance infrared spectrum measured by in-situ technique, Energy Fuels 15 (2001) 599–610.

[25] L. Feng, X.C. Liu, L.L. Song, X.H. Wang, Y. Zhang, T.W. Cui, H.Y. Tang, The effect of alkali treatment on some physico–chemical properties of Xilinhaote lignite, Powder Technol. 247 (2013) 19–23.

[26] X.C. Liu, L. Feng, X.H. Wang, Y. Zhang, X.F. Shi, Effect of K^+, Na^+, Ca^{2+} and Mg^{2+} on equilibrium adsorption of water content of Shengli lignite, J. Fuel Chem. Technol. 42 (2014) 385–391.

[27] D. Charrière, P. Behra, Water sorption on coals, J. Colloid Inter. Sci. 344 (2010) 460–467.

[28] J. Nishino, Adsorption of water vapor and carbon dioxide at carboxylic functional groups on the surface of coal, Fuel 80 (2001) 757–764.

[29] J.V. Ibarra, E. Muñoz, R. Moliner, FTIR study of the evolution of coal structure during the coalification process, Org. Geochem, 24 (1996) 725–735.

[30] J.V. Ibarra, R. Moliner, A.J. Bonet, FTIR Investigation on char formation during the early stages of coal pyrolysis, Fuel 73 (1994) 918–924.

[31] A. Tahmasebi, Y. Jiang, J.L. Yu, X.C. Li, J. Lucas, Solvent extraction of Chinese lignite and chemical structure changes of the residue during H_2O_2 oxidation, Fuel Process. Technol. 129 (2015) 213–221.

[32] D.J. Allardice, L.M. Clemow, W.R. Jackson, Determination of the acid distribution and total acidity of low-rank coals and coal-derived materials by an improved barium exchange technique, Fuel 82 (2003) 35–40.

[33] M.M. Maroto-Valer, C.S. Song, Y. Soong, Environmental Challenges and Greenhouse Gas Control for Fossil Fuel Utilization in the 21st Century, Kluwer Academic/Plenum Publishers, New York, 2002.

[34] A. Tahmasebi, J.L. Yu, S. Bhattacharya, Chemical structure changes accompanying fluidized-bed drying of Victorian brown coals in superheated steam, nitrogen, and hot air, Energy Fuels 27 (2013) 154–166.

[35] A. Tahmasebi, J.L. Yu, Y.N. Han, X.C. Li, A Study of chemical structure changes of Chinese lignite during fluidized-bed drying in nitrogen and air, Fuel Process. Technol. 101 (2012) 85–93.

[36] S.J. Grabowski, Ab Initio calculations on conventional and unconventional hydrogen bond-study of the hydrogen bond strength, J. Phys. Chem. A 105 (2001) 10739–10746.

[37] N. Spegazzini, H.W. Siesler, Y. Ozaki, Activation and thermodynamic parameter study of the heteronuclear C=O···H−N hydrogen bonding of diphenylurethane isomeric structures by FT-IR spectroscopy using the regularized inversion of an eigenvalue problem, J. Phys. Chem. A 116 (2012) 7797–7808.

[38] J. Hayashi, K. Norinaga, N. Kudo, T. Chiba, Estimation of size and shape of pores in moist coal utilizing sorbed water as a molecular probe, Energy Fuels 15 (2001) 903–909.

[39] M. Blazsó, E. Jakab, A. Vargha, T. Székely, H. Zoebel, H. Klare, G. Keil, The effect of hydrothermal treatment on a Merseburg lignite, Fuel 65 (1986) 337–341.

CHAPTER 3

Effects on some physicochemical properties of Loy Yang lignite during hydrothermal treatment coupled with mechanical expression dewatering and upgrading process

3.1 Introduction

Fundamental studies of forms of water in Loy Yang (LY) lignite and changes in hydrogen bonds between lignite and water during hydrothermal treatment (HT) have been investigated in **Chapter 2**. Furthermore, environmentally friendly and efficient use of lignite and a better understanding of dewatering and water re-adsorption mechanisms should consider special physicochemical properties. Consequently, the discussion of the changes in some physicochemical properties during HT and HT coupled mechanical expression (HT–ME) is the subject of this chapter.

A variety of techniques, which are in general grouped into evaporative and non-evaporative drying techniques, have been investigated to remove water from lignite [1–13]. Detailed explanation of evaporative and non-evaporative drying techniques has been given in **Sections 1.4.1 and 1.4.2**, respectively.

Conventionally, HT and HT–ME are carried out by adding extra water or steam to lignite before or during treatment process. However, this will increase the volume of wastewater and energy requirement [1]. Furthermore, conventional HT–ME consists of two successive stages: HT (stage 1) and then ME at the same temperature of HT process with autogenously saturated pressure (Stage 2). To our knowledge, there are no researches that were conducted to investigate stage 1 and HT–ME products separately.

Furthermore, we wanted to explore stage 2 under more moderate conditions. In the present work, stage 1 was conducted without adding extra water, and stage 2 was performed at low temperature (110 ^{o}C) under atmosphere environment. We aimed to separately investigate stage 1 and HT–ME products. Of particular interest was the microscopic description of the process of HT–ME considering the types of water in lignite.

3.2 Experimental

3.2.1 Sample

Sample is the same as **Section 2.2.1**.

3.2.2 Hydrothermal treatment

About 6 g raw lignite was placed in a steel filter (ϕ = 60 μm), and three of the steel filters were fixed in the middle of the cylinder of a 0.5 L batch-type reactor equipped with an automatic temperature controller (MA22, Taiatsu Techno, Japan; **Fig. 2.1**). N_2 gas was flushed through the sealed system to remove air. The reactor was then pressurized with N_2 gas to 1.5 MPa at room temperature. A series of hydrothermal treatments were performed at different temperatures (50, 100, 150, 200, and 250 ^{o}C) with the desired time of 40 min at an average heating rate of ca. 5 ^{o}C/min. Gaseous, solid, and wastewater products were collected after the reactor was cooled to room temperature. Samples were labeled as HT50, HT100, HT150, HT200, and HT250 (samples obtained by stage 1).

3.2.3 Hydrothermal treatment coupled with mechanical expression

HT solid products (samples obtained by stage 1) and raw lignite were placed in the fixed regions of filter papers so that the sizes of samples treated by the next ME are the same. A small press machine (AH-2003, ASONE, Japan; **Fig. 3.1**) was heated to a prescribed temperature (110 ^{o}C). After confirmation that the temperature had reached the desired value, mechanical pressure of 6 MPa was applied to the samples by the small press machine for 20 min under atmosphere environment. For brevity, the treated samples are named as HT50–ME and the like (HT–ME products). We refer to raw lignite directly treated by ME as RL–ME.

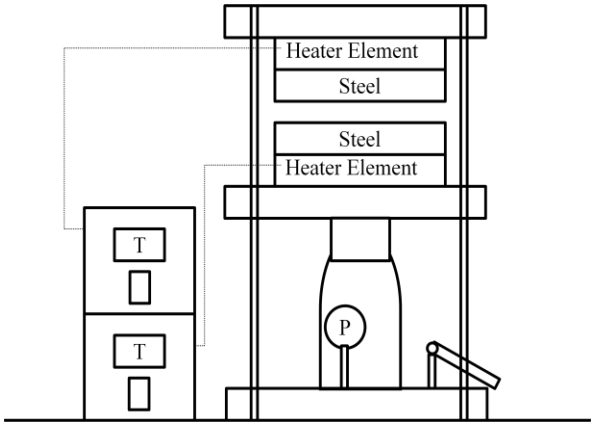

Fig. 3.1 Schematic of ME equipment

3.2.4 Characterization

The residual water contents of all of the solid samples was measured immediately after HT and HT–ME treatment. In brief, samples (m_{li}, weight of treated lignite) were separately placed in weighing bottles (m_1, mass of the weighing bottle, lid, and sample). Then, the open weighing bottles were placed in the oven at 105 ℃. After 6 h, the weighing bottles were taken out, cooled in a desiccator, and weighed with lids (m_i). The residual water content was calculated using

$$\text{Residual water content (\%)} = [(m_1 - m_i)/m_{li}] \times 100\%. \quad (1)$$

Ash content was determined by the weight of waste left after lignite was burned in a furnace (TFM-2200, Eyela, Japan) at 815 ℃ for 2.5 h. Volatile matter was measured by the mass release observed in the furnace at 900 ℃ for 7 min.

Other characterizations were according to the same procedures as reported in the literature [14,15]. In brief, the gas composition was determined by gas chromatography (GC, GC-2014, Shimadzu, Japan) using Molecular Sieve 5A and Porapak Q columns, whose temperature was set at 60 °C, and a Shimadzu GC-4C thermal conductivity detector. Ar gas was the carrier gas. Total organic carbon (TOC) content was measured by a Shimadzu TOC-5000A VCSH TOC analyzer. Inorganic matter was analyzed using inductively coupled optical emission spectroscopy (ICP-OES, optima 8300, PerkinElmer, USA). The composition of organic compounds in the wastewater was determined by high performance liquid chromatography (HPLC, JASCO, Japan) using a JASCO UV-2075 Plus detector and a Shodex KS-811 column with a CO-2065 Plus column oven and the eluent was 2 mM $HClO_4$ at a flow rate of 0.7 mL/min. The FT-IR spectra were recorded with the diffuse reflectance infrared Fourier transform (DRIFT) technique using a FT-IR spectrometer (670 Plus, JASCO, Japan). The concentrations of carboxyl groups and the total acidic values were measured by an improved barium exchange technique, and the concentration of phenolic hydroxyl groups equaled to the difference between total acidic values and carboxyl groups [16]. In brief, sample (ca. 250 mg, d) was mixed with either 60 ml $BaCl_2$/triethanolamine/HCl buffer (carboxyl groups determination) or 50 ml $BaCl_2/Ba(OH)_2$ buffer (total acidic determination) for 30 min and then the mixture was filtered and rinsed with 3 × 5 ml either distilled water (carboxyl groups determination) or

$BaCl_2$/NaOH solution (total acidic determination). The filter cake was collected and stirred with 10 ml, 0.2 M HCl for 30 min. Then, the acid solution was filtered and rinsed with 3 × 10 ml distilled water (carboxyl groups and total acidic determination) and the filtrate made up to 100 ml. Titrate a 20 ml the filtrate using 0.005 M NaOH. The volume of NaOH used was recorded at the titration endpoint of pH 5.00. All characterization was repeated 3–4 times.

3.3 Results and discussion

3.3.1 Gaseous products

Pressures generated with gaseous products and initial N_2 gas of experiment (after the reactor was cooled to room temperature) varied from ca. 1.5 to 1.7 MPa in the processing temperature range of 50 to 250 ^oC. It should be mentioned that the initial pressure generated with N_2 gas of experiment was 1.5 MPa at room temperature. This indicates that some gases were produced. To investigate what kinds of gases were released during dewatering process, GC was used to measure the gaseous products. N_2 was the most abundant gas in the whole process, which originates from initial atmospheric N_2 gas in the reactor, and proportion of N_2 gradually decreased with increasing temperature because some gaseous products were progressively released during the process. CO_2 started to be detected from 200 ^oC, a significant contribution to the formation of CO_2 results from decarboxylation. CO_2 made up 0.46 and 1.92% of the gaseous products at 200 and 250 ^oC, respectively. The amount of released CO_2 increased with increasing temperature as increased temperature accelerates decarboxylation. The increase in the amount of CO_2 is consistent with the loss of carboxyl groups. Wu et al. [17] and Blazsó

et al. [18] suggested that CO_2 product during HT process can be attributed to CO_2 release from coal micropores and CO_2 formation from decarboxylation.

3.3.2 Wastewater products

3.3.2.1 Changes in the volumes of wastewater through HT process

Wastewater was generated during the process of HT, which was acidic, and contained significant amounts of dissolved inorganic and organic compounds. It should be mentioned that wastewater cannot be collected from the sample treated at 50 ^{o}C in this paper, because it existed in the form of droplet on the surface of the reactor at room temperature.

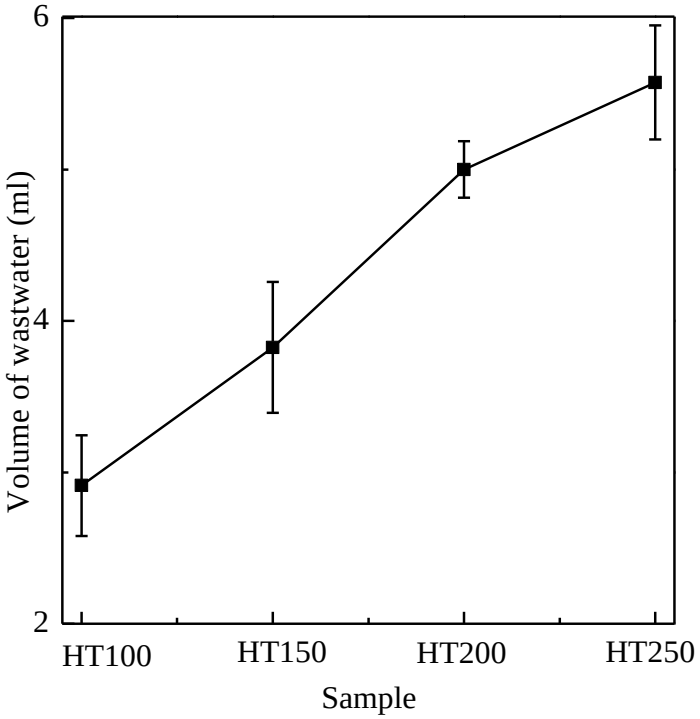

Fig. 3.2 Effects of temperature on the volume of wastewater

Fig. 3.2 shows effect of temperature from 100 to 250 ^{o}C on the volume of wastewater. It was observed that the volume of wastewater generally increased with increasing temperature, which is in agreement with the result that more and more water was

dewatered with increasing temperature. Noteworthy thing is that because the volumes of the wastewater collected from samples treated at different temperatures are not big, it easily causes big experimental errors during collection process, as shown by big error bars in **Fig. 3.2.**

3.3.2.2 Changes in TOC values through HT process

Shown in **Fig. 3.3** is the effect of temperature on TOC value. TOC is the carbon content, which is bound in organic matter, and is generally employed as a guideline for wastewater treatment. TOC values in the wastewater products showed a significant increase from 28 to 698 mg/L between 100 and 250 ^{o}C, which suggests that more and more dissolved organic matter were removed from lignite during HT process. Therefore, the severity of the problems of direct use of wastewater without treatment toward environment, such as contaminating surface water and damaging soil structure, increased with increasing processing temperature. In other words, increased TOC value would prevent the direct disposal of wastewater to the environment. The effect has been observed by others [17,19,20]. It can also be noted that the leaching of soluble organic compounds was greatly enhanced at 250 ^{o}C, indicating that the amount of organic compounds leached, especially aliphatic compounds because there are some low molecular weight aliphatic compounds in lignite's macromolecular structure and aromatic compounds are difficult to decompose at the temperature, were increased at high temperature. In the study of Wu et al. [17], HT was employed to a Chinese lignite between 200 and 320 ^{o}C, and TOC contents of HT320 and HT200 are 5350 and 615 mg/L, respectively. Yu et al. [20] reported that TOC values of the wastewater produced from HT process range from 540 mg/L at 220 ^{o}C to 4792 mg/L at 320 ^{o}C. In summary,

TOC value of sample treated at 250 ^{o}C is not too big but still require some remediation prior to disposal. It is necessary to develop remediation technologies for HT wastewater. If the technologies are successfully investigated, the wastewater may be a valuable resource [19].

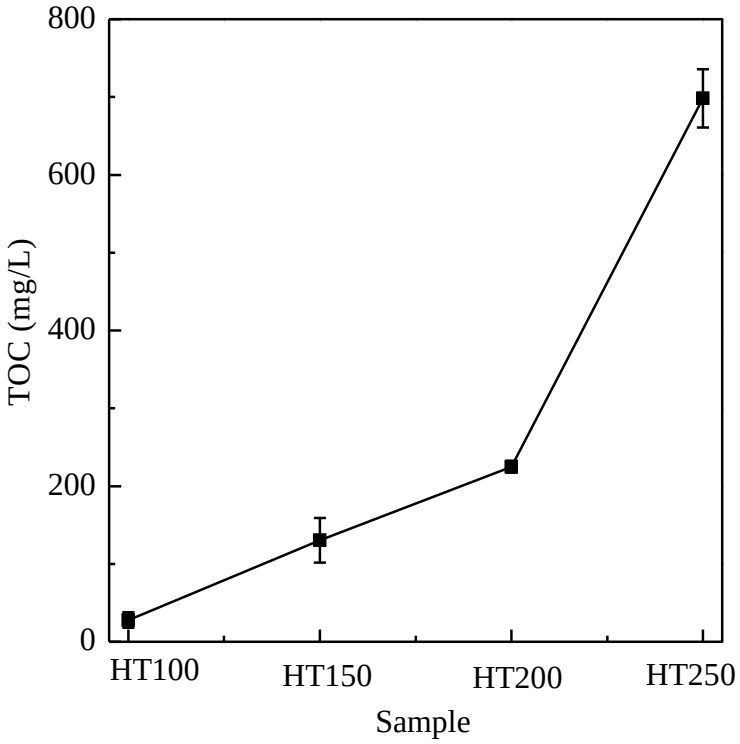

Fig. 3.3 Effects of temperature on TOC value

3.3.2.3 Changes in inorganic compounds through HT process

To provide a guideline that what kinds of inorganic components may exist in the wastewater, X-ray Fluorescence (XRF) was used to measure the composition of the ash of raw lignite (**Table 3.1**). pH values of the wastewater, which were in the range of 3.5 to 4.2, were measured by pH meter. As seen, the main cation was Si^{4+}, which is commonly in the form of quartz and difficult to dissolve into wastewater. Besides, raw sample also contained a large amounts of Al, alkali and alkaline earth metal ions, which may be

present primarily as exchangeable and soluble metal ions [21,22]. Na^+, K^+, Ca^{2+}, Mg^{2+}, and Al^{3+} in wastewater were measured by ICP-OES, since these dissolved salts can be expressed with the wastewater during dewatering. The concentrations of these cations in the wastewater can be measured by ICP-OES and the volumes of wastewater also were known (**Fig. 3.2**). Therefore, total amount of these cations in the wastewater can be calculated. Experiments were repeated four times; the results are given in **Table 3.2**, which suggests quite large error bars. Thus, we will discuss the trends of the removal of these cations with increasing HT temperature.

Table 3.1 Concentrations of major elements of the ash of raw lignite as determined by XRF

Element compounds	SiO_2	Al_2O_3	MgO	Na_2O	CaO	K_2O	Others
Amount (wt.%)	27.70	26.20	11.30	8.59	5.01	0.81	20.39

Table 3.2 Total amounts of main cation components in wastewater of HT (10^{-6}g)

Sample	Na^+	K^+	Mg^{2+}	Ca^{2+}	Al^{3+}
HT100	47.85±27.62	53.67±28.60	6.41±5.66	5.75±7.12	1.07±1.14
HT150	153.25±68.01	69.47±51.57	29.75±6.84	11.66±4.33	2.19±3.50
HT200	159.02±16.21	70.24±12.93	60.09±5.07	32.22±7.84	1.12±1.12
HT250	189.97±60.01	71.62±25.36	51.38±15.67	47.91±13.42	4.08±2.70

Dewatering treatment removed significant amount of Na^+ from lignite. This stands out because Na^+ partly is present as soluble cation. Similar change in Na^+ has been reported previously [23], who stated that 70% of Na^+ in the coals is leached out into the wastewater. Furthermore, the total amounts of Na^+ and K^+ in wastewater increased significantly from 100 to 150 ^oC and then changed slight with increasing temperature. It

can be seen that the relative abundance of K^+ in wastewater was not roughly consistent with its amount in the ash of raw lignite compared with Ca^{2+} and Mg^{2+}. As can be seen, the total amount of Mg^{2+} in wastewater was a little at 100 ^oC and increased apparently from 100 to 200 ^oC then changed little from 200 to 250 ^oC, and the total amount of Ca^{2+} in wastewater was also a little at 100 ^oC and increased apparently from 150 to 250 ^oC. One possible explanation of the trend is that most divalent cations are more strongly bound to carboxyl groups than monovalent cations, which can be more easily removed under severe conditions (high temperature) [19]. Hence the temperature where divalent cations (Ca^{2+} and Mg^{2+}) were greatly removed was higher than that of monovalent cations (Na^+ and K^+). The relative movement rates of Ca^{2+} and Mg^{2+} because of the removal of water from lignite are in the order of: $Ca^{2+} < Mg^{2+}$ [3]. Therefore, the amount of Ca^{2+} in the wastewater increased at 250 ^oC relative to 200 ^oC but kept almost constant for Mg^{2+}. Although the amount of Al^{3+} was larger than that of the other fours, its concentration was the lowest in the wastewater, which can be attributed to that it is likely to be representative of a large proportion of insoluble clay [19].

3.3.2.4 Changes in organic compounds through HT process

HPLC was used to measure the wastewater to find that what kinds of major organic compounds exist in the wastewater. **Table 3.3** is the amount (wt.%) of organic matter in the wastewater products determined by HPLC. Sugar compound glucose was observed at all processing temperatures. Its presence increased up to maximum at 200 ^oC then decreased at 250 ^oC. This may be because of its decomposition with increasing temperature or the big error bars of wastewater volume. Sugar compound xylose began to be detected at 250 ^oC. The detection of glucose and xylose agrees well with the study [24]

that glucose and xylose are detected from lignite humic acids. Small peaks of glyceraldehyde were detected in the temperature range 100–200 ^{o}C, indicating that the amount of glyceraldehyde in wastewater was small, and it was not present at 250 ^{o}C, as also shown in **Table 3.3**. For acetic acid, it can be detected within the range 100–200 ^{o}C. As to levulinic acid, it was first detected at 250 ^{o}C. Mursito et al. [15] analyzed the wastewater obtained from HT of raw peat, and reported that the wastewater contains glyceraldehydes, acetic acid, and levulinic acid. Changes in sugar compounds, organic acid, and aldehyde indicate that organic matter in the treated lignite underwent some decomposition during HT process.

Table 3.3 The amount of organic matter in the wastewater produces determined by HPLC

Amount (wt.%)	Glucose	Xylose	Glyceraldehyde	Acetic acid	Levulinic acid
HT100	0.84±0.60	0	0.01±0.01	0.02±0.02	0
HT150	7.61±0.81	0	0.15±0.03	1.61±0.35	0
HT200	12.49±2.47	0	0.17±0.11	5.05±3.50	0
HT250	7.56±2.05	2.94±2.04	0	0	0.003±0.001

3.3.3 Solid products

3.3.3.1 Changes in functional groups through HT and HT–ME processes

Oxygen-containing functional groups on the surface of lignite play an important role in lignite–water interactions by providing active sites for the adsorption of water. Shown in **Fig. 3.4** are DRIFT spectra of raw lignite and the treated samples obtained by HT or HT–ME at varying temperature. The relative intensity of the bands at 1780 cm^{-1}, which can be attributed to the carbonyl stretching vibration of carboxyl groups C=O [25,26], gradually decreased, suggesting the decomposition of carboxyl groups, which is in

agreement with the results of **Table 3.4**. The bands at around 1690 cm^{-1} revealed the presence of ketone carboxyl band C=O groups [15]. The increase in its relative intensity of peak is probably due to the reaction between side chains of oxygen-containing functional groups during dewatering process under N_2 atmosphere. An aromatic C=C stretch at 1520 cm^{-1} changed slightly in relative intensity with increasing temperature, suggesting decomposition or formation of aromatic hydrocarbons was negligible for temperature lower than 250 ^oC under N_2 atmosphere. Murakami et al. [27] also showed that aromatic ring structures appear to decompose very slowly up to 250 ^oC. The assignment of 1360 cm^{-1} is C–H bond of $–CO–CH_2–$ or $–CO–CH_3$ [28,29]. Its relative intensity sharpened gradually with temperature, which is consistent with the changes in the band at ca. 1690 cm^{-1}. It can also be noted that the difference in DRIFT spectra was hardly found between HT and corresponding HT–ME solid products. Overall, it can be concluded that the changes in functional groups is the result of decomposition during dewatering process.

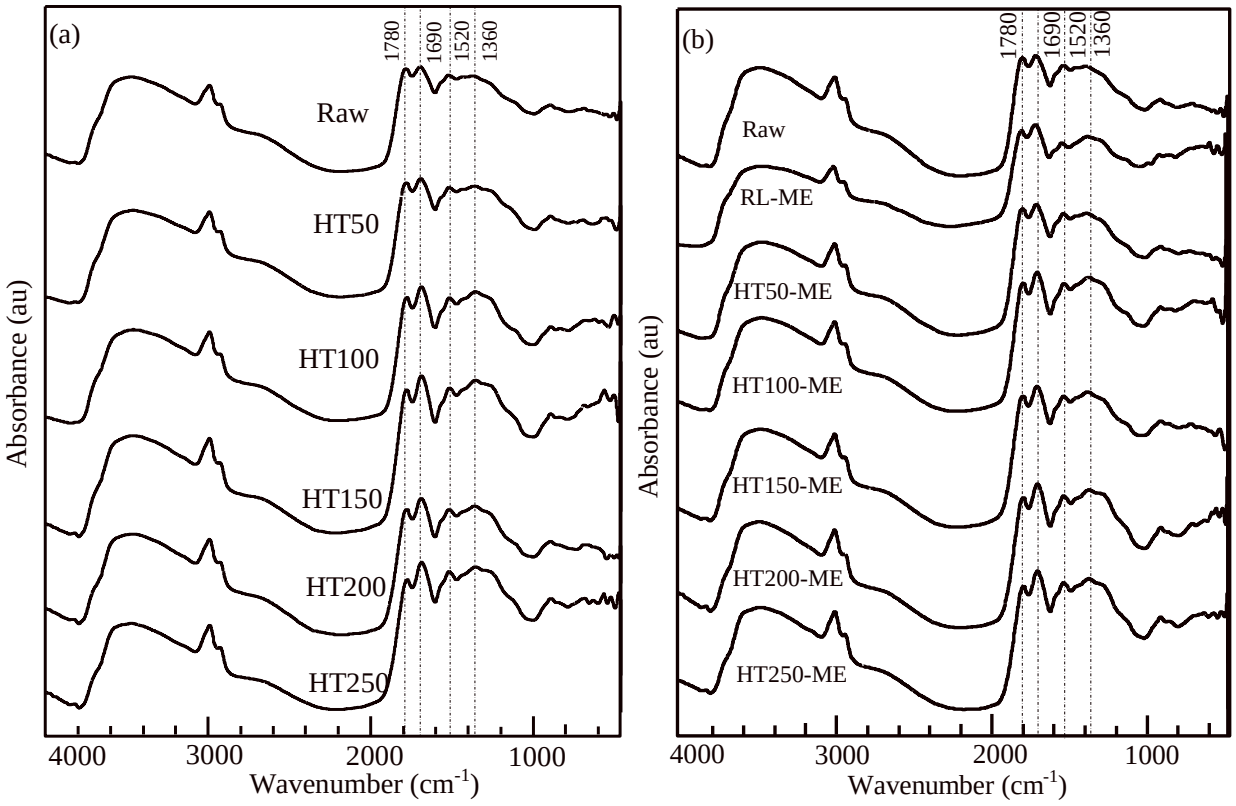

Fig. 3.4 DRIFT spectra of: (a) hydrothermally treated LY lignite; (b) hydrothermally coupled with mechanically expression treated LY lignite. 1780 cm^{-1}: carboxyl groups C=O groups; 1690 cm^{-1}: ketone carboxyl band C=O groups; 1520 cm^{-1}: aromatic C=C stretch; 1360 cm^{-1}: C–H bond of –CO–CH_2– or –CO–CH_3

Table 3.4 Concentrations of carboxyl groups and total acidity of all of the samples (mmol/g, dry basis)

Sample	–COOH	Total acidity	Phenolic hydroxyl groups
Raw	1.74±0.10	6.95±0.02	5.21±0.11
HT50	1.63±0.26	6.80±0.02	5.17±0.22
HT100	2.00±0.16	7.23±0.07	5.23±0.14
HT150	1.54±0.11	6.03±0.39	4.49±0.24
HT200	1.45±0.05	5.87±0.10	4.42±0.47
HT250	0.78±0.10	3.40±0.31	2.77±0.36
RL–ME	1.98±0.09	6.97±0.04	5.00±0.05
HT50–ME	1.71±0.12	6.95±0.11	5.24±0.23
HT100–ME	1.83±0.06	7.01±0.06	5.18±0.06
HT150–ME	1.60±0.13	6.74±0.26	5.14±0.14
HT200–ME	1.40±0.14	5.81±0.02	4.41±0.13
HT250–ME	0.88±0.13	2.95±0.27	2.07±0.33

Because acidic groups (carboxyl and phenolic hydroxyl groups), especially, carboxyl groups [3], are the main hydrophilic groups in lignite and one of the primary factors influencing the high water content in lignite [10,11], quantitative determination of carboxyl, phenolic hydroxyl groups, and total acidic groups is shown in **Table 3.4**. It can be seen that carboxyl groups changed a little below 200 ^{o}C and drastically decomposed above 200 ^{o}C. Similar results have been reported by other researchers [4,26]. At 250 ^{o}C, ca. a half of carboxyl groups was eliminated. Up to 200 ^{o}C, the number of carboxyl groups reached the maximum value at 100 ^{o}C and then decreased. As can be seen from TOC and HPLC results, some dissolved organic compounds were released including some dissolved carboxyl groups. Furthermore, the number of carboxyl groups can be

reduced by decompostion. Concentration of carboxyl groups is the ratio of the number of carboxyl groups to the weight of total organic compounds of lignite. Therefore, the changes in the concentration of carboxyl groups are mainly associated with the removal of dissolved organic compounds below 100 ^{o}C, and the small but steady decrease in the concentration of carboxyl groups can be mainly attributed to the dissolution and decomposition of carboxyl groups above 100 ^{o}C. When temperature was increased to 250 ^{o}C, a significant decrease in the concentration of carboxyl groups was observed because of the drastic decomposition of carboxyl groups. From the GC result, it can be known that CO_2 was first detected at 200 ^{o}C, which is the product of the decomposition of carboxyl groups. However, from **Table 3.4**, it can be known that carboxyl groups started to decompose at temperature lower than 200 ^{o}C. Maybe this is because at low temperature H_2O is produced as the result of the decomposition of carboxyl groups and at high temperature the product is CO_2. Murray et al. [4] reported that the products of the decomposition of carboxyl groups are probably CO_2. However, based on Miura et al. [30], H_2O can be formed during the decomposition process of carboxyl groups. It should be stressed that changes in the concentration of carboxyl groups of samples treated by HT and HT–ME were slight, suggesting that the subsequent ME at 110 ^{o}C under atmosphere condition has a little effect on the concentration of acidic groups. Furthermore, changes in phenolic hydroxyl groups and total acidic groups were similar to that of carboxyl groups.

3.3.3.2 Changes in proximate and ultimate analyses through HT and HT–ME processes

Table 3.5 shows the changes in proximate and ultimate analyses of all of the samples. Lignite contains a large amount of volatile matter, and is also easily susceptible to devolatilization. It can be seen from **Table 3.5** that volatile matter and ash contents of the sample HT50 changed only slightly relative to raw lignite. Up to a temperature of 100 ^{o}C, contents of the volatile matter and ash of samples treated by HT and HT–ME reached their maximum values. The increase is probably because that some soluble organic matter, which is in the form of fixed carbon (e.g., some low molecular weight aliphatic compounds), is removed during dewatering process.

At the temperatures of 100–250 ^{o}C, the volatile matter contents decreased with increasing temperature for HT and HT–ME treated samples, indicating volatile matter started to be released at 100 ^{o}C. As to ash contents of HT and HT–ME treated samples, they decreased gradually at temperature from 100 to 200 ^{o}C because of the dissolution of inorganic and organic compounds during dewatering. More specifically, it is that the removal of inorganic matter surpasses that of organic matter. Then, ash content of HT250 (HT250–ME) increased compared to that of HT200 (HT200–ME). From TOC and FT-IR results, it can be known that TOC values increased significantly and carboxyl groups decomposed drastically at the temperatures of 200–250 ^{o}C. This suggests that a considerable amount of organic matter was removed, which will lead to corresponding gain in the ash content. Furthermore, the changes in volatile and ash contents between samples RL–ME and HT50–ME can be negligible, which is consistent with their similar water content removed from lignite. Compared to raw lignite, their volatile matter decreased and ash contents increased. This can be attributed to that a large amount of water is removed [**Fig. 3.5(b)**], which is accompanied by the great loss of organic matter.

Table 3.5 Proximate and ultimate analyses of all of the samples (wt.%)

Sample	Proximate analysis			Ultimate analysis (daf)			
	V_{daf}	FC_{daf}	A_d	C	H	N	(O+S) (diff.)
Raw	51.34±0.09	48.66±0.09	0.74±0.02	64.8	4.9	0.6	29.7
HT50	51.20±0.37	48.80±0.37	0.80±0.06	64.2	4.9	0.6	30.3
HT100	52.45±0.14	47.55±0.14	0.84±0.03	63.8	4.9	0.6	30.7
HT150	51.45±0.03	48.55±0.03	0.71±0.01	63.8	4.9	0.6	30.7
HT200	49.73±0.56	50.27±0.56	0.43±0.05	64.2	4.9	0.6	30.3
HT250	49.06±0.62	50.94±0.62	0.72±0.02	66.5	4.8	0.7	28.0
RL–ME	50.52±0.09	49.48±0.09	0.84±0.01	63.1	4.9	0.6	31.4
HT50–ME	50.39±0.40	49.61±0.40	0.83±0.01	63.1	5.0	0.6	31.3
HT100–ME	51.08±0.20	48.92±0.20	0.85±0.01	63.0	4.9	0.6	31.5
HT150–ME	50.62±0.16	49.38±0.16	0.70±0.01	64.0	4.9	0.6	30.5
HT200–ME	49.25±0.38	50.75±0.38	0.61±0.02	65.6	4.6	0.7	29.1
HT250–ME	49.28±0.11	50.72±0.11	0.75±0.02	66.2	4.7	0.6	28.5

In generally, volatile matter contents of HT treated samples was higher than that of corresponding HT–ME treated samples but lower for ash contents, because more amount of water is removed by HT–ME relative to HT. The amount of removed organic and matter during HT–ME dewatering process exceeds that during corresponding HT process. Thus, these results were observed.

For HT treated samples, the carbon content slightly decreased up to a temperature of 100 °C when compared with that of raw sample and then increased a little relative to that of HT100. The decrease is because some volatile matter is removed during dewatering (**Table 3.5**) and the increase is attributed to that the decomposition of oxygen-containing

functional groups increases with increasing temperature, which can reduce oxygen content. Furthermore, the contents of hydrogen and nitrogen kept almost unchanged. The same phenomena of HT–ME treated sample were also observed.

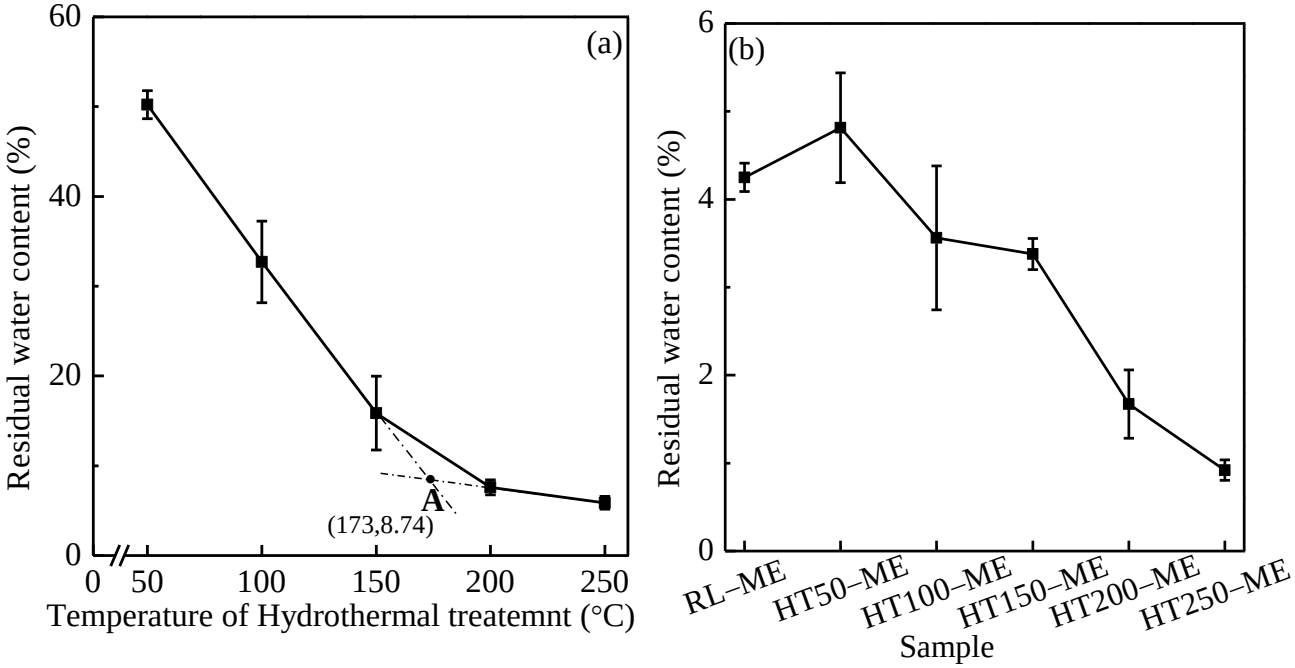

Fig. 3.5 Residual water contents of HT and HT–ME samples

Fig. 3.5 presents residual water contents of HT solid products (stage 1 products) treated by the following ME (stage 2) decreased significantly compared to the corresponding HT solid products, indicating that the next ME is an effective dewatering method. Since changes, such as oxygen-containing functional groups, TOC values, and inorganic matter, are slight by HT in this temperature, the upgrading of HT solid products is not enough. Considering the contradiction between reducing the amounts of gaseous, wastewater products, and energy consumption and upgrading solid products, a temperature of 250 ^{o}C is close to optimum for HT process. In addition, residual water content of HT250–ME was low (0.92%). In summary, HT–ME method described here

produced low water content solid products with using less water, releasing less wastewater for HT stage, and utilizing lower temperature for ME stage relative to conventional HT–ME.

3.3.4 Microscopic description of HT–ME process

Fig. 3.6 shows the simplified schematic diagram of the changes in gaseous, liquid and solid products obtained from HT–ME. Chemically and physically, lignite can be described as an average of one to two aromatic rings per cluster with macromolecular network and is highly porous [3,31]. The active sorption sites on the surface of lignite that significantly affect the amount of water in lignite main are carboxyl groups and carboxylate [3,32]. It is known that some organic matter and inorganic ions dissolve in the water of lignite. Furthermore, interfacial water is difficult to be removed because it likely to condense in micropores and/or bind to active sorption sites via specific interaction such as hydrogen bonds and its layer is around one to two, and non-interfacial water includes free water (without specific interaction with lignite matrix) and bound water (condensed in capillary; Chapter 2). According to these, sketch of lignite was drawn, as shown in the part of magnified sketch of sample in **Fig. 3.6**. When lignite is treated by HT at temperature lower than 173 ℃, the main removed water is non-interfacial water (**Section 2.3.1**). Meanwhile, organic matter, containing glucose, glyceraldehydes, and acetic acid, dissolved in the water of lignite are leached out along with the removal of water from lignite. As to inorganic matter, most Na^+ and K^+ are removed in this temperature range, and the total amounts of Na^+ and K^+ in wastewater increase significantly from 100 to 150 ^oC and then change slight with increasing temperature. Total acidity (carboxyl and phenolic hydroxyl groups) in lignite starts to be

dissolved and decomposed at 100 ^{o}C where its concentration reaches the maximum value (**Table 3.4**) and volatile matter begins to be released also at 100 ^{o}C where their mass percent is the maximum value (**Table 3.5**). As to HT–ME samples, their residual water contents are lower than 5% which are lower that the interfacial water content [8.74%, **Fig. 3.5(a) and Section 2.3.1**] and the remaining water in HT treated samples at temperature lower than 173 ℃ was non-interfacial and interfacial water. Thus, the subsequent ME treatment in this temperature range leads to the release of all of the non-interfacial water and a large proportion of interfacial water. At the same time, organic and inorganic compounds are also removed based on the changes in contents of volatile matter and ash. The subsequent ME treatment affects the number of acidic groups little. Moreover, devolatilization results in the loss of volatile matter in lignite during the subsequent MT process. With further increasing the HT processing temperature from 173 to 250 ^{o}C, interfacial water is the main form of water removed (**Section 2.3.1**). Organic matter continues to be leached out, and new organic matters (xylose and levulinic acid) are first detected at 250 ^{o}C. The total amount of Mg^{2+} significantly increases up to 200 ^{o}C and then changes little, and the total amount of Ca^{2+} removed increases within this temperature range. Besides, decarboxylation results in the detection of CO_2 in gaseous products by GC. For the subsequent ME treatment in this temperature range, interfacial water is the main type of water released. Residual water content of sample HT250–ME is 0.92%, and the remaining water in HT treated samples at temperature higher than 173 ℃ includes interfacial water, meaning that the subsequent ME treatment in this temperature range leads to the removal of interfacial water. Organic and inorganic compounds, acidic

groups containing carboxyl and phenolic hydroxyl groups, and volatile matter are continued to be released during the following ME treatment.

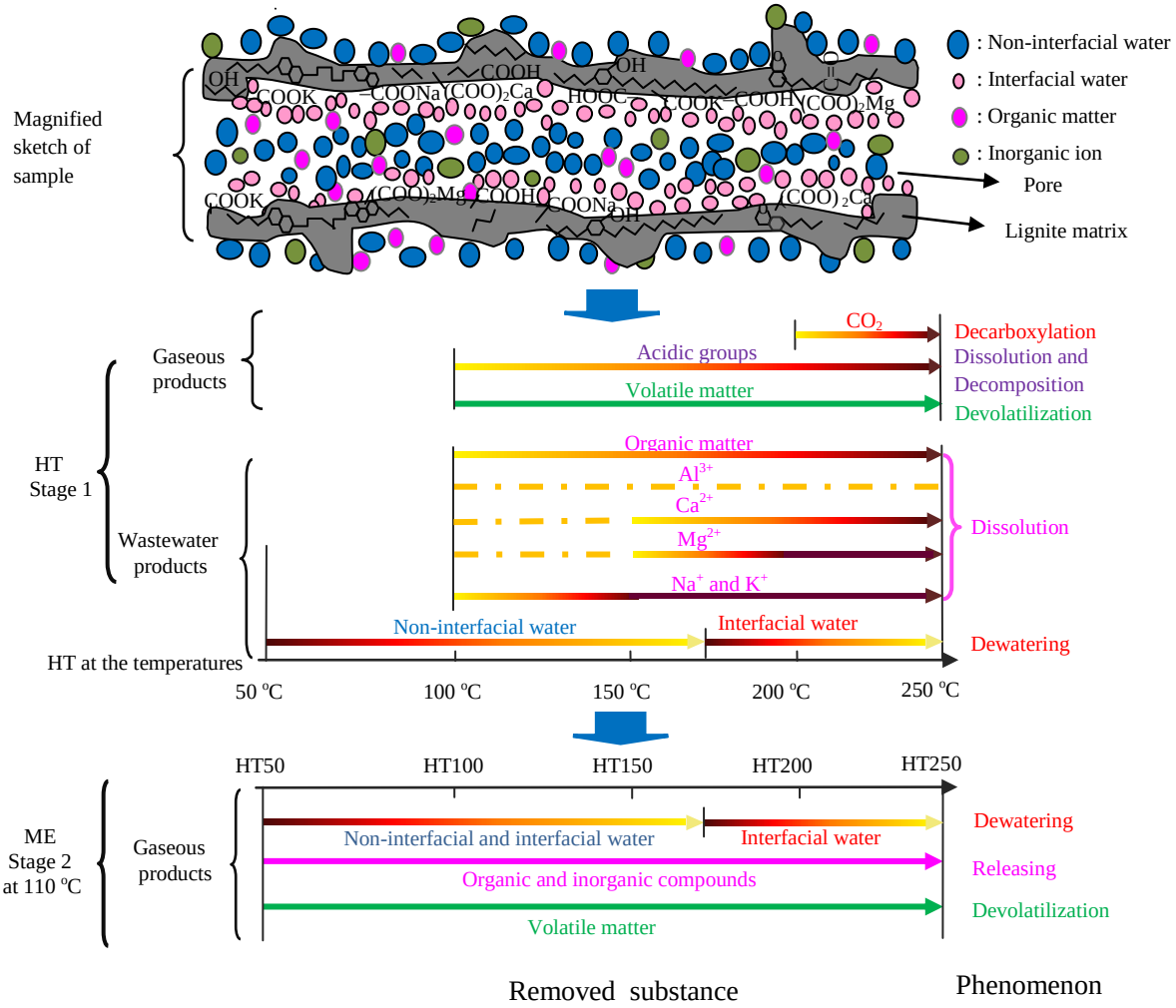

Fig. 3.6 Simplified schematic diagram of the changes in gaseous, liquid, and solid products obtained from HT–ME

Note: A small amount Low High

3.4 Conclusions

In this study, considering the contradiction between reducing the amounts of gaseous and wastewater products and upgrading solid products, a temperature of 250 ^{o}C is close to optimum for HT process without adding extra water. The subsequent ME treatment at 110 ^{o}C under atmosphere condition can reduce the residual water content to 0.92%. HT–ME method described here produced low water content of solid products with using less water, releasing less wastewater at HT stage, and utilizing lower temperature at ME stage compared with conventional HT–ME.

At temperatures ($T \leq 173$ ℃), the main removed water was non-interfacial water. Meanwhile, most monovalent cations (Na^+ and K^+) were removed from lignite in this temperature range, and the total amounts of Na^+ and K^+ in wastewater increased significantly from 100 to 150 ^{o}C and then changed slight with increasing temperature. Acidic groups containing carboxyl and phenolic hydroxyl groups in lignite first dissolved and decomposed at 100 ^{o}C. Furthermore, volatile matter released was also observed. Non-interfacial and interfacial water left after HT were removed by the following ME treatment, and organic and inorganic compounds were also removed. There were little effects of the subsequent ME treatment on the concentration of acidic groups. As to volatile matter, its loss can be attributed to devolatilization. At temperatures ($173 < T \leq 250$ ℃), the main released water was interfacial water. The amount of removed organic compound began to significantly increase at 200 ℃. As to inorganic matter, most divalent cations (Ca^{2+} and Mg^{2+}) were leached out in this temperature range. The total amount of Mg^{2+} in wastewater increased apparently up to 200 ^{o}C then changed little with increasing temperature, and the total amount of Ca^{2+} increased apparently up to 250 ^{o}C. Furthermore, one explanation for the detection of CO_2 in gaseous products is

decarboxylation. For the following ME treatment in this temperature range, the main removed water was interfacial water.

References

[1] M. Sakaguchi, K. Laursen, H. Nakagawa, K. Miura, Hydrothermal upgrading of Loy Yang Brown coal–Effect of upgrading conditions on the characteristics of the products, Fuel process. Technol. 89 (2008) 391–396.

[2] M. Liu, J.J. Yan, B.F. Bai, D.T. Chong, X.K. Guo, F. Xiao, Theoretical study and case analysis for a predried lignite-fired power system, Dry. Technol. 29 (2011) 1219–1229.

[3] C.Z. Li, Advances in the Science of Victorian Brown Coal, Elsevier, Amsterdam, Netherlands, 2004.

[4] J.B. Murray, D.G. Evanst, The brown-coal/water system: Part 3. Thermal dewatering of brown coal, Fuel 51 (1972) 290–296.

[5] H. Fleissner, Method of drying coal and the like, U.S. Patent US1632829, 1927.

[6] D.G. Evans, S.R. Siemon, Dewatering brown coal before combustion, J. the Institute of Fuel 43 (1970) 413–419.

[7] T. Nakajima, H. Hasegawa, H. Takanashi, A. Ohki, Ecotoxicity of effluents from hydrothermal treatment process for low-rank coal, Fuel 104 (2013) 36–40.

[8] G. Favas, W.R. Jackson, Hydrothermal dewatering of lower rank coals. 1. Effects of process conditions on the properties of dried product, Fuel 82 (2003) 53–57.

[9] C. Bergins, Kinetics and mechanism during mechanical/thermal dewatering of lignite, Fuel 82 (2003) 355–364.

[10] C. Vogt, T. Wild, C. Bergins, K. Straußß, J. Hulston, A.L. Chaffee, Mechanical/thermal dewatering of lignite. Part 4: Physico–chemical properties and pore structure during an acid treatment within the MTE process, Fuel 93 (2012) 433–442.

[11] C. Bergins, J. Hulston, K. Strauss, A.L. Chaffee, Mechanical/thermal dewatering of lignite. Part 3: Physical properties and pore structure of MTE product coals, Fuel 86 (2007) 3–16.

[12] M. Karthikeyan, Z.H. Wu, A.S. Mujumdar, Low-rank coal drying technologies—current status and new developments, Dry. Technol. 27 (2009) 403–415.

[13] H. Osman, S.V. Jangam, J.D. Lease, A.S. Mujumdar, Drying of low-rank coal (LRC)—a review of recent patents and innovations, Dry. Technol. 29 (2011) 1763–1783.

[14] A.T. Mursito, T. Hirajima, K. Sasaki, Upgrading and dewatering of raw tropical peat by hydrothermal treatment, Fuel 89 (2010) 635–641.

[15] A.T. Mursito, T. Hirajima, K. Sasaki, S. Kumagai. The effect of hydrothermal dewatering of Pontianak tropical peat on organics in wastewater and gaseous products, Fuel 89 (2010) 3934–3942.

[16] D.J. Allardice, L.M. Clemow, W.R. Jackson, Determination of the acid distribution and total acidity of low-rank coals and coal-derived materials by an improved barium exchange technique, Fuel 82 (2003) 35–40.

[17] J.H. Wu, J.Z. Liu, X. Zhang, Z.H. Wang, J.H. Zhou, K.F. Cen, Chemical and structural changes in XiMeng lignite and its carbon migration during hydrothermal dewatering, Fuel 148 (2015) 139–144.

[18] M. Blazsó, E. Jakab, A. Vargha, T. Székely, H. Zoebel, H. Klare, G. Keil, The effect of hydrothermal treatment on a Merseburg lignite, Fuel 65 (1986) 337–341.

[19] C.J. Butler, A.M. Green, A.L. Chaffee, Assessment of the water quality produced from mechanical thermal expression processing of three Latrobe Valley lignites, Fuel 85 (2006) 1364–1370.

[20] Y.J. Yu, J.Z. Liu, K.F. Cen, Properties of coal water slurry prepared with the solid and liquid products of hydrothermal dewatering of brown coal, Ind. Eng. Chem. Res. 53 (2014) 4511−4517.

[21] Y. Artanto, A.L. Chaffee, Dewatering low rank coals by mechanical thermal expression (MTE) and its influence on organic carbon and inorganic removal, Int. J. Coal Prep. Util. 25 (2005) 251–267.

[22] N. Wijaya, T.K. Choo, L. Zhang, Generation of ultra-clean coal from Victorian brown coal: Effect of hydrothermal treatment and particle size on coal demineralization and the extraction

kinetic of individual metals, Energy Fuels 26 (2012) 5028–5035.

[23] G. Favas, W.R. Jackson, Hydrothermal dewatering of lower rank coals. 2. Effects of coal characteristics for a range of Australian and international coals, Fuel 82 (2003) 59–69.

[24] B. Allard, A comparative study on the chemical composition of humic acids from forest soil, agricultural soil and lignite deposit: Bound lipid, carbohydrate and amino acid distributions, Geoderma 130 (2006) 77–96.

[25] F. Jiang, Z.H. Li, Z.W. Lv, T.G. Gao, J.S. Yang, Z.H. Qin, H.L. Yuan, The biosolubilization of lignite by Bacillussp. Y7 and characterization of the soluble products, Fuel 103 (2013) 639–645.

[26] A. Tahmasebi, J.L. Yu, Y.N. Han, X.C. Li, A study of chemical structure changes of Chinese lignite during fluidized-bed drying in nitrogen and air, Fuel Process. Technol. 101 (2012) 85–93.

[27] K. Murakami, H. Shirato, Y. Nishiyama, In situ infrared spectroscopic study of the effects of exchanged cations on thermal decomposition of a brown coal, Fuel 76 (1997) 655–661.

[28] S.H. Wang, P.R. Griffiths, Resolution enhancement of diffuse reflectance IR spectra of coal by Fourier self-deconvolution. 1. C–H stretching and bending modes, Fuel 64 (1985) 229–236.

[29] A. Tahmasebi, Y. Jiang, J.L. Yu, X.C. Li, J. Lucas, Solvent extraction of Chinese lignite and chemical structure changes of the residue during H_2O_2 oxidation, Fuel Process. Technol. 129 (2015) 213–221.

[30] K. Miura, K. Mae, W. Li, T. Kusakawa, F. Morozumi, A. Kumano, Estimation of hydrogen bond distribution in coal through the analysis of OH stretching bands in diffuse reflectance infrared spectrum measured by in-situ technique, Energy Fuels 15 (2001) 599–610.

[31] M.L. Gorbaty, Prominent frontiers of coal science: Past, present and future, Fuel 73 (1994) 1819–1828.

[32] D. Charrière, P. Behra, Water sorption on coals. J. Colloid Interf. Sci. 344 (2010) 460–467.

[33] K. Norinaga, J.I. Hayashi, N. Kudo, T. Chiba, Evaluation of effect of predrying on the porous structure of water-swollen coal based on the freezing property of pore condensed water, Energy Fuels 13 (1999) 1058–1066.

CHAPTER 4

Effects of hydrothermal treatment coupled with mechanical expression on equilibrium water content of Loy Yang lignite and mechanism

4.1 Introduction

Water re-adsorption is placed in a separate chapter to explore its mechanism. Water re-adsorption is an important parameter to characterize dewatering and upgrading effect and its mechanism can provide useful guidelines for the targeted control of the water re-adsorption of lignite and its storage.

Dried lignite is easy to re-adsorb water under atmosphere environment, which can be attributed to relative humidity (RH) of atmosphere environment and some physico-chemical properties of lignite. It is well known that RH changes with time, temperature, pressure, location, and so on. Thus, it is essential to investigate the mechanism of equilibrium water content (EWC) in lignite at different RHs.

Valuable works on the EWC behavior of lignite have been presented. These studies showed that there are many factors [e.g., oxygen-containing functional groups, residual water content (RWC), pore volume, and RH] that affect EWC of dewatered lignite [1–13]. Early work was based on the measurement of adsorption–desorption isotherms of water, and water in lignite can be categorized into free, capillary, multilayer, and monolayer water, which is the basis for the scientific studies today [7,8]. Generally, monolayer and the second layer of adsorbed water roughly belong to non-freezable water [9]. Other multilayer and capillary water are called bound water. Schafer [10] studied the effects of carboxyl and phenolic hydroxyl groups on the EWC and found that the EWC

depends primarily on the carboxyl groups and, to a lesser extent, on the phenolic hydroxyl groups. Further research [11] showed that water adsorption is assumed to occur on the active adsorption sites, and carboxyl groups are the preferential active adsorption sites on the surface of lignite when compared with the other oxygen-containing functional groups. Correlation between the RWC of Loy Yong lignite dewatered by mechanical thermal expression and the EWC at RH=96% was investigated by Hulston et al. [3], who found that the EWC increases with increasing RWC. This is because the difference between the internal water content of sample and water vapor in the external environment determines the ultimate steady state [12]. Furthermore, during dewatering process, the pore structure may collapse, become cross-linked, or shrink, which leads to significant change in water adsorption capacity of dewatered lignite [13]. Yang et al. [14] reported that the change in mesopore is the main factor that influences the EWC of dewatered lignite.

Numerous studies showed that dewatered lignite with different RWCs either re-adsorb or evaporate water at various RHs [6–15]. As reported by Shigehisa et al. [6] and Charrière et al. [15], adsorption process includes three steps. (1) Adsorption on active adsorption sites; (2) formation of water clusters; and (3) pores filling of water clusters and capillary condensation in narrow pores. As to evaporation process, the relative difficulty of removing different types of water is in the order: free water < capillary water < multilayer water < monolayer water [8,16].

Although some studies on the performance of EWC of lignite have been published [11–15], there are little detailed analysis of the phenomenon. Systematical investigation of this can provide useful guidelines for the targeted control of the water re-adsorption of

lignite and its storage. In this study, Loy Yang (LY) lignite was treated by hydrothermal treatment (HT) and HT coupled with mechanical expression (HT–ME). We detailedly reported the influence of carboxyl groups, monolayer water content, mesopore volume, and RWC on the EWCs at various RHs. Of particular interest was the analysis of the changes in the mechanism with increasing RH.

4.2 Experimental

4.2.1 Sample

Sample is the same as **Section 2.2.1**.

4.2.2 Hydrothermal treatment

The as-received raw lignite (about 6 g) was placed in a steel filter (ϕ = 60 μm), and three of the steel filters were fixed in the middle of a 0.5 L batch-type reactor that was equipped with an automatic temperature controller and had a maximum temperature of 400 ^{o}C and a maximum pressure of 30 MPa (MA22, Taiatsu Techno, Japan; **Fig. 2.1**). In order to remove air, N_2 gas was flushed through the sealed system, which was then pressurized to 1.5 MPa with N_2 gas at room temperature. A series of hydrothermal treatments were conducted at 50, 100, 150, 200, and 250 ^{o}C for 40 min at an average heating rate of ca. 5 ^{o}C/min. Products, which were referred to as HT50, HT100, HT150, HT200, and HT250, were collected after the reactor was cooled to room temperature.

4.2.3 Hydrothermal treatment coupled with mechanical expression

HT solid products and raw lignite were placed in the fixed regions of filter papers so that the sizes of samples treated by the next ME are the same. A small press machine (AH-2003, ASONE, Japan; **Fig. 3.1**) was heated to a prescribed temperature (110 ^{o}C).

After confirmation that the temperature had reached the desired value, mechanical pressure of 6 MPa was applied to the samples by the small press machine for 20 min under atmosphere environment. For brevity, the treated samples are named as HT50–ME and the like. We refer to raw lignite directly treated by ME as RL–ME.

4.2.4 Residual water content, water content, and equilibrium water content determination

Samples (ca. 1.00 g) were separately placed in weighing bottles (m_1, mass of the weighing bottle, lid, and sample). Then, the open weighing bottles were positioned in a desiccator with one of a set of saturated salt solutions inside. The desiccator was placed in a 25 ^{o}C room, and each saturated salt solution can maintain a specific RH, as shown in **Table 4.1**. RH was measured by hygrometer. After several hours the weighing bottles were taken out, closed with lids, and weighted (m_i). Experiments were repeated until reaching the equilibrium ($m_{i,e}$), and water content is called EWC in such a case. The RWC and EWC of sample were measured by the method used in our previous work [17]. In brief, after reaching equilibrium, weighing bottles without lids were placed in an oven (WFO-50, Eyela, Japan) at 105 ℃. After 6 h, the weighing bottles were taken out, cooled in a desiccator, and weighed with lids (m_b). The RWC of the total weight (tw) of sample was calculated using

$$\text{RWC (\%, tw)} = [(m_1 - m_b)/(m_1 - m_w)] \times 100\%, \quad (1)$$

where m_w is the mass of the weighing bottle and lid.

The water content of the total weight (tw) of sample was calculated using

$$\text{Water content (\%, tw)} = [(m_i - m_b)/(m_i - m_w)] \times 100\% \quad (2)$$

EWC of the total weight (tw) of sample was calculated using

$$\text{EWC (\%, tw)} = [(m_{i,e} - m_b)/(m_{i,e} - m_w)] \times 100\% \quad (3)$$

EWC of lignite of 100 g, on a dry (d) basis, was calculated using

$$\text{EWC (g/100g–lignite, d)} = \{(\text{EWC (\%, tw)}/[100-\text{EWC (\%, tw)}]\} \times 100 \quad (4)$$

The experiments were repeated three times.

Table 4.1 RH of saturated salt solution at 25 ^{o}C measured by hygrometer

Salt solution	LiBr	LiCl	K_2CO_3	KNO_3	K_2SO_4
RH (%)	6	10	42	92	97

4.2.5 Characterization

The number of carboxyl groups was measured by an improved barium exchange technique [18]. Mesopore (pores 2 to 50 nm diameter) volume was calculated based on N_2 gas adsorption–desorption isotherms, which were measured by a high precision–special surface area/pore size distribution unit (BELSORP–max, BEL, Japan) using Barrett, Joyner, and Halenda proposed method, BJH method. For N_2 adsorption–desorption experiment, pretreatment under vacuum at 110 ^{o}C for 15 h was performed to remove the adsorbed gases. All experiments were performed at least two times.

4.3. Results and discussion

4.3.1 Analysis of factors that control EWC at various RHs

To investigate the relationship between RH and EWC, EWCs variations against all of the RHs are shown in **Fig. 4.1**. These isotherms can be divided into three regions. The slope of region 1 (RH ≤ 10%) is greater than that of region 2 (10 < RH ≤ 92%), suggesting a stronger monolayer adsorption capacity. The higher monolayer adsorption

capacity can be attributed to that monolayer water molecules interact with the surface of lignite by hydrogen bonds with the adsorption active sites. As mentioned above, hydrophilic carboxyl groups act in the primary active adsorption sites, which have a greater affinity to chemically bind the water. With increasing RH, a decreased slope is observed in region 2 because the extra adsorbed water is in the form of bound water. The amount of bound water is mainly determined by the amount of monolayer water and mesopore volume. The lower adsorption capacity in region 2 is because water–water bonding energy and capillary force are smaller than the bonding energy of hydrogen bonds. As the RH increased further, the increased slope of region 3 (RH > 92%) corresponds to more free volume allowing the filling of more amount of free water. The division is coincident with Allardice et al. [19], Fei et al. [20], and Charrière et al. [15], who reported that the factors that control water adsorption at RHs lower than 92% differ from those that control the extra water adsorbed at RHs higher than 92% [19]; there is a good linear correlation between the EWCs at RHs=11, 32, and 51% [20]; and adsorption process of water vapor in coal with increasing RH includes four stages, and the slopes of the second and third stages are similar [15]. The factors that control EWCs at different RHs are systematically discussed later (**Sections 4.3.1.1, 4.3.1.2, and 4. 3.1.3**).

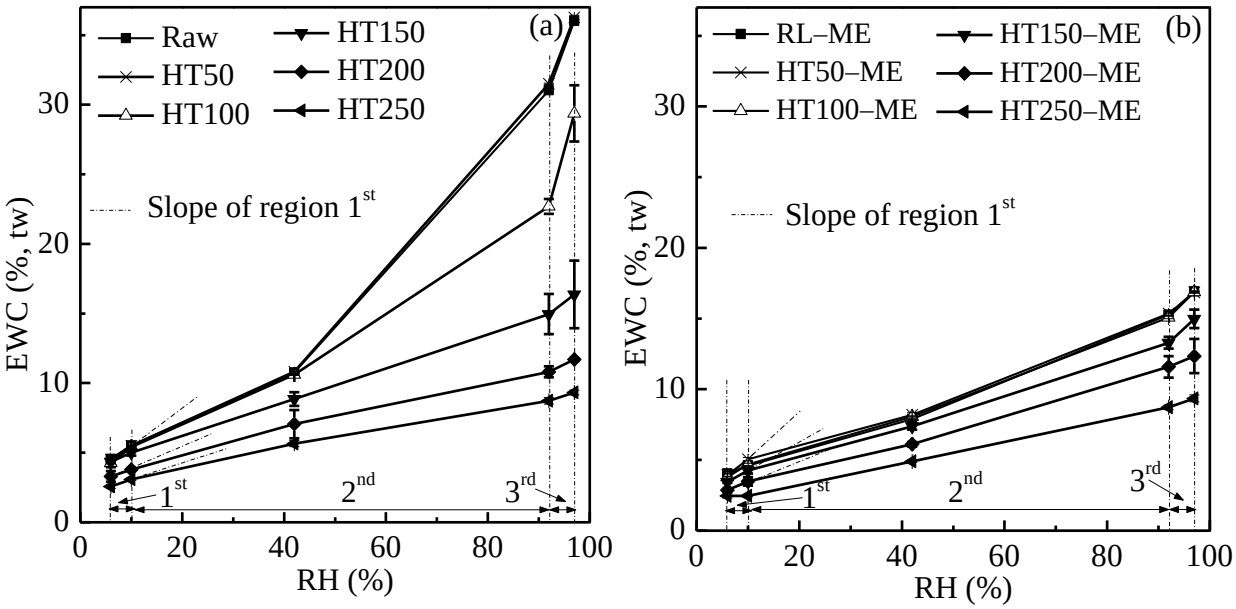

Fig. 4.1 EWCs of all of the samples at various RHs. EWC (%, tw): EWC of the total weight (tw) of sample

It is interesting that for raw lignite and HT50, there was the non-linear correlation between the EWCs and RHs=10, 42, and 92%. **Fig. 4.2** shows the effect of time on water content at RH=92%. As can be seen, raw and HT50 dewatered at RH=92% [**Fig. 4.2(a)].** Furthermore, RWCs of raw lignite and HT50 were 57.47 and 50.22%, respectively, which were significantly relatively high. It also known that free water is the most easily removed one among all types of water. These indicate that the removed water was mainly in the form of free water for raw and HT50. Meanwhile, for sample of HT100, its water content changed slightly with time. However, the other HT treated samples and HT–ME treated samples re-adsorbed water under the same condition (**Fig. 4.2**). The EWCs of raw lignite and HT50 at RH=92%, whose values were 31.03 and 31.50%, respectively, were apparently higher than that of HT100, HT150, HT200, and HT250, whose values were 22.70, 14.96, 10.81, and 8.72%, respectively. On the basis of the above analyses, the

forms of EWCs at RH=92% for raw lignite and HT50 include fractional free water besides bound water. Consequently, one possible explanation of the changed slope in the RH range of 42–92% is that the existing water includes fractional free water besides bound water for raw lignite and HT50, while the other samples just contain bound water.

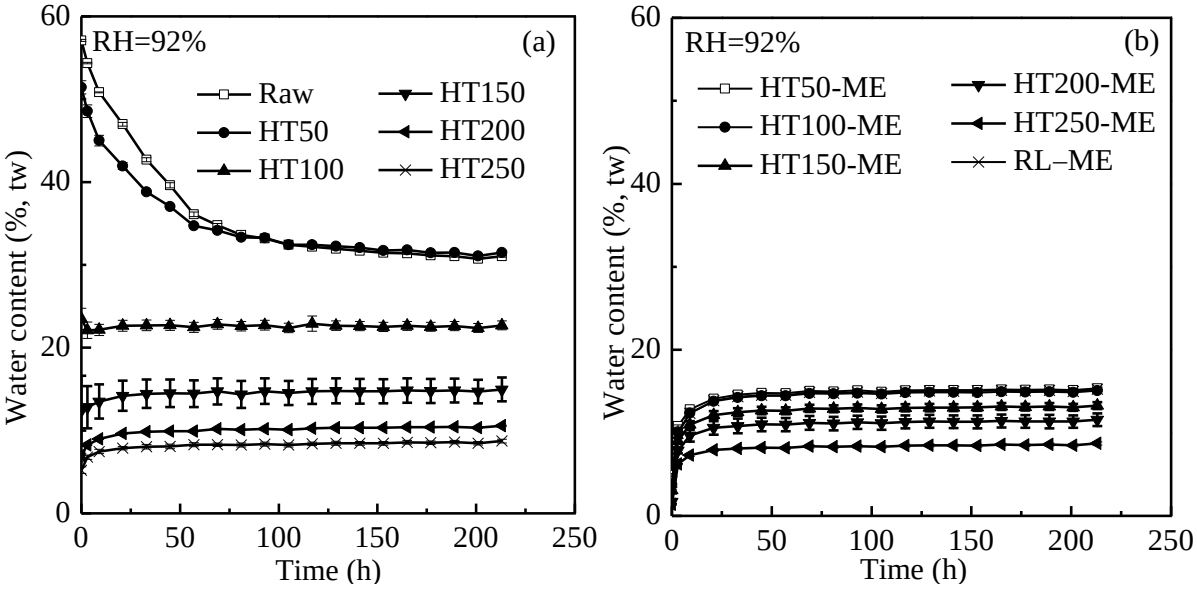

Fig. 4.2 Effects of time on water content of HT treated samples at RH=92%. Water content at 0 h is RWC

As to HT–ME treated samples, their changes in EWC with increasing RH were similar to those of HT treated samples at temperature higher than 100 ^{o}C. Note that the slope of HT–ME250 at RH below 10% is extraordinary relative to the other HT–ME samples in the same RH range, which can be attributed to that the measurement uncertainty in EWC of HT–ME250 at RH=6% is greater than those of the others because in this narrow RH range EWC of HT–ME250 sample changes more slightly compared with the others.

It was also observed that EWCs at all of the RHs decreased with increasing processing temperature of HT and HT–ME. EWCs of samples obtained from HT–ME were lower

than those of samples obtained from HT, which suggests that HT and HT−ME can upgrade the lignite by reducing water loading capacity and HT−ME was better than HT. At low RHs (RH ≤ 10%), the factor that controls EWC is water molecules−active sites interactions (Detailed analysis is shown **in Section 4.3.1.1**). Therefore, the decrease in EWC with increasing temperature of HT and HT−ME within low RH range is because of the decrease trend in the concentrations of carboxyl groups (**Table 4.2**). The difference between EWCs of HT and HT−ME treated samples at low RHs was not significant due to the slight changes in carboxyl groups between HT and HT−ME samples. At medium RHs (10 < RH ≤ 92%), the effects of the amount of monolayer water and mesopore volume on EWC are important (Detailed analysis is shown in **Section 4.3.1.2**). Thus, the difference between EWCs of HT and HT−ME treated samples at medium RHs became more clearly, which can be attributed to mesopore volumes of HT−ME samples are smaller than those of corresponding HT samples (**Table 4.2**). At high RHs (RH > 92%), EWC is strongly influenced by the comprehensive factors including total volume of macropores and cracks, the size of spaces between the particles, the concentration of carboxyl groups, and interaction between water molecules (Detailed analysis is shown in **Section 4.3.1.3**). Hence, the changes in EWC with increasing temperature and the lower EWCs of HT−ME samples relative to HT samples are dependent on the factors that affect EWC in this RH range.

Table 4.2 Concentrations of carboxyl groups and mesopore volumes of all of the samples

Sample	Carboxyl groups (mmol/g, d)	Mesopore volume (cm^3/g, d)
Raw	1.74±0.10	$0.0076 \pm 6.8\times10^{-5}$
HT50	1.63±0.26	$0.0084 \pm 3.2\times10^{-4}$
HT100	2.00±0.16	$0.0109 \pm 6.4\times10^{-4}$
HT150	1.54±0.11	$0.0073 \pm 4.5\times10^{-4}$
HT200	1.45±0.50	$0.0092 \pm 3.1\times10^{-4}$
HT250	0.78±0.10	$0.0040 \pm 1.0\times10^{-3}$
RL–ME	1.98±0.09	$0.0111 \pm 2.4\times10^{-4}$
HT50–ME	1.71±0.12	$0.0074 \pm 1.7\times10^{-4}$
HT100–ME	1.83±0.06	$0.0088 \pm 1.1\times10^{-4}$
HT150–ME	1.60±0.13	$0.0068 \pm 8.9\times10^{-5}$
HT200–ME	1.40±0.14	$0.0041 \pm 3.3\times10^{-5}$
HT250–ME	0.88±0.13	$0.0041 \pm 2.4\times10^{-5}$

4.3.1.1 Analysis of factor that controls EWC at low RHs

The EWC at ca. RH=10% corresponds to monolayer adsorption water, which is not strongly related to the surface area but significantly influenced by the active adsorption sites on the surface of lignite [8]. Carboxyl groups are the primary active adsorption sites [10]. Furthermore, the slope of RHs lower than 10% is different from those of the other RH regions (**Fig. 4.1**). Therefore, the concentrations of carboxyl groups are plotted against the EWC at RH=10% for a quantitative discussion of the relationship between carboxyl groups and monolayer adsorption capacity, as shown in **Fig. 4.3**. The slope is 1.31 with a moderately good correlation (R^2=0.66), which means that each carboxyl group bound one to two water molecules to complete the monolayer adsorption.

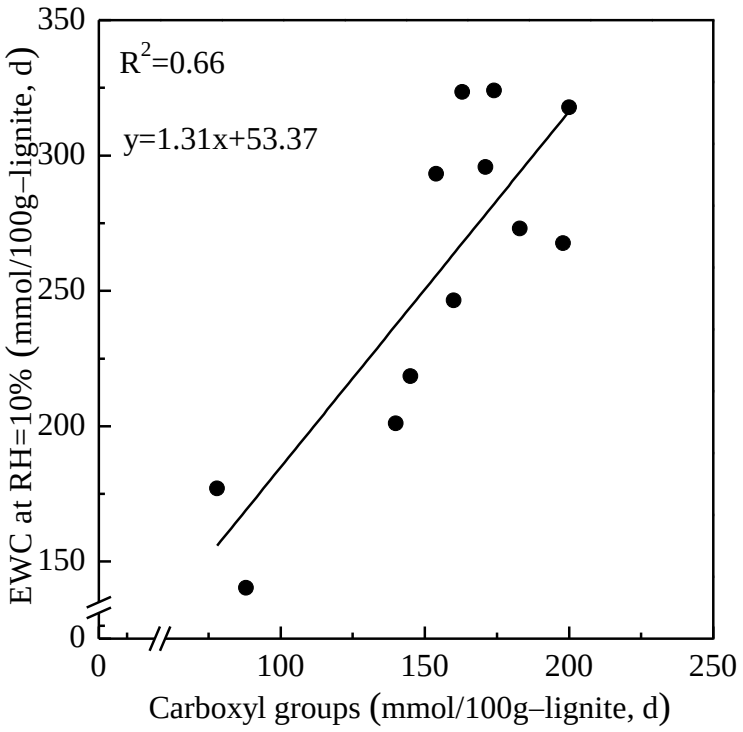

Fig. 4.3 Relationship between carboxyl groups and EWC at RH=10%

Carboxyl groups are the preferential active adsorption sites of monolayer water adsorption. Meanwhile, other oxygen-containing functional groups (e.g., hydroxyl and carbonyl groups), whose water adsorption capacity is less significant compare with that of carboxyl groups, and cations-exchanged oxygen-containing functional groups (e.g., carboxylate and phenolate), which could result in a greater affinity for water relative to corresponding oxygen-containing functional groups, are also able to act as the active adsorption sites of monolayer adsorption [11,21]. In summary, carboxyl groups are the main factor that controls monolayer adsorption capacity but not the only one. Therefore, a moderately good correlation between carboxyl groups and EWCs at RH=10% was observed.

4.3.1.2 Analysis of factor that controls EWC at medium RHs

The EWC at RH=42% is main in the form of multilayer water. Literature has proposed that water adsorption is involved at active adsorption sites on the surface of lignite, which have high binding energies. Afterward, the monolayer water molecules occupied the active adsorption sites play the role of the secondary adsorption sites, having lower binding energies, because of water molecules interactions [13]. This phenomenon induces the formation of water clusters [15]. Charrière et al. [15] also concluded that after the adsorption of water on active adsorption sites on the surface of lignite, the surface is weakly hydrophilic. Actually, the amount of multilayer water is determined by monolayer water content. Therefore, the EWC at RH=10% is plotted against the EWC at RH=42% to investigate the effect of monolayer water on multilayer water, as shown in **Fig. 4.4**. The slope is 2.05 with a high correlation coefficient (R^2=0.90), suggesting that ca. two multilayer water molecules were bound to each monolayer water molecule via water−water interaction. At the RH, the amount of EWC is high enough to form water clusters around active adsorption sites.

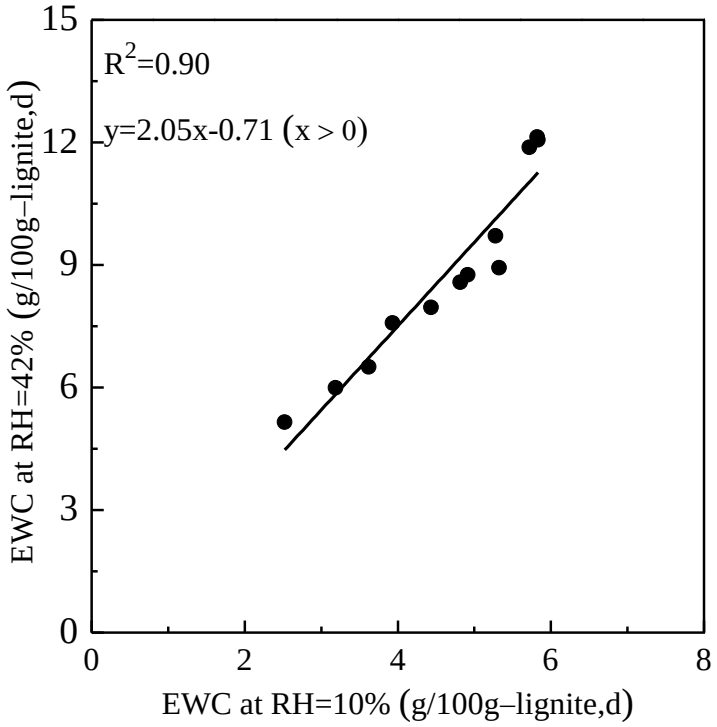

Fig. 4.4 Relationship between EWC at RH=10% and EWC at RH=42%

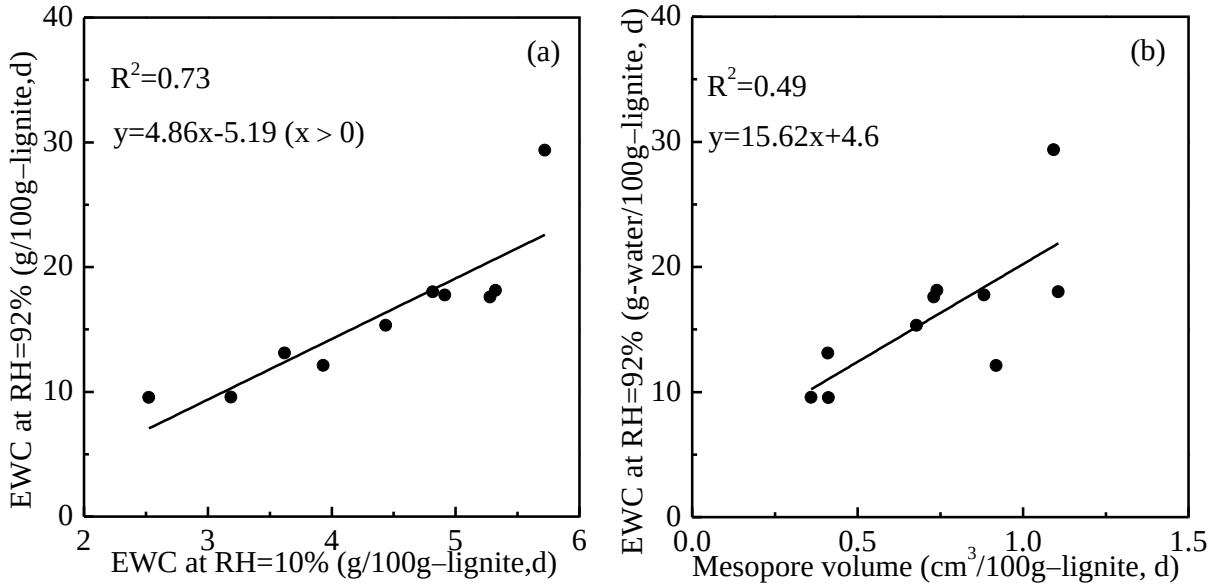

Fig. 4.5 Effects of EWC at RH=10% and mesopore volume on EWC at RH=92%

A high correlation between the EWCs at RHs of 10% and 42% was found, but moderately good between the EWCs at RHs of 10% and 92% [R^2=0.73, **Fig. 4.5(a)**]. A RH increase will lead to an increase in EWC with water clusters growing and pores filling, and the main type of the EWC at RH=92% in lignite is capillary water which is also affected by the mesoproe volume. Therefore, **Fig. 4.5(b)** plots EWC at RH=92% as a function of mesopore volume. It was found that the linear correlation between the EWC at RH=92% and mesopore volume decreased further (R^2=0.49). These results are because the EWC at the RH is mainly determined by both monolayer water content and mesopore volume. However, other factors, such as capillary force and bonding energies between capillary water molecules, also have an effect on EWC. Furthermore, multilayer water also exists at the RH. As shown in **Fig. 4.1** (big error bar), the measurement uncertainty in the EWC at RH=92% was greater than that at low RHs. Consequently, the comprehensive effect of the above factors finally leads to the results.

Generally, there was a good linear correlation between EWC in the RH range 10–92% (**Fig. 4.1**). However, based on the above analyses, the factor that control EWCs in the RH from 10 to 42% differs from that in the RH range 42–92%. It is known that multilayer water exists in the RH range 10–42% and the extra adsorbed water is in the form of capillary with further increasing RH. Allardice et al. [8] reported that the transition in the isosteric heat from capillary water to multilayer water is indistinct, which can be attributed that some overlap where the more-loosely-held multilayer water is desorbed simultaneously with capillary water held tenaciously in small pores. Furthermore, Multilayer (except the second layer) and capillary water are bound water [9]. These may be the reason for the same slope of the two RH ranges.

4.3.1.3 Analysis of factor that controls EWC at high RHs

As RH increases further, more water is being adsorbed on lignite, and finally EWC increases. In this stage, the increased EWC is in the type of free water which is contained in the places such as spaces between the lignite particles, macropores, and intraparticle cracks [22]. Meanwhile, forms of monolayer, multilayer, and capillary water also exist. Furthermore, the slope in the RH range higher than 92% changes (**Fig. 4.1**). Therefore, the factors that control EWC at high RHs changed. Based on the forms of water in lignite at high RHs and their influence factors, it can be concluded that these factors (e.g., total volume of macropores and cracks, the size of spaces between the particles, the content of carboxyl groups, and interaction between water molecules) significantly affect the EWC at high RHs. Because the comprehensive effect of these factors on EWC is very complicated, it is difficult to further discuss.

4.3.2 Mechanism of EWC in lignite at various RHs

The porous structure of lignite mainly comprises of mesopores and macropores [23] and the similar result that micropores of the lignite can be negligibly was found by adsorption−desorption isotherms of N_2 at 77 K (not shown). These suggest that EWC is greatly controlled by mesopores and macropores in porous structure aspect, which is one of the most important factors that influence EWC. Furthermore, spaces between lignite particles and intraparticle cracks also have a significant effect on EWC. Based on the results and discussion presented above, a mechanism of EWC in lignite at various RHs is proposed, as shown in **Fig. 4.6**. At low RHs, water molecules are bound to active adsorption sites on the surface of lignite and carboxyl groups are the preferential active adsorption sties. Each carboxyl group binds one to two molecules. This roughly falls in

the range of monolayer adsorption. The monolayer water is in the types of non-freezable water. Because the van der Waals diameter of a water molecule is ca. 0.3 nm [24], the thickness of the monolayer adsorption is about 0.3 nm [**Fig. 4.6(a)**]. With increasing RH, water molecules are associated with monolayer water molecules, which act in the secondary active adsorption sites. Each monolayer water molecule is occupied by ca. two multilayer water molecules via water–water interactions, meaning the formation of water clusters [**Fig. 4.6(b)**]. The second layer water belongs to non-freezable water and the other multilayer water is a part of bound water. As the RH increases further, more water molecules are filled in mesopores, which causes the growth of water clusters and the continuous filling of mesopores [**Fig. 4.6(c)**]**.** The increased water in this RH range exists in the form of capillary water, a constituent of bound water. At high RHs, with increased EWC as a result of increased RH, the filling of spaces between lignite particles, macropores, and cracks occurs. The additional increased EWC is in the forms of free water [**Fig. 4.6(d)**].

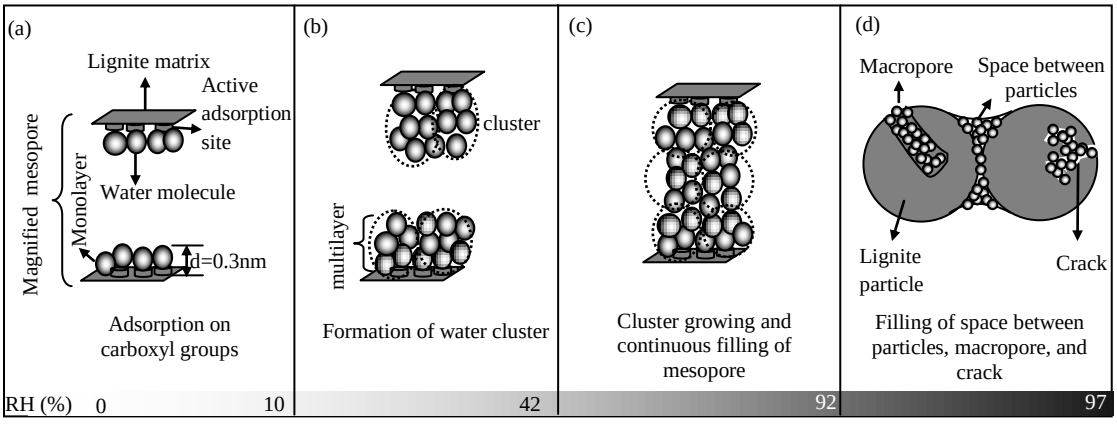

Fig. 4.6 Simplified schematic diagram of the mechanism of EWC in lignite at various RHs

4.3.3 Effects of RWC on EWC at various RHs

Shown in **Fig. 4.7** is the relationship between EWCs at various RHs and RWCs. As can be seen, if the RWC of one HT treated sample was higher than that of another sample, its EWC showed a general trend of higher than that other sample at all of the RHs. The same relationship between EWCs and RWCs was also obtained for HT−ME treated samples. It is interesting that for a sample below a threshold residual water level (ca. 5 to 16%), its EWC was higher than its RWC. This trend was generally observed. The opposite relationship was found for samples with RWC higher than 16%. However, for samples within the threshold, EWC can be either higher or lower than RWC depending on RH. The study of Hulston et al. [3] on samples with RWC higher than ca.16% showed that the EWCs at RH=96% are slightly lower than the RWCs in the RWC range of about 16–44%. Above a RWC of 44%, the EWCs at RH=96% is substantially lower than the RWCs. Similar results have also been reported by Vogt et al [1]. Compared with the previous works [1,3], we extended the ranges of RWC and RH, and found that the relationships between RWC and EWC below a RWC of 5%, within a threshold residual water level (ca. 5 to 16%), and above a RWC of 16% differ from each other, which is significant and can provide information for the operation of lignite dewatering technique, the control of its water re-adsorption, and storage. If RWC of a sample is below 5%, EWC of the sample will increase, indicating that water re-adsorption will occur under atmosphere condition during storage. Therefore, some measures should be taken to forbid the re-adsorption. If RWC of a samples is within a threshold level (ca. 5 ~ 16%), EWC of the sample will increase or decrease, suggesting that the sample will either re-adsorb or dewater depending on the RH in the locality. As a consequence, corresponding measures

should be taken according to the RH. If RWC of a sample is above 16%, EWC of the sample will decrease. Consequently, measures do not need to be taken. On the other hand, taking relationship between EWC and RWC and avoiding re-adsorption into account, some information for the extent of dewatering of lignite can be obtained in target-user location.

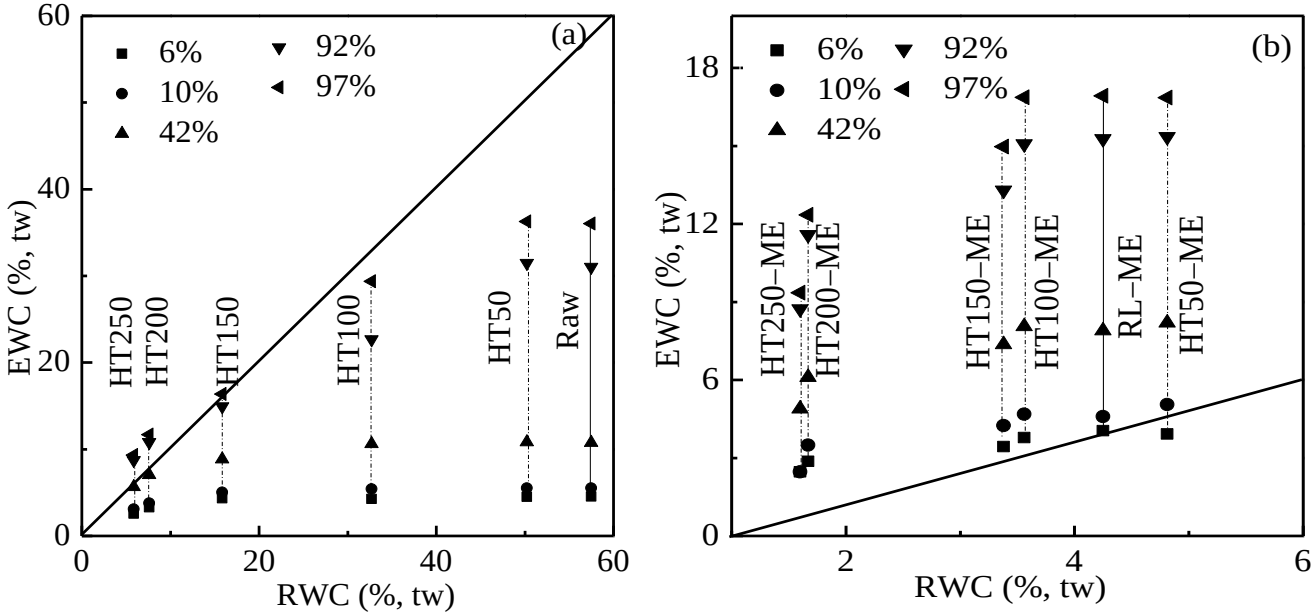

Fig. 4.7 Relationship between EWCs of HT and HT–ME treated samples at various RHs and RWCs. (a) HT treated samples. (b) HT–ME treated samples

4.4. Conclusions

In the present work, EWCs at all of the RHs decreased with increasing temperature of HT and HT–ME, and EWCs of HT–ME samples were lower than those of corresponding HT samples, suggesting that HT and HT–ME can upgrade the lignite by reducing water loading capacity and HT–ME was better than HT.

At low RHs (RH ≤ 10%), the factor that controls EWC is water molecules–active sites interactions and each carboxyl group is occupied by one water molecule. Within 10 < RH ≤ 42%, monolayer water content is relative important and each monolayer water molecule binds ca. two multilayer water molecules. At medium RHs (10 < RH ≤ 92%), the amount of monolayer water and mesopore volume are more important.. However, at high RHs (RH > 92%), EWC is related to the comprehensive factors including total volume of macropores and cracks, the size of spaces between the particles, the amount of carboxyl groups, and interactions between water molecules.

The relationship between RWC and EWC has a threshold residual water level (ca. 5 to 16%). EWC was generally higher than RWC below a RWC of ca. 5% and the opposite relationship was observed in the RWC range above ca. 16%. Within the threshold, EWC can be either higher or lower than RWC depending on RH. These can provide information for the operation of lignite dewatering technology, the control of its water re-adsorption, and storage.

References

[1] C. Vogt, T. Wild, C. Bergins, K. Strauß, J. Hulston, A.L. Chaffee, Mechanical/thermal dewatering of lignite. Part 4: Physico–chemical properties and pore structure during an acid treatment within the MTE process, Fuel 93 (2012) 433–442.

[2] Y. Fe, Y. Artanto, L. Giroux, M. Marshall, W.R. Jackson, J.A. MacPhee, Comparison of some physico–chemical properties of Victorian lignite dewatered under non-evaporative conditions, Fuel 85 (2006) 1987–1991.

[3] J. Hulston, G. Favas, A.L. Chaffee, Physico–chemical properties of Loy Yang lignite dewatered by mechanical thermal expression, Fuel 84 (2005) 1940–1948.

[4] C.Z. Li, Advances in the Science of Victorian Brown Coal, Elsevier, Amsterdam, Netherlands,

2004.

[5] M. Sakaguchi, K. Laursen, H. Nakagawa, K. Miura, Hydrothermal upgrading of Loy Yang brown coal-Effect of upgrading conditions on the characteristics of the products, Fuel process. Technol. 89 (2008) 391–396.

[6] T. Shigehisa, T. Inoue, H. Kumagai, Water adsorption and desorption of upgraded brown coal. Part 1: isotherms of adsorption and desorption, Energy Fuels 28 (2014) 4986−4992.

[7] D.G. Evans, The brown-coal/water system: Part 4. Shrinkage on drying, Fuel 52 (1973) 186−190.

[8] D.J. Allardice, D.G. Evans, The-brown coal/water system. Part 2. Water sorption isotherms on bed-moist Yallourn brown coal, Fuel 50 (1971) 236−253.

[9] J.I. Hayashi, K. Norinaga, N. Kudo, T. Chiba, Estimation of size and shape of pores in moist coal utilizing sorbed water as a molecular probe, Energy Fuels 15 (2001) 903-909.

[10] H.N.S. Schafer, Factors affecting the equilibrium moisture contents of low-rank coals, Fuel 51 (1972) 4–9.

[11] J. Nishino, Adsorption of water vapor and carbon dioxide at carboxylic functional groups on the surface of coal, Fuel 80 (2001) 757−764.

[12] C.F. You, H.M. Wang, K. Zhang, Moisture adsorption properties of dried lignite, Energy Fuels 27 (2013) 177−182.

[13] C.B. Man, Y.H. Liu, X. Zhu, D.F. Che, Moisture readsorption performance of air-dried and hydrothermally dewatered lignite, Energy Fuels 28 (2014) 5023−5030.

[14] Y.L. Yang, X.X. Jing, Z.Q. Li, X. Liu, Y.L. Zhang, L.P. Chang, Effect of drying conditions on moisture re-adsorption performance of dewatered lignite, Dry. Technol. 31 (2013) 1430–1437.

[15] D. Charrière, P. Behra, Water sorption on coals, J. Colloid Interf. Sci. 344 (2010) 460–467.

[16] J.L. Yu, A. Tahmasebi, Y.N. Han, F.K. Yin, X.C. Li, A review on water in low rank coals: The existence, interaction with coal structure and effects on coal utilization, Fuel Process. Technol. 106 (2013) 9–20.

[17] X.C. Liu, T. Hirajima, M. Nonaka, K. Sasaki, Investigation of the changes in hydrogen bonds during low-temperature pyrolysis of lignite by diffuse reflectance FT-IR combined with forms of

water, Ind. Eng. Chem. Res. 54 (2015) 8971–8978.

[18] D.J. Allardice, L.M. Clemow, W.R. Jackson, Determination of the acid distribution and total acidity of low-rank coals and coal-derived materials by an improved barium exchange technique, Fuel 82 (2003) 35–40.

[19] D.J. Allardice, L.M. Clemow, G. Favas, W.R. Jackson, M. Marshall, R. Sakurovs, The characterisation of different forms of water in low rank coals and some hydrothermally dried products, Fuel 82 (2003) 661–667.

[20] Y. Fei, C.F. Zhang, M. Marshall, W.R. Jackson, A.L. Chaffee, D.J. Allardice, The effect of cation content of some raw and ion-exchanged Victorian lignites on their equilibrium moisture content and surface area, Fuel 86 (2007) 2890–2897.

[21] X.C. Liu, L. Feng, X.H. Wang, Y. Zhang, H.Y. Tang, Effect of Mg^{2+} content in ion-exchanged Shengli lignite on its equilibrium adsorption water content and its mechanism, Chinese J. Chem. Eng. 23 (2015) 456–460.

[22] S.C. Deevi, E.M. Suuberg, Physical changes accompanying drying of western US lignites, Fuel 66 (1987) 454–460.

[23] M.Y. Ogaki, H. Usui, O. Okuma, The advantages of vacuum-treatment in the thermal upgrading of low-rank coals on the improvement of dewatering and devolatilization, Fuel Process. Technol. 84 (2003) 147–160.

[24] K. Norinaga, J.I. Hayashi, N. Kudo, T. Chiba, Evaluation of effect of predrying on the porous structure of water-swollen coal based on the freezing property of pore condensed water, Energy Fuels 13 (1999) 1058–1066.

CHAPTER 5

Effects of hydrothermal treatment coupled with mechanical expression on combustion performance of Loy Yang lignite

5.1 Introduction

Previous three chapters focused on effects of hydrothermal treatment (HT) and HT coupled with mechanical expression (HT–ME) on physicochemical properties. Now, lignite is primarily used for electricity generation at power stations located at or near a mine. In addition, the changes in physicochemical properties of lignite can lead to the changes in the combustion performance. Moreover, Investigation of the utilization in combustion aspect of HT and HT–ME treated samples help to evaluate upgrading effect of lignite. Therefore, changes in combustion performance are the subject of this chapter.

The combustion performance of lignite for use in industrial pulverized coal furnaces can be investigated using thermogravimetric (TG) analysis. TG analysis is an effective and simple technique [1–9]. It provides a rapid quantitative method for examining the overall combustion process and estimating the effective kinetic parameters; these are useful in engineering design and economic assessment. The ignition temperature, peak temperature (T_p), burnout temperature, and maximum combustion rate (MCR) are generally used to characterize combustion [2–11]. The activation energy (E), which is associated with the energy barrier, the pre-exponential factor (A), which is related to the vibrational frequency of the activated complex, and the dependence on the extent of conversion (α) by the reaction model [$f(\alpha)$], which is regarded as the reaction mechanism, are used to analyze the combustion kinetics [2–11]. Many studies of the combustion

performance of lignite have been performed using TG analysis. In early studies, the combustion performance of lignite alone was studied [5–8]. Recently, researchers have focused on co-combustion of lignite and other substances such as coal gangue, sewage sludge, and chemical wastewater [9–11]. The combustion performance depends greatly on a number of factors such as the operating conditions (e.g., heating rate, reaction atmosphere, sample size, and water content of the sample) and physicochemical properties [e.g., specific surface area (SSA), pore volume, and amounts of volatile matter and char]. Different operating conditions can give different combustion characteristics and kinetic parameters. However, under the same conditions, TG analysis is a valuable tool for investigating changes in the combustion characteristics and kinetic parameters, which are useful for evaluating the combustion performance [2].

In this study, instead of conventional hydrothermal treatment (HT), HT without addition of extra water was performed; this reduces the amounts of wastewater and energy consumption. Solid samples obtained using HT were also treated using ME (HT–ME) at 110 °C under atmospheric conditions. Few studies have considered how the changes in the physicochemical properties caused by HT and HT–ME influence the combustion performance. In this work, TG analysis was used to investigate changes in the combustion performances of samples treated using HT and HT–ME with changes in the physicochemical properties, namely the SSA, pore volume, and amounts of volatile matter and fixed carbon. Non-isothermal thermogravimetry was performed at four different heating rates and the Kissinger–Akahira–Sunose (KAS) isoconversional method was used to calculate the kinetic parameters.

5.2 Experimental

5.2.1 Sample

Sample is the same as **Section 2.2.1**.

5.2.2 Hydrothermal treatment

Raw lignite (about 6 g) was placed in a steel filter (ϕ = 60 μm), and three of the steel filters were fixed in the middle of the cylinder of a 0.5-L batch-type reactor equipped with an automatic temperature controller with a maximum temperature of 400 ℃ and a maximum pressure of 30 MPa (MA22, Taiatsu Techno, Japan; **Fig. 2.1**). N_2 gas was flushed through the sealed system to remove air. The reactor was then pressurized with N_2 gas to 1.5 MPa at room temperature. A series of HTs were performed at different temperatures (150, 200, and 250 ℃) for 40 min at an average heating rate of ca. 5 ℃/min. The reactor was cooled to room temperature and the solid products were collected. The samples are denoted by HT150, HT200, and HT250 for HT temperatures of 150, 200, and 250 ℃, respectively.

5.2.3 Hydrothermal treatment coupled with mechanical expression

The HT solid products and raw lignite were placed in fixed regions of filter papers to ensure that the sizes of the samples treated using ME were the same. A small pressing machine (AH-2003, ASONE, Japan; **Fig. 3.1**) was heated to a prescribed temperature (110 ℃). When the desired temperature was reached, the machine was used to apply a mechanical pressure of 6 MPa to the samples for 20 min under atmospheric conditions. The treated samples were denoted by HT150–ME, HT200–ME, and HT250–ME, and raw lignite directly treated by ME was denoted by RL–ME.

5.2.4 Calculation of kinetic parameters

The isoconversional method does not depend on prior assumptions or any particular form of the reaction model. It has been proved to be effective and is highly recommended for kinetic analysis by the International Confederation for Thermal Analysis and Calorimetry (ICTAC) Kinetics Committee [5]. The principle of the isoconversional method is that the reaction rate at a constant α is a function of temperature only. The KAS method is one of the most popular isoconversional methods for determining thermal kinetic parameters because it is computationally simple and its accuracy is adequate for most practical purposes [5,12]. The KAS equation can be obtained from the literature [12]. Briefly, the Arrhenius law is

$$\frac{\mathrm{d}\alpha}{\mathrm{d}t} = A\mathrm{e}^{\left(\frac{-E}{RT}\right)} f(\alpha), \quad (1)$$

where $\alpha = (m_0 - m_i)/(m_0 - m_\infty)$ is the extent of conversion (m_0, m_∞, and m_i are the initial, final, and instantaneous mass, respectively); t is the combustion time (s); A is the pre-exponential factor; E is the activation energy [J/(mol K)]; R is the gas constant [J/(mol K)]; and T is the temperature (K). The heating rate (°C/min) is

$$\beta = \mathrm{d}T/\mathrm{d}t. \quad (2)$$

Combining Eqs. (1) and (2) gives

$$\frac{\mathrm{d}\alpha}{f(\alpha)} = \frac{A}{\beta} \cdot \mathrm{e}^{\left(\frac{-E}{RT}\right)} \mathrm{d}T. \quad (3)$$

Integrating Eq. (3) gives

$$\int_0^\alpha \frac{\mathrm{d}\alpha}{f(\alpha)} = \frac{A}{\beta} \int_0^T \mathrm{e}^{\left(-\frac{E}{RT}\right)} \mathrm{d}T = \frac{AE}{\beta R} \int_y^\infty \frac{e^{(-y)}}{y^2}\, dy, \quad (4)$$

where

$$y = E/RT, \quad (5)$$

$$\int_y^\infty \frac{e^{(-y)}}{y^2}\,dy = \frac{e^{(-y)}}{y^2}\left(1+\frac{2!}{y}+\frac{3!}{y^2}+\frac{4!}{y^3}+\cdots\right). \quad (6)$$

Truncating the series to the first-order approximation gives

$$\int_y^\infty \frac{e^{(-y)}}{y^2}\,dy \approx \frac{e^{(-y)}}{y^2}. \quad (7)$$

The KAS equation can therefore be obtained by taking the logarithm of Eq. (4) and using Eq. (7):

$$\ln\frac{\beta}{T^2} = -\frac{E}{RT} + \ln\frac{AR}{E\int_0^\alpha d\alpha/f(\alpha)}. \quad (8)$$

The ICTAC Kinetics Committee recommends performing a series of three to five runs for calculation of reliable kinetic parameters [5]. The following form of the KAS equation is therefore frequently used:

$$\ln\frac{\beta_i}{T_{\alpha,i}^2} = \frac{E_\alpha}{RT_{\alpha,i}} + \ln\frac{AR}{E\int_0^\alpha d\alpha/f(\alpha)}, \quad (9)$$

where *i* denotes various heating rates. $T_{\alpha,i}$ is the temperature at a given α at the *i*th heating rate. The second term on the right-hand side of Eq. (9) is a constant at a given α for different heating rates, based on isoconversional methods [12]. The *E* at each given α value (E_α) is determined from the slope of a plot of $\ln(\beta_i/T_{\alpha,i}^2)$ against $1/T_{\alpha,i}$ at heating rates of 2, 4, 8, and 16 °C/min. An example is shown in **Fig. 5.1**. Note that the experimentally determined *E* is appropriate to call an "effective", "apparent", "empirical", or "global" *E* to stress that it can deviate from the intrinsic value of a specific individual step [5].

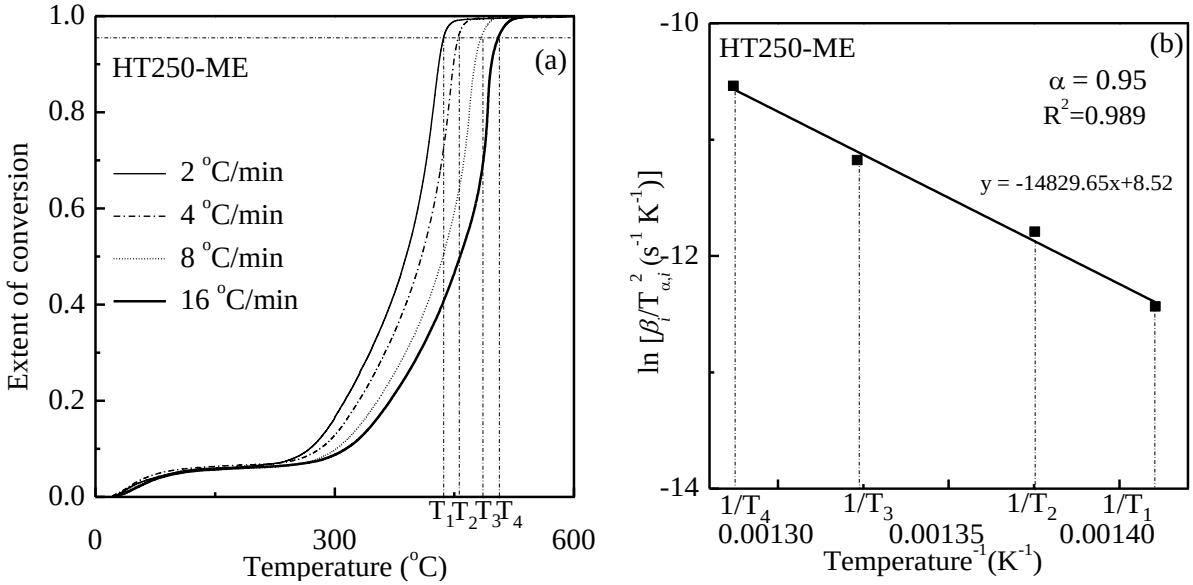

Fig. 5.1 An example of kinetics calculation by the KAS method. (a) Relationship between temperature and α of HT250–ME. (b) curve of fitting to kinetic model by the KAS method to α = 0.95 corresponding to the combustion of HT250–ME at β = 2, 4, 8, and 16 °C/min

5.2.5 Characterization

The lignite water content was measured based on the fractional mass release during heating in an oven (WFO-50, Eyela, Japan) at 105 ℃ for 6 h. The ash content was calculated as the mass of waste remaining after treatment of the lignite in a furnace (TFM-2200, Eyela, Japan) at 815 ℃ for 2.5 h. The volatile matter was calculated as the mass release observed on heating in the furnace at 900 ℃ for 7 min. The SSAs, macro- and mesopore size distributions, and micropore size distributions were calculated using the Brunauer–Emmett–Teller, Barrett–Joyner–Halenda, and Horvath–Kawazoe equations, respectively, based on the adsorption isotherms, which were measured by N_2 gas adsorption at 77 K using a high-precision SSA and pore size distribution analyzer (BEL-Max, BEL, Japan). For the N_2 gas adsorption experiments, pretreatment under vacuum at 110 °C for 15 h was preformed to remove adsorbed gases. TG tests were performed by

placing the sample (3 mg) in a platinum crucible on a thermal analyzer (2000SA, Bruker, USA). The samples were heated from room temperature to 600 °C at a series of different heating rates (2, 4, 8, and 16 °C/min) under an air flow rate of 25 mL/min. The characterizations were repeated at least twice. The morphologies of the samples before and after treatment were observed using scanning electron microscopy (SEM; VE-9800, Keyence, Japan).

5.3 Results and discussion

5.3.1 Effects of HT and HT–ME on pore size distribution

The pore structure has a significant effect on the combustion performance of lignite; the pore size distributions of all the samples are shown in **Fig. 5.2**. According to the International Union of Pure and Applied Chemistry classification, the diameter ranges of macropores, mesopores, and micropores are >50 nm, 2–50 nm, and <2 nm, respectively. The pore size range was divided into three regions, i.e., macro-, meso-, and micropore regions, to aid analysis of the pore size distribution data (**Fig. 5.2**).

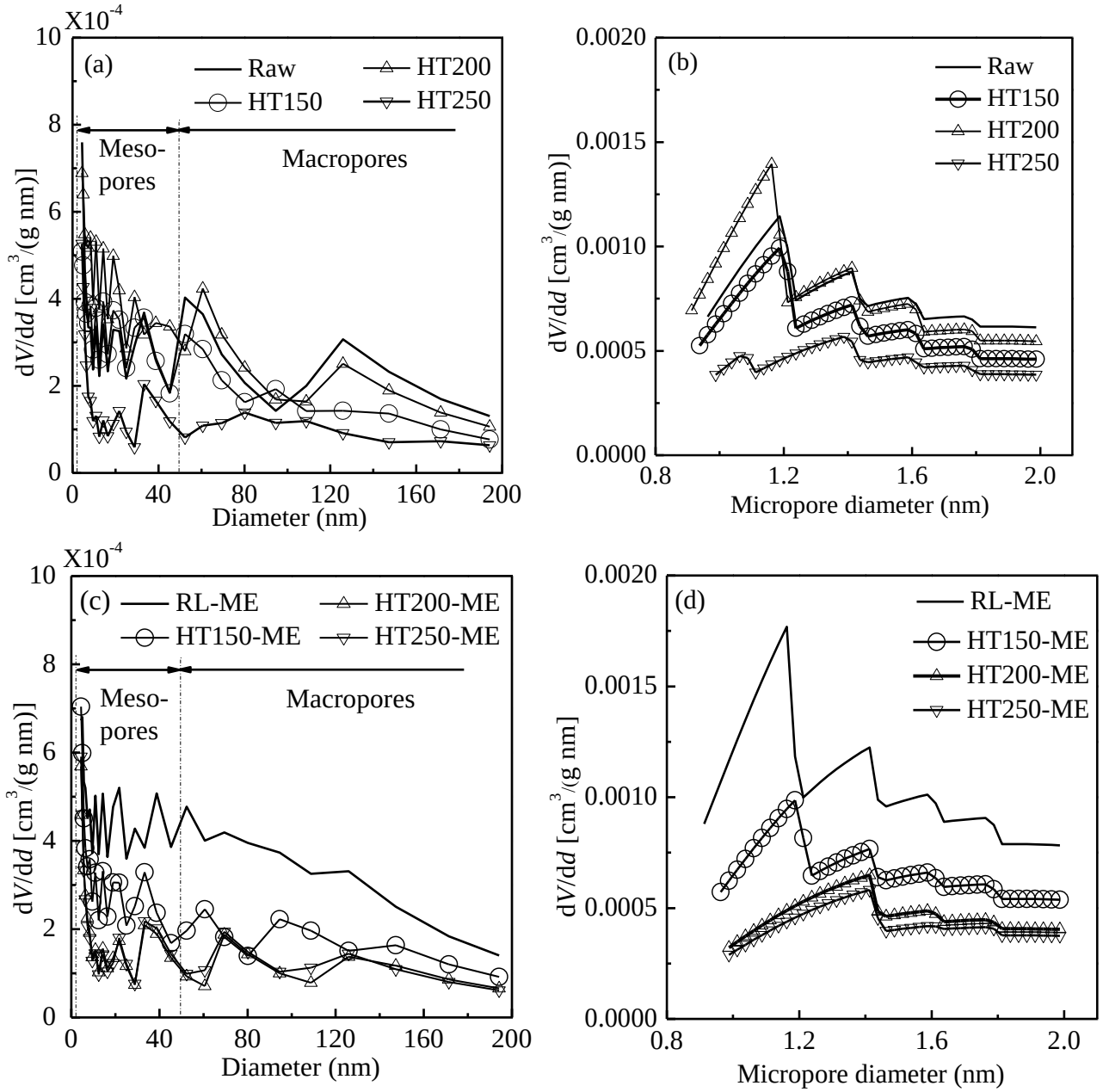

Fig.5.2 Effects of HT and HT–ME on pore size distribution

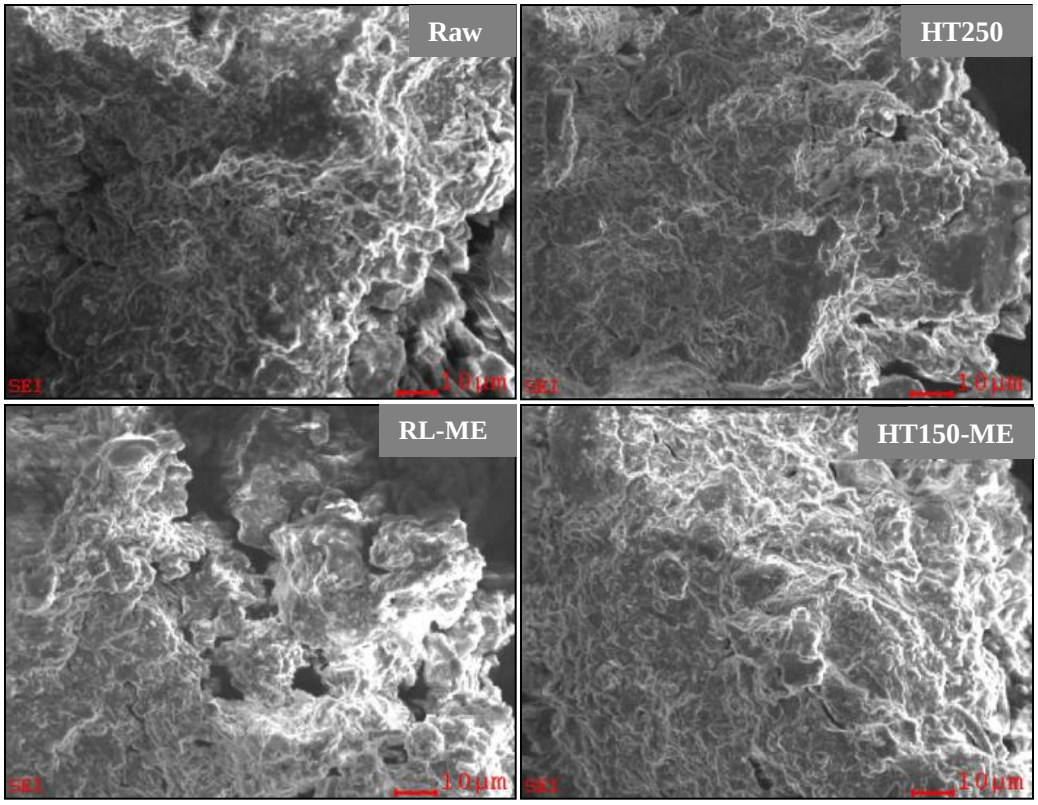

Fig.5.3 Typical samples under SEM observation

Fig. 5.2(a) and **5.2(b)** show that the porosities of the macro- and micropores of HT150 were lower than those of raw lignite, whereas the mesopore porosity was slightly higher than that of raw lignite. The porosities of the macro-, meso-, and micropores of HT200 were higher than those of HT150, which were significantly higher than those of HT250. The porosity changes at temperatures below 200 °C can be understood in terms of competition between development and collapse of pores. Pores develop because of opening and cross-linking of closed pores, as well as removal of organic matter during dewatering. The collapse of pores is caused by increases in the diameters of old pores and shrinkage forces caused by drying. Above 200 °C, not only pore collapse but also disintegration of the macromolecular structure as a result of significant thermal

decomposition occurs [1]. As a result of these two factors, the porosity of HT250 was markedly lower than that of HT200.

Table 5.1 Effects of HT and HT–ME on combustion characteristic parameters and some physicochemical properties of all of the samples

Sample	T_c (°C)	TP_2 (°C)	MCR (%/s)	SSA (m^2/g)	Total volume of macro- and mesopore (cm^3/g)	M / [(g/g) 100%][a]	A/[(g/g) 100%][a]	V/[(g/g) 100%][a]	FC/[(g/g) 100%][a]
Raw	381	449	0.09	3.6±0.2	0.023±0.001	57.47±0.14	0.31±0.02	21.67±0.09	20.54±0.03
HT150	405	460	0.15	3.0±0.5	0.018±0.001	15.85±4.11	0.60±0.01	42.99±0.03	40.57±0.02
HT200	409	463	0.15	3.7±0.3	0.024±0.001	7.60±0.84	0.40±0.05	45.75±0.56	46.24±0.56
HT250	415	463	0.17	2.2±0.3	0.010±0.004	5.87±0.71	0.68±0.02	45.85±0.62	47.61±0.59
RL–ME	404	459	0.19	4.9±0.1	0.032±0.002	4.25±0.16	0.80±0.01	47.97±0.09	46.98±0.09
HT150–ME	406	456	0.18	3.2±0.1	0.018±0.000	3.38±0.18	0.68±0.01	48.57±0.16	47.37±0.15
HT200–ME	410	463	0.17	2.3±0.2	0.012±0.001	1.67±0.39	0.60±0.02	48.13±0.38	49.59±0.39
HT250–ME	419	463	0.18	2.2±0.2	0.012±0.000	0.92±0.12	0.74±0.02	48.46±0.11	49.87±0.08

[a] on the basis of the total mass of sample

The porosities of the macro-, meso-, and micropores of the treated samples [(**Fig. 5.2(c)** and **5.2(d**)) continuously decreased from RL–ME to HT250–ME. This is the result of the effects of compression during ME treatment and pore collapse. Note that the porosities of the macro-, meso-, and micropores of RL–ME were higher than those of raw lignite. The water content of RL–ME was low (**Table 5.1**). The release of water from closed and blind pores of RL–ME led to opening and linking of these pores [13]. As a result, the pore volume increased. Furthermore, the colloidal properties of raw lignite cannot be destroyed without HT. The effect of compression during ME treatment on the porosity, which can decrease the pore volume, was therefore negligible without HT. The

differences among the surface morphologies were examined using SEM; images of some representative samples are shown in **Fig. 5.3**. **Figs. 5.2** and **5.3** show that the number of pore networks in RL–ME was higher than that in raw lignite because of pore development, whereas the numbers of pore networks in HT250 and HT150–ME were lower as a result of collapse, disintegration, and compression of pores.

5.3.2 Effects of HT and HT–ME on lignite combustion characteristics

A large sample mass causes heat accumulation in the sample, therefore a small amount of sample is better for TG experiments. To obtain high-quality experimental data, a series of experiments using 2, 3, and 5 mg of lignite were performed to determine the most suitable sample mass; the results are shown in **Fig. 5.4**. The derivative TG (DTG) curve for 2 mg of sample contained too much noise. The 3 mg sample gave the best result. Therefore, this amount was used for subsequent experiments.

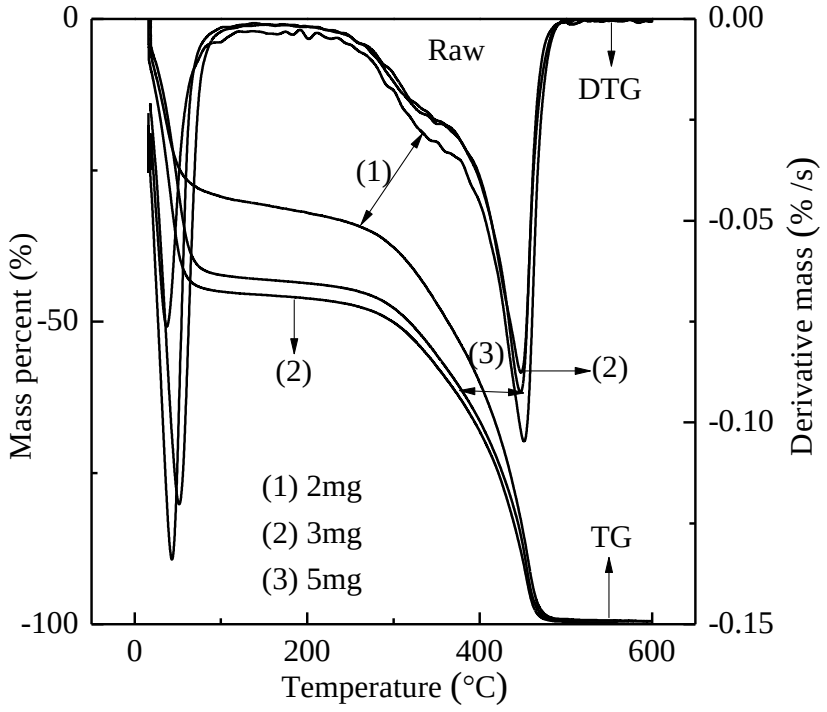

Fig.5.4 Effects of sample mass on TG and DTG curves

The combustion characteristics of lignite are usually investigated by TG analysis. The plot of mass against temperature (TG curve) clearly shows a gradual process of mass loss. The mass loss against temperature (DTG curve) plot provides the combustion rate. In the heat released against temperature plot [differential thermal analysis (DTA) curve], either exothermic or endothermic processes can be observed [14–17]. As mentioned in the Introduction, TG analysis under the same conditions is a valuable tool for comparing combustion characteristics. In this study, a heating rate of 8 °C/min was used to investigate changes in the combustion characteristics. Combustion process was divided into three regions, based on the approximate start and end points of the DTA curves. An example of this method is shown in **Fig. 5.5**. The first region ($T \leq 150$ °C) mainly represents removal of water, and the second region ($150 < T \leq 370$ °C) represents devolatilization and combustion of volatile matter. In the third region ($370 < T \leq 490$ °C), burning of solid char formed by decomposition, polycondensation, solidification, and shrinkage of fixed carbon occurs, and continues until the ash level is reached. The higher the fixed carbon content, the higher the obtained char content will be. In this study, attention was primarily focused on regions 2 and 3.

The combustibility of coal can be expressed in terms of T_c, T_p, and the MCR [2–11]. The definition of T_c in this study is taken from the literature [15]. In brief, as shown in **Fig. 5.5**, a vertical line is first made through the DTG peak point A, to meet the TG curve at point B. The tangent to the TG curve through point B and the initial baseline of the TG curve meet at point C. T_c is the corresponding temperature at point C. In the present work, T_c was in region 3, which corresponded to the initial temperature of rapid-weight-loss of char. The temperature of peak 2 (TP_2) is defined as the point at which the rate of mass

loss is maximum (DTG curve), mainly because of char combustion. The rate of maximum mass loss at TP_2 is called the MCR (**Fig. 5.5**). These combustion parameters and some physicochemical properties of all the samples are listed in **Table 5.1**. It should be noted that the pore structure of lignite consisted mainly of macro- and mesopores [18]. The total volume of macro- and mesopores (TV) without the micropore volume is given in **Table 5.1**.

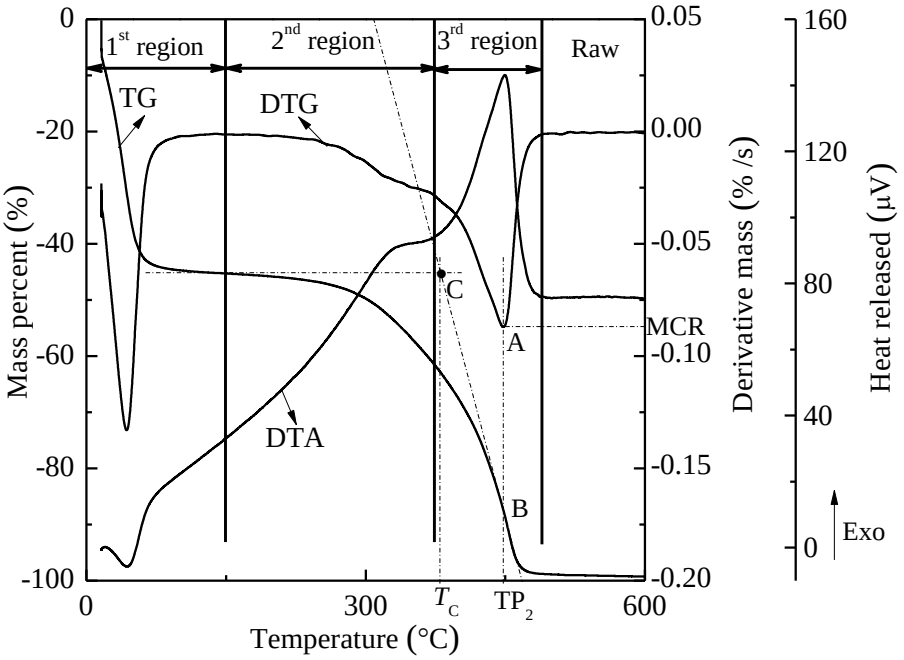

Fig. 5.5 TG, DTG, and DTA curves of raw lignite at β = 8 °C/min. T_c as the initial temperature of rapid-weight-loss of char, TP_2 as the peak temperature of the 3rd region, MCR as the maximum combustion rate

T_c depends on the amount and boiling point of volatile matter, the char content, and the speed of heat released by volatile matter and char combustion. The combustion of volatile matter plays a preheating role in char combustion. Char acts as a diffusion barrier for combustible components (e.g., oxygen and char) and a thermal insulation barrier [3]. The MCR is mainly determined by the char content, the accessibility of an oxidizer to the

active sites in the sample, and the SSA for oxidation [19]. These factors, which control T_c and the MCR, influence TP_2.

Table 5.1 shows that the T_c, TP_2, and MCR values of raw lignite and the samples treated using HT and HT–ME varied greatly, suggesting that HT and HT–ME affected the combustion characteristics of lignite. T_c and TP_2 are related to ignition property and are inversely proportional to the reactivity of lignite, i.e., the lower T_c (or TP_2), the more reactive the coal is [20]. The T_c and TP_2 values for the samples treated using HT and HT–ME were significantly higher than those for raw lignite, and they increased with increasing processing temperature. This is because the raw lignite contains a relatively high amount of low-boiling-point volatile matter, which is released from the lignite at relative low temperatures, and a small amount of char (**Table 5.1**). After HT, the content of high-boiling-point volatile matter, which is removed at relative high temperatures, increased and the char in the treated samples led to increases in the T_c and TP_2 values. For the samples treated using HT–ME, although the changes in their volatile matter contents were negligible, the char content increased slightly, i.e., the same phenomenon were observed as for the samples treated using HT and HT–ME. For the samples treated using HT and HT–ME, the amounts of high-boiling-point volatile matter and char increased slightly with increasing processing temperature; this is the reason for the slight increases in the T_c and TP_2 values. In summary, the changes in T_c and TP_2 indicate that HT and HT–ME can significantly decrease the reactivity of raw lignite and the reactivities of the treated samples gradually decrease as a result of these two processes.

A comparison of the MCRs shows that the values for the samples treated using HT and HT–ME were higher than those for raw lignite, and the changes in the MCRs of the

treated samples with increasing temperature were negligible. A higher char content and larger SSA can provide more active sites, and increasing the TV can improve accessibility for the oxidizer. For RL–ME and HT200, the synergistic effect of the increases in char content, SSA, and TV relative to those of raw lignite resulted in higher MCRs compared with that of raw lignite. For the other samples, the increases in the MCRs can be attributed to competition between the increases in char contents and the decreases in the SSAs and TVs. In addition, the increased MCRs show that the combustion intensities of the samples treated using HT and HT–ME can be improved.

The T_c and MCR values of the samples treated using HT–ME were slightly higher than those of the corresponding samples treated using HT. The TP_2 values of the samples treated using HT–ME were similar to those of the corresponding samples treated using HT. These results suggest that HT–ME slightly changed the reactivity and combustion intensity of LY lignite compared with those obtained using HT.

5.3.3 Effects of HT and HT–ME on lignite combustion kinetics

Lignite combustion is a complicated process that generally involves removal of water, release and combustion of volatile matter, and char burning. The total mass loss in TG experiments is therefore the result of the combined changes in the amounts of water, volatile matter, and char. The ICTAC Kinetics Committee recommends that an α interval not greater than 0.05 should be used in the determination of E_α. An α interval of 0.05 was chosen in this work. E_α was calculated for α values of 0.20–0.95 because most solid-state reactions are not stable in the initial and final periods [12]. The E_α values calculated from plot slopes using the KAS method had high correlation coefficients (R^2), as shown in

Tables 5.2 and 5.3. For raw lignite, the initial α value was 0.6 because at $\alpha < 0.6$ removal of water occurs, which was not considered in this study.

The changes in E_α with α, determined using an isoconversional method, show whether the sample combustion obeys multistep kinetics or single rate-limiting step kinetics, in which the mechanism involves several steps but one of them dominates the overall kinetics [5]. For raw lignite, the E_α value varied significantly with changes in α and the difference between the maximum and minimum values was 70.5 kJ/mol, which was more than 20–30% of the average activation energy (E_a). This suggests that the raw lignite combustion kinetics was multistep [5]. However, for the other samples, the E_α values did not vary significantly with α, indicating that these processes can be described by single rate-limiting step kinetics.

Table 5.2 Combustion kinetic parameters of samples treated by HT calculated by KAS method

	Raw		HT150		HT200		HT250	
α	E(kJ/mol)	R^2	E(kJ/mol)	R^2	E(kJ/mol)	R^2	E(kJ/mol)	R^2
0.20			94.4±3.5	0.967	101.2±4.0	0.993	96.7±9.3	0.985
0.25			97.4±4.2	0.985	101.7±1.3	0.990	97.9±8.7	0.988
0.30			98.3±3.7	0.993	102.4±1.1	0.987	100.6±8.3	0.988
0.35			100.8±3.1	0.995	104.6±0.5	0.986	103.6±7.6	0.989
0.40			104.2±2.9	0.996	107.9±0.1	0.986	106.2±6.6	0.989
0.45			107.5±2.9	0.997	111.0±0.6	0.988	108.3±6.1	0.991
0.50			110.8±3.1	0.997	112.9±1.2	0.990	110.1±5.3	0.991
0.55			112.4±3.4	0.996	114.7±1.5	0.992	111.2±4.8	0.992
0.60	63.8±1.3	0.973	113.2±3.4	0.994	115.2±2.1	0.994	111.2±4.2	0.992
0.65	75.2±1.1	0.977	113.7±3.1	0.995	115.7±2.0	0.995	111.9±3.9	0.993
0.70	87.5±3.2	0.980	114.7±2.2	0.995	117.2±2.0	0.996	113.0±3.9	0.994
0.75	102.5±6.0	0.984	116.8±1.7	0.996	118.9±2.2	0.996	114.7±3.7	0.994
0.80	116.7±8.7	0.988	119.3±2.2	0.996	121.7±2.6	0.996	115.6±4.3	0.993
0.85	125.5±10.6	0.990	120.3±3.1	0.995	123.5±3.9	0.995	114.6±5.1	0.990
0.90	130.5±10.8	0.991	119.0±4.1	0.991	123.7±5.8	0.994	112.3±5.1	0.988
0.95	134.3±12.1	0.991	116.1±3.9	0.985	121.3±5.4	0.995	110.0±4.6	0.990
(E_a)[a]	104.5±6.1		109.9±3.1		113.3±1.4		108.6±5.7	

[a] as average activation energy

Table 5.3 Combustion kinetic parameters of samples treated by HT–ME calculated by KAS method

	RL–ME		HT150–ME		HT200–ME		HT250–ME	
α	E(kJ/mol)	R^2	E(kJ/mol)	R^2	E(kJ/mol)	R^2	E(kJ/mol)	R^2
0.20	114.4±13.3	0.957	98.8±4.9	0.972	121.5±4.0	0.999	103.2±2.7	0.987
0.25	91.1±24.2	0.941	99.8±2.4	0.976	117.5±5.6	0.999	102.2±1.0	0.988
0.30	105.7±2.4	0.991	100.9±0.7	0.977	117.0±6.4	0.999	102.3±0.2	0.989
0.35	104.6±1.2	0.993	103.7±1.0	0.979	118.3±6.6	0.999	103.9±0.1	0.990
0.40	105.5±0.0	0.994	107.3±2.0	0.981	119.7±7.1	0.999	105.1±0.6	0.992
0.45	107.3±1.0	0.996	110.5±3.0	0.983	121.2±7.6	0.999	106.7±1.4	0.994
0.50	109.1±1.8	0.997	113.0±3.9	0.984	121.8±7.7	0.999	107.4±1.4	0.995
0.55	110.3±2.0	0.997	115.0±4.3	0.985	120.9±6.7	0.999	107.4±1.6	0.996
0.60	110.4±2.5	0.997	115.4±4.6	0.985	119.4±5.9	0.998	107.2±1.7	0.996
0.65	109.5±2.7	0.996	115.8±4.5	0.986	119.1±5.3	0.998	108.0±1.7	0.996
0.70	108.0±0.8	0.994	116.2±4.3	0.986	120.5±4.5	0.998	109.9±2.3	0.996
0.75	108.8±0.9	0.996	118.5±5.0	0.988	119.7±8.4	0.995	112.1±3.0	0.996
0.80	111.3±2.0	0.997	122.6±5.6	0.989	124.4±7.6	0.998	114.2±5.3	0.996
0.85	116.7±1.8	0.998	127.0±6.6	0.990	125.6±9.1	0.998	115.5±8.4	0.994
0.90	123.7±1.8	0.998	129.8±8.0	0.989	124.8±10.6	0.998	115.7±10.2	0.992
0.95	128.4±7.6	0.998	128.3±9.7	0.984	123.4±10.3	0.998	114.4±8.9	0.991
E_a	110.3±1.6		113.9±3.4		120.9±7.1		108.4±2.7	

Changes in E_α with α reflect general trends in the combustion process. The E_α values generally increased with increasing α. This is because combustion of low-boiling-point volatile matter changes to combustion of high-boiling-point volatile matter, where E_α gradually increases, and then changes to char burning with increasing α. The E of volatile matter combustion is lower than that of char [21,22]**.** This is consistent with the findings of Vyazovkin et al. [5], who reported that the E_α of fossil fuels increases with increasing α because the residual material becomes increasingly refractory. Furthermore, the change trends in the E_α values with α for HT200–ME and HT250–ME were smaller than those for the other samples. The changes in E_α with α reflect a change from combustion of volatile matter to char combustion. More low-boiling-point volatile matter is released from HT200–ME and HT250–ME, leading to an increase in E at low α values. Therefore, the differences between the E_α values of the volatile matter remaining in the samples and char decreased. As a result, the smaller change trends were found. The E_α of HT200–ME

was higher than that of HT250−ME; this can be explained by the effects of increased diffusion and formation of new lower-*E* char. A more detailed analysis of this point is provided later.

The E_a values for the samples treated using HT and HT−ME (108.6–113.3 and 108.4–120.9 kJ/mol, respectively) were higher than that for raw lignite (104.5 kJ/mol), indicating that HT and HT−ME can lower the overall reactivity in LY lignite combustion. For the samples treated using HT and those treated using HT−ME, the E_a values increased slightly and reached the maximum values for HT200 and HT200−ME. This can be attributed to increases in the amounts of char carbon and high-boiling-point volatile matter (**Table 5.1**), leading to increased E_a values. The E_a values decreased for HT250 and HT250−ME. As we previously reported [23], the carboxyl group contents of HT200, HT250, HT200−ME, and HT250−ME were 1.45, 0.78, 1.40, and 0.88 (mmol/g, d), respectively. The char contents of HT250 and HT250−ME, respectively, were higher than those of HT200 and HT200−ME, respectively (**Table 5.1**). This suggest that more oxidizer from the external environment was required for HT250 and HT250−ME than for HT200 and HT200−ME. Furthermore, the TV of HT250 decreased significantly relative to that of HT200 and the TVs of HT250 and HT250−ME changed slightly (**Table 5.1**). These factors increased the effect of diffusion on E_a. The *E* value for chemical control, i.e., control by a chemical reaction, is higher than that for diffusion, which involves physical control. This perhaps is one reason for the phenomenon. On the other hand, as shown in our previous study [23], glucose and xylose were found in a liquid product obtained using HT because lignite is low-rank coal and contains plant materials. Iryani [24] found that in HT above 200 °C, 5-hydroxymethylfurfural (5-HMF) and furfural are

generated from the decomposition of glucose and xylose, respectively. Further conversions of 5-HMF and furfural above 240 °C, e.g., 5-HMF polymerization, increase the amount of char [24]. Similarly, it is possible that some new lower-*E* char was formed for HT250 and HT250–ME, which may be another reason for the decrease in E_a. In summary, HT can decrease the reactivity of LY lignite and ME can further slightly decrease the reactivity.

5.4 Conclusions

The T_c and TP_2 values for samples treated using HT and HT–ME were significantly higher than the corresponding values for raw lignite, and they increased with increasing treatment temperature. This is because the amounts of high-boiling-point volatile matter and char in the treated samples are higher than those in raw lignite, leading to increases in the T_c and TP_2 values. The changes with increasing temperature in the amount and boiling point of volatile matter and the char content are small, resulting in only a slight increase in their T_c and TP_2 values. The MCRs of the treated samples were slightly higher than that of raw lignite, and the MCRs did not change significantly with increasing temperature. This may arise from the overall effects of differences among the char contents, SSAs, and TVs.

The combustion of raw lignite follows multistep kinetics, whereas the other samples follow single rate-limiting step kinetics. The E_a values of the treated samples were higher than that of raw lignite.

The T_c, MCR, and E_a values of the samples treated using HT–ME were slightly higher than those of the corresponding samples treated using HT. In summary, HT and HT–ME

both decrease the reactivity and increase the combustion intensity of LY lignite, and the changes are slightly higher for HT–ME than for HT.

References

[1] C.Z. Li, Advances in the science of Victorian brown coal, Elsevier, Amsterdam, 2004.

[2] X.C. Liu, L. Feng, L.L. Song, X.H. Wang, Y. Zhang, Effect of NaOH treatment on combustion performance of Xilinhaote lignite, Int. J. Min. Sci. Technol. 24 (2014) 51–55.

[3] S.Y. Yorulmaz, A.T. Atimtay, Investigation of combustion kinetics of treated and untreated waste wood samples with thermogravimetric analysis, Fuel Process. Technol. 90 (2009) 939–946.

[4] A.P. Schniewind, Concise Encyclopedia of Wood and Wood Based Materials, 1st ed, Pergamon Press, Elmsford, 1989.

[5] S. Vyazovkin, A.K. Burnham, J.M. Criado, L.A. Pérez-Maqueda, C. Popescu, N. Sbirrazzuoli, ICTAC Kinetics Committee recommendations for performing kinetic computations on thermal analysis data, Thermochim. Acta, 520 (2011) 1–19.

[6] S. Ma, J.O. Hill, S. Heng, A thermal analysis study of the combustion characteristics of Victorian brown coals, J. Therm. Anal. 35 (1989) 1985–1996.

[7] M.L. Contreras, F.J. Garcí a-Frutos, A. Bahillo, Study of the thermal behaviour of coal/biomass blends during oxy-fuel combustion by thermogravimetric analysis, J. Therm. Anal. 123 (2016) 1643–1655.

[8] H.P. Tseng, T.F. Edgar, Identification of the combustion behaviour of lignite char between 350 and 900 ℃, Fuel 63 (1984) 385–393.

[9] Y.Y. Zhang, J. Nakano, L.L. Liu, X.D. Wang, Z.T. Zhang, Co-combustion and emission characteristics of coal gangue and low-quality coal, J. Therm. Anal. 120 (2015) 1883–1892.

[10] D. Vamvuka, S. Sfakiotakis, S. Saxioni, Evaluation of urban wastes as promising co-fuels for energy production–A TG/MS study, Fuel 147 (2015) 170–183.

[11] J.B. Chen, L. Mu, J.C. Cai, H.C. Yin, X.G. Song, A.M. Li, Thermal characteristics and kinetics of refining and chemicals wastewater, lignite and their blends during combustion, Energ.

Convers. Manage. 100 (2015) 201–211.

[12] C.A. Wang, Y.B. Du, D.F. Che, Reactivities of coals and synthetic model coal under oxy-fuel conditions, Thermochim. Acta. 553 (2013) 8–15.

[13] J.Z. Liu, J.F. Zhu, J. Cheng, J.H. Zhou, K.F. Cen, Pore structure and fractal analysis of Ximeng lignite under microwave irradiation, Fuel 146 (2015) 41–50.

[14] F.M. Ren, F. Yue, M. Gao, M. Yu, Combustion characteristics of coal and refuse from passenger trains, Waste Manage. 30 (2010) 1196–1205.

[15] X.G. Li, B.G. Ma, X. Liu, Z.W. Hu, X.G. Wang, Thermogravimetric analysis of the cocombustion of the blends with high ash coal and waste tyres, Thermochim. Acta. 441 (2006) 79–83.

[16] P. Pranda, K. Prandová, V. Hlavacek, Combustion of fly-ash carbon Part I. TG/DTA study of ignition temperature, Fuel Process. Technol. 61 (1999) 211–221.

[17] X.G. Liu, B.Q. Li, K. Miura, Analysis of pyrolysis and gasification reactions of hydrothermally and supercritically upgraded low-rank coal by using a new distributed activation energy model, Fuel Process. Technol. 69 (2001) 1–12.

[18] Mahidin, Y. Ogaki, H. Usui, O. Okuma, The advantages of vacuum-treatment in the thermal upgrading of low-rank coals on the improvement of dewatering and devolatilization, Fuel Process. Technol. 84 (2003) 147–60.

[19] M.A. Serageldin, W. Hai, A thermogravimetric study of coal decomposition under ignition conditions. Thermochim. Acta, 171 (1990) 193–206.

[20] J.W. Cumming, Reactivity assessment of coals via a weighted mean activation energy, Fuel 63 (1984) 1436–1440.

[21] Z. Liu, W.H. Li, Y.S. Zhang, J.W. Wang, W. Orndorff, W.P. Pan, Influence of biomass on coal combustion based on thermogravimetry and Fourier transform infrared spectroscopy, J. Therm. Anal. 122 (2015) 1289–1298.

[22] G. Hakvoot, J.C. Schouten, P.J.M. Valkenburg, The determination of coal combustion kinetics with thermogravimetry, J. Therm. Anal. 35 (1989) 335–346.

[23] X.C. Liu, T. Hirajima, M. Nonaka, K. Sasaki, Hydrothermal treatment coupled with mechanical expression for Loy Yang lignite dewatering and the microscopic description of the process, Dry. Technol. 34 (2016) 1471–1483.

[24] D.A. Iryani, S. Kumagai, M. Nonaka, Y. Nagashima, K. Sasaki, T. Hirajima, The hot compressed water treatment of solid waste material from the sugar industry for valuable chemical production, Int. J. Green Energy 11 (2014) 577–588.

CHAPTER 6

Experimental study on freeze drying of Loy Yang lignite and inhibiting water holding capacity of dried lignite

6.1 Introduction

Previous four chapters are fundamental and utilization investigations of hydrothermal treatment coupled with mechanical expression (HT–ME). In this chapter, freeze drying (FD) was used to examine non-interfacial and interfacial water contents determined by HT. Moreover, for HT and HT–ME, pores, residual water content, and oxygen-containing functional groups change simultaneously. As to FD, it affects oxygen-containing functional groups slightly and effects of pore volumes of the FD treated samples on water re-adsorption are not clear. Effects of FD on water re-adsorption was also investigated. Kerosene covering oxygen-containing functional groups by means of coating with different amounts of kerosene either by direct mixing or desiccator adsorption methods was used to study effects of oxygen-containing functional groups on water re-adsorption.

The requirement, distribution, and characteristics of lignite and why lignite needs to be dewatered have been detailedly presented in **Sections 1.1 and 1.2,** respectively. Various drying and upgrading technologies have been developed to dry lignite. These can be grouped into two categories: evaporative and non-evaporative drying [1–7]. Detailed information is shown in **Section 1.4**. FD is another alternative dehydration technique, which is widespread and plays an indispensable role among various drying techniques [8–13]. Its general operation process, advantage, and disadvantage have been given in **Section 1.4.1**.

A study of drying kinetics has significantly academic and practical meanings for the design of a lignite drying system. Thin-layer empirical equations are widely employed to investigate the drying process mainly because these empirical models do not need assumptions in mass diffusivity, geometry, and conductivity aspects [14–17]. Zhao et al. [15] investigated the effects of mineral matter on the drying kinetics of lignite using thin-layer models and argued that high-ash lignite reveals more promising drying kinetics with lower activation energy than does low-ash lignite. Pickles et al. [16] and Tahmasebi et al. [17] obtained the drying kinetics of low-rank coal in the microwave and using a superheated steam fluidized-bed.

Another problem related to water in lignite is that dewatered lignite easily re-adsorbs water, which has a negative effect on its storage and causes a loss of the drying effects. There are many factors that influence the water re-adsorption capacity of dried lignite, such as oxygen-containing functional groups, pore structure, the diffusion force between the internal water content in the sample and the water vapor in the external environment, and the storage environment. Shigehisa et al. [18] and Choi et al. [19] reported that the water re-adsorption content of dried lignite is reduced markedly by coating with asphalt. The asphalt was coated during coal-oil slurry dewatering, which mixed kerosene containing a small amount of asphalt with the raw lignite to produce the slurry. Although the kerosene was recovered by heating, there was still a certain amount of kerosene that remained in the pores and on the surface of lignite and the authors did not focus on this. Coating with different amounts of kerosene to prevent water re-adsorption is discussed in this study.

6.2 Experimental

6.2.1 Sample

Sample is the same as **Section 2.2.1**.

6.2.2 Freeze drying treatment

Raw lignite (6 g) was placed in a FD flask (diameter of 7 cm and height of 7 cm). Then, the FD flask was connected with a laboratory freeze-dryer (FDU–1200, EYELA, Japan). Its temperature and pressure had already been reduced to ca. −45 °C and 10 Pa, respectively. A series of FD treatments were performed at a temperature of about −45 °C and a pressure of approximately 10 Pa with different times (1, 2, 3, 4, and 6 h). Samples were labeled as FD1, FD2, FD3, FD4, and FD6, respectively.

6.2.3 Coating with kerosene by direct mixing

A 1 g sample of FD4 was directly mixed with kerosene in a beaker. A series of mixing experiments were performed at different mass ratios of kerosene to FD4 (2.5, 5, and 10%). The samples are called FD4KM2.5, FD4KM5, and FD4KM10, respectively.

6.2.4 Coating with kerosene by adsorption

Sample FD4 (1 g) was placed into a Petri dish (diameter of 8.3 cm) and finely separated. The Petri dish was put in the upper part of a desiccator, the bottom of which contained kerosene. After a given time (1 min, 1 h, and 12 h), the Petri dish was taken out and measured. The mass ratios of kerosene to lignite were 0.7, 2.0, and 4.0% for the adsorption times of 1 min, 1 h, and 12 h, respectively, which were referred to as FD4KA0.7, FD4KA2.0, and FD4KA4.0, respectively. Blank experiments were also performed and it was found that kerosene did not adsorb on the surface of Petri dish. The

blank experiments consisted of the Petri dish without a sample, but placed into the desiccator for the same period of time.

6.2.5 Residual water content and moisture holding capacity determination

Details of the measurement of the residual water content have been specified previously [4]. In brief, samples were separately placed in weighing bottles (m_i, mass of the weighing bottle, lid, and initial treated sample). Then, the open weighing bottles were placed in an oven (WFO-50, Eyela, Japan) at 105 °C. After 6 h, the weighing bottles were taken out, closed with their respective lids, cooled, and weighed (m_f). The residual water content was calculated on a dry (d) basis using

$$\text{Residual water content (g/g-lignite, d)} = [(m_i - m_f)/(m_f - m_b)], \quad (1)$$

where m_b is the mass of weighing bottle and lid. The experiments were repeated three times.

The moisture ratio was calculated using

$$\text{Moisture ratio} = [(M_t - M_e)/(M_0 - M_e)], \quad (2)$$

where M_t and M_e are the residual water contents at time t and at the end of FD, respectively. M_0 is the initial water content. Because M_e was assumed to be zero, Eq. (2) was used in the following form [17]:

$$\text{Moisture ratio} = M_t/M_0. \quad (3)$$

Moisture holding capacity (MHC), that is, the equilibrium water content at relative humidity of 97%, was measured by a desiccator method. Samples (1.00 g) were separately placed in weighing bottles. Then, the open weighing bottles were positioned in a desiccator containing saturated K_2SO_4 salt solution, which was placed in a 25 °C room. The relative humidity in the desiccator was measured by a hygrometer and its value was

97%. The weighing bottles were taken out, closed with their respective lids, and weighed (m_1) after several hours. These experiments were repeated until equilibrium was reached and the water content is called MHC at that point. After reaching equilibrium, weighing bottles without lids were heating in the oven at 105 °C for 6 h and then were cooled in a desiccator and weighed with lids (m_2). The water content was calculated using

$$\text{Water content (g/g-lignite, d)} = [(m_1 - m_2)/(m_2 - m_b)] \times 100\%. \quad (4)$$

The experiments were repeated at least two times.

6.2.6 Pore size distribution determination

The macro- and mesopore size distributions were calculated based on adsorption isotherms, which were measured by N_2 gas adsorption at 77 K using a high-precision special surface area and pore size distribution analyzer (BEL-Max, BEL, Japan), and calculated using the Barrett–Joyner–Halenda (BJH) equation. For this experiment, adsorbed gases were removed by pre-treatment under vacuum at 110 °C for 15 h.

6.2.7 Mathematical thin-layer drying models

The best drying model among different thin-layer models given by various authors (**Table 6.1** [20–27]) was selected by curve-fitting analysis using a non-linear regression (least-squares method) and multiple regression analysis. The correlation coefficient (R^2) is one of the primary criteria for determining the best-fitting drying mode. Furthermore, the *F-value*, the residual sum of square (*RSS*), and the reduced chi-square (χ^2) were also employed to evaluate the goodness of fit of the models. In summary, a higher quality of fit was associated with higher values of R^2 and *F-value* and lower values of RSS and χ^2 [17,28].

Table 6.1 Mathematical thin-layer drying models proposed by various authors

No.	Model	Expression	No.	Model	Experssion
1	Lewis	$MR = \exp(-kt)$[20]	6	Modified Page	$MR = \exp[-(kt)^n]$ [25]
2	Henderson and Pabis	$MR = a\exp(-kt)$ [21]	7	Simplified Fick diffusion	$MR = a\exp[-c(t/L^2)]$ [25]
3	Logarithmic	$MR = a\exp(-kt) + c$[22]	8	Midilli–Kucuk	$MR = a\exp(-kt^n) + bt$ [26]
4	Diffusion approach	$MR = a\exp(-kt) + (1-a)\exp(-kbt)$ [23]	9	Wang and Singh	$MR = 1 + at + bt^2$ [27]
5	Two-term	$MR = a\exp(-k_1t) + b\exp(-k_2t)$ [24]			

6.3 Results and discussion

6.3.1 Forms of water in lignite

Fig. 6.1 shows the effects of FD time on the residual water content. It can be seen that the residual water content almost linearly decreased with increasing time in the range of 0–2 h, suggesting that a single type of water was removed in this range. We refer to this type of water as non-interfacial water. Above 2 h, the slope decreases with increasing time, indicating that another type of water was removed and it was more difficult to be removed than the non-interfacial water, which was named as interfacial water. To quantitatively determine the non-interfacial and interfacial water contents, the two slopes in the time ranges of 0~2 h and 3~6 h were extended (dashed lines in **Fig. 6.1**). They meet at point A (**Fig. 6.1**), which is the border between non-interfacial and interfacial water. From point A, the amounts of non-interfacial and interfacial water were 1.258 and 0.093 (g/g-lignite, d), respectively (**Table 6.2**). **Table 6.2** also shows non-interfacial and interfacial water contents, 1.255 and 0.096 (g/g-lignite, d), respectively, determined by HT, which coincides quite well with FD result. This confirms the reliability of the measurements of non-interfacial and interfacial water contents determined by these two

methods.

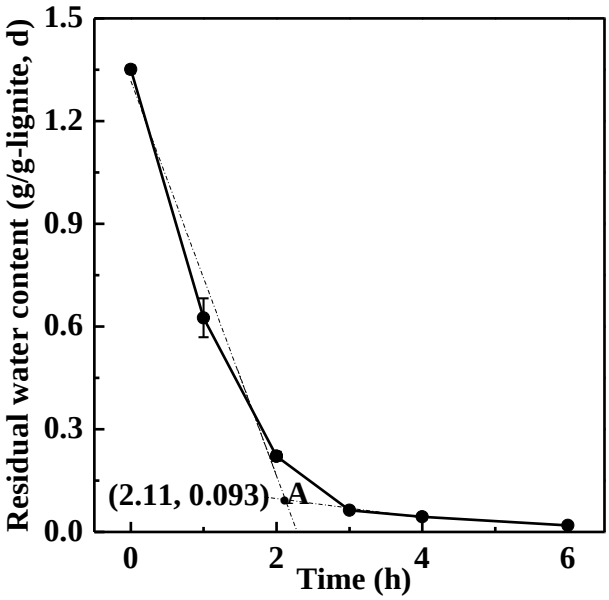

Table 6.2 Non-interfacial and interfacial water contents (g/g-lignite, d) determined by HT and FD

Method	Non-interfacial water	Interfacial water
HT	1.255	0.096
FD	1.258	0.093

Fig. 6.1 Effects of FD time on residual water content

Furthermore, the changes in the slopes of the drying curve of time against residual water content show that there were three drying stages: the fast dewatering region (~2 h) which is controlled by non-interfacial water, followed by the reduced drying rate region (2~3 h) in which non-interfacial and interfacial water dominate throughout, and significantly falling rate period (> 3 h) which is dominated by interfacial water. It should be mentioned that FD method, however, still remains a conceptual one for the dewatering of lignite. What the authors wish to emphasize here is that the proposed concept will present a possible option for lignite dewatering and will extend the utilization range of FD.

6.3.2 Drying kinetics modeling

To determine the FD kinetics, the residual water contents obtained from the drying experiments were demonstrated as the curve of moisture ratio against drying time, as shown in **Fig. 6.2**, which was curve-fitted with each of the 9 thin-layer drying models listed in **Table 6.1**. The R^2, *F-value*, *RSS*, and χ^2 were used as the criteria to evaluate goodness of fit for FD dewatering of LY lignite at different times. The estimated and statistical parameters of all of the models are presented in **Table 6.3**.

Table 6.3 Estimated and statistical parameters obtained from all of the thin-layer drying models

Model	Estimated parameter	Statistical parameter			
		R^2	*F-value*	*RSS*	χ^2
Lewis	k = 0.8625	0.9965	2.37×10^{3}	2.61×10^{-3}	5.21×10^{-4}
Henderson and Pabis	a = 1.0079, k =0.8677	0.9958	9.71×10^{2}	2.54×10^{-3}	6.35×10^{-4}
Logarithmic	a = 1.0191, k = 0.8388, c = -0.0125	0.9950	5.40×10^{2}	2.28×10^{-3}	7.61×10^{-4}
Diffusion approach	a = -0.4919, k = 2.6843, b = 0.4156	0.9991	3.14×10^{3}	3.93×10^{-4}	1.31×10^{-4}
Two-term	a = 0.6177, k_1 = 0.8674, b = 0.3902, k_2 = 0.8681	0.9916	2.42×10^{2}	2.54×10^{-3}	1.27×10^{-3}
Simplified Fick diffusion	a = 1.0079, c = 24.2147, l = 5.2823	0.9944	4.85×10^{2}	2.54×10^{-3}	8.47×10^{-4}
Modified Page	k = 0.8223, n = 1.2144	0.9993	5.70×10^{3}	4.33×10^{-4}	1.08×10^{-4}
Midilli–Kucuk	a = 0.9999, k = 0.7902, n = 1.2558, b = 0.0025	0.9995	3.80×10^{3}	1.62×10^{-4}	8.11×10^{-5}
Wang and Singh	a = 0.0567, b = -0.4975	0.9495	7.90×10	3.05×10^{-2}	7.62×10^{-3}

The R^2, *F-value*, *RSS*, and χ^2 values were between 0.9495 and 0.9995; 79 and 5.70×10^{3}; 1.62×10^{-4} and 3.05×10^{-2}; and 8.11×10^{-5} and 7.62×10^{-3}, respectively. **Table 6.3** shows that

the highest value of R^2, the second highest value of the *F-value*, and the lowest values of *RSS* and χ^2 were obtained from the Midilli–Kucuk thin-layer drying model compared with those obtained from the other models. Consequently, the Midilli–Kucuk thin-layer drying model was found to be the most suitable among the 9 models to represent the drying performance in this study.

To demonstrate the established model, the comparison of the experimental and the predicted moisture ratios by the Midilli–Kucuk thin-layer drying model is shown in **Fig. 6.2**, which shows that the model provided a good conformity between experimental and predicted moisture ratios. This suggests that the Midilli–Kucuk thin-layer drying model fitted the drying kinetics of LY lignite in FD very well. As a consequence, this expression can be used to predict the residual water content in LY lignite at any time during the FD process with high accuracy.

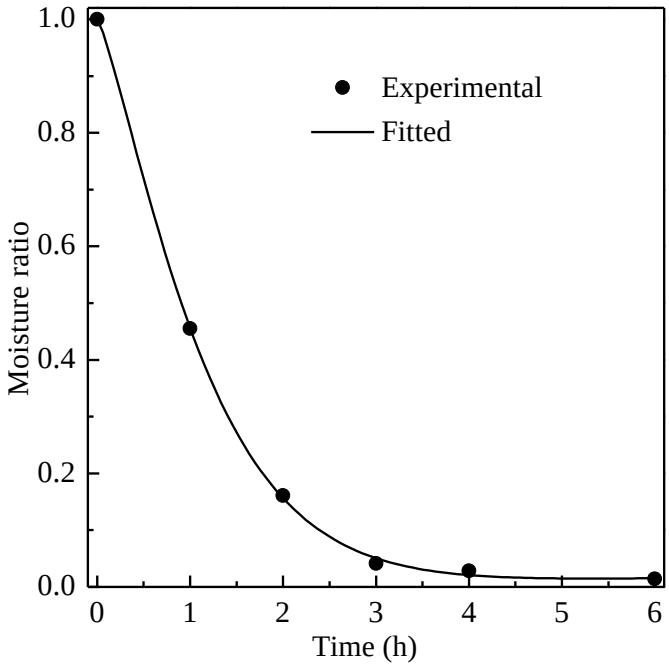

Fig. 6.2 Variations of experimental and predicted moisture ratios by the Midilli–Kucuk thin-layer drying model

Tahmasebi et al. [17] reported that the Midilli–Kucuk thin-layer drying model is the best-fitted model for N_2 fluidized-bed drying and superheated steam fluidized-bed drying while the Page model is the most suitable model for microwave drying. This is because of the different drying mechanisms. Microwave energy can penetrate into a coal particle and water can be evaporated within the particle, leading to an increase in the water vapor pressure inside the coal particle. The increased vapor pressure is an additional mechanism of microwave dewatering. This is absent in conventional drying techniques, in which water is gradually vaporized and transferred to the surface until the drying front extends to the particle center [17]. The Midilli–Kucuk thin-layer drying model was also selected as the best model for FD. The above discussion implies that the drying mechanism of FD is similar to that of traditional drying methods, which is that ice is sublimed from the outer surface and is progressively removed until the sublimation front between the frozen and dry regions reaches the particle center.

6.3.3 Effects of FD treatment on MHC

FD has a little influence on oxygen-containing functional groups because the experimental temperature is –45 °C. Furthermore, pore volumes of the FD treated sample were enlarged significantly compared with that of raw. In other words, effect of pore volumes of the FD treated samples on MHC was insignificant (detailed analysis is provided later). Therefore, the part focused on effects of residual water content on MHC.

It is easy for dried lignite to re-adsorb water and attention should be paid to water re-adsorption by dewatered lignite, which is important to the storage of lignite. **Fig. 6.3** shows the water contents of the FD treated samples and raw lignite. As seen, the water content decreased substantially during the first 105 h for raw lignite and then changed

slightly. Finally, equilibrium was attained. For sample FD1, its water content decreased a little with increasing time. The water contents of FD2, FD3, FD4, and FD6 increased with increasing time up to 21 h and equilibrium eventually was approached as time went on. In summary, water evaporation was dominant in raw lignite and FD1 at a relative humidity of 97%, whereas water vapor adsorption occurred in FD2, FD3, FD4, and FD6 under the same condition. The difference in water re-adsorption or desorption performances can be understood in terms of the difference between the water content in the sample and water vapor in the external environment, which is one of the main factors that determine the ultimate steady state [29].

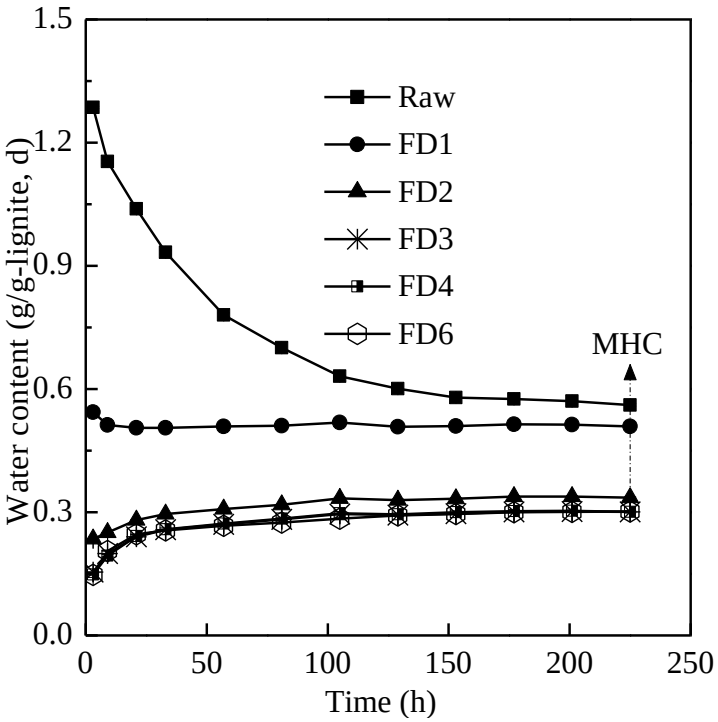

Fig. 6.3 Water contents of the FD treated samples and raw lignite. MHC: Moisture holding capacity

As mentioned above, the equilibrium water content at relative humidity of 97% is also defined as the MHC. The value of the last point of each curve is the MHC of the corresponding sample, as shown in **Fig. 6.3**. It was observed that the MHCs of the FD

treated samples decreased compared with that of raw lignite. The MHC gaps between raw lignite and the FD treated samples increased with increasing FD time and then remained almost constant. The same phenomenon that partially or completely dried lignite cannot regain its original water content after treatment with conventional heating dewatering techniques has been widely observed [1,30,31]. Researchers attribute this irreversible loss of water to an irreversible reduction in pore volume, which provides less space for the existence of water, and also the decomposition of oxygen-containing functional groups, which increases the hydrophobicity of treated samples [1,2,32]. The shrinkage forces caused by removal of the water in small capillaries and on the surface of lignite lead to the collapse of the pore structure [31,33,34]. On the other hand, at temperatures higher than 200 °C, a disintegration of the macromolecular structure occurs because of thermal decomposition, which also reduces pore volume [35]. For FD treatment, its effect on oxygen-containing functional groups can be negligible. Therefore, the changes in the MHCs of the FD treated samples are attributed to the changes in pore structure and diffusion force between the internal water content of sample and water vapor in external environment.

According to the IUPAC classification, the diameter ranges of macro-, meso-, and micropores are > 50 nm, 2–50 nm, and < 2 nm, respectively. The pore structure of lignite, which is mainly composed of macro- and mesopores, has a significant effect on MHC and the number of micropores can be negligible [36]. Consequently, the pore size distributions of all the samples are shown in **Fig. 6.4(a)**. To allow easy comparisons to be made, the effects of FD treatment on pore volume are also shown in **Fig. 6.4(b)**.

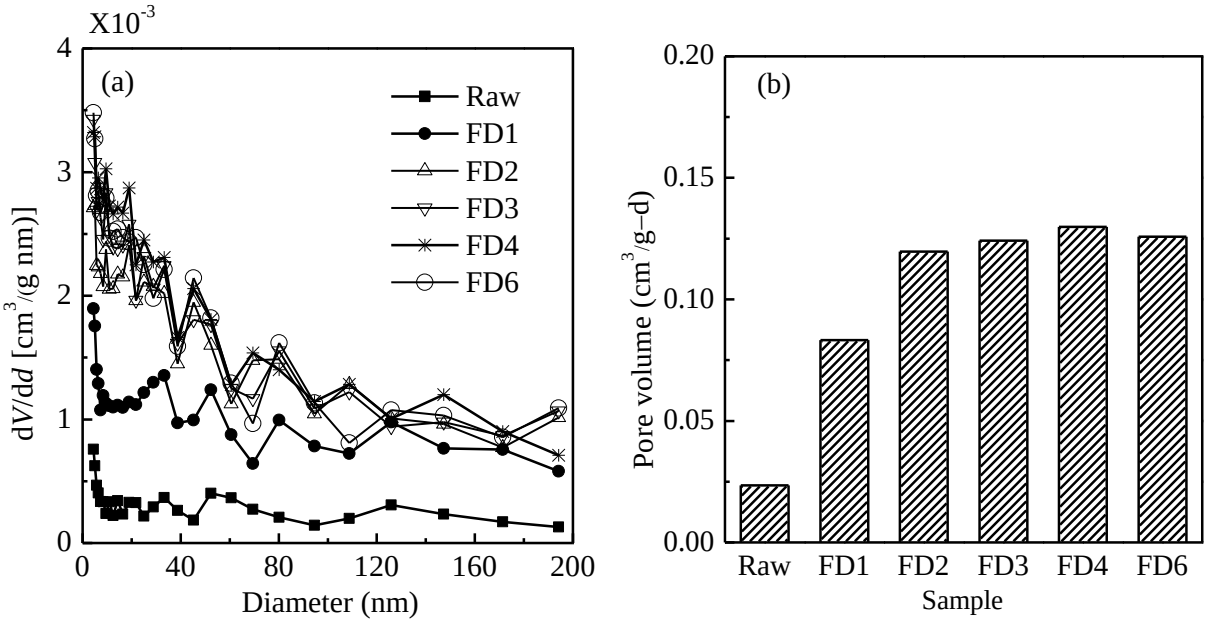

Fig. 6.4 Effects of FD treatment on pore size distributions and pore volumes

It can be seen that the porosities of macro- and mesopores of the FD treated samples were significantly higher than those of raw lignite. This is because during the FD process the water in lignite changes to ice and the volume of ice is greater than that of water with the same mass. The enlarged volume because of the conversion of water into ice expands the pore volumes of the FD treated samples. Moreover, the porosities of macro- and mesopores of FD2, FD3, FD4, and FD6 were similar to each other but were higher than those of FD1, suggesting that when the FD time was above 2 h, the effect of time on porosity was small. To demonstrate the surface morphologies, SEM images of some representative samples are shown in **Fig. 6.5**. As seen, surface roughness and the number of pore networks increased from raw lignite to FD4, which are consistent with the results of pore size distribution.

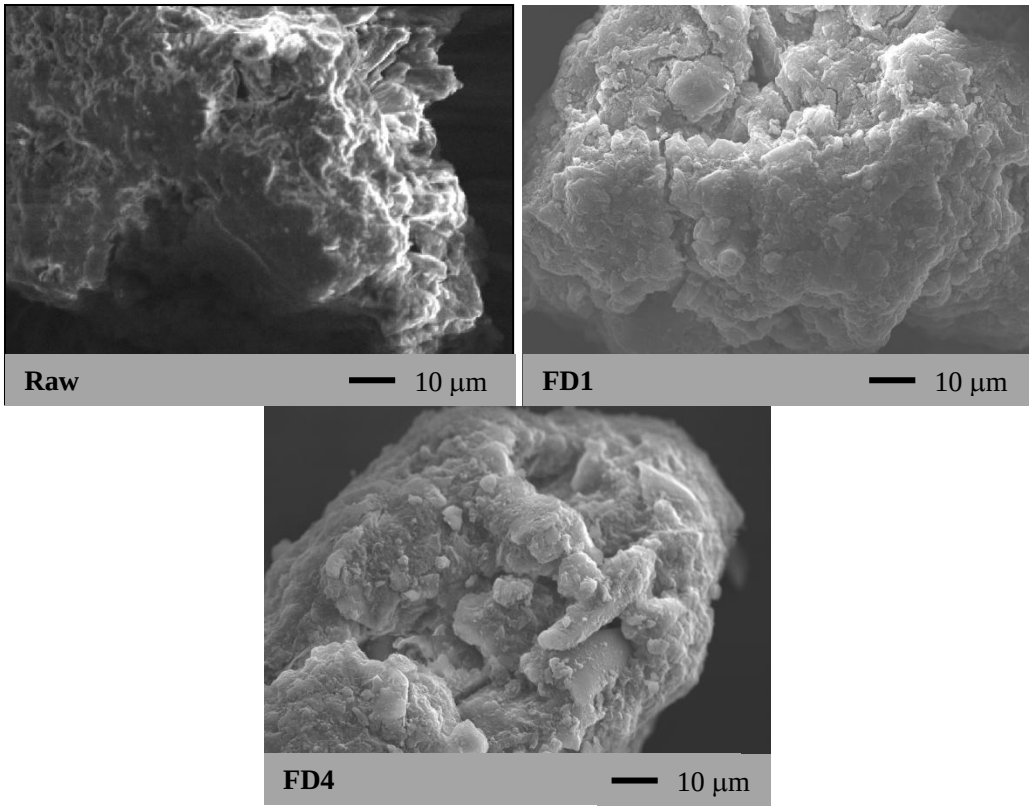

Fig. 6.5 SEM images of some representative samples

Furthermore, as described earlier, raw lignite and FD1 dewatered, whereas the other samples adsorbed water. This means that the mechanisms of reaching equilibrium of these two types of samples are different. In detail, water desorbs in order of increasing bond strength. Water without any interaction with lignite is first removed, followed by weakly adsorbed water. Water strongly adsorbed at active sites on the surface of lignite is the last desorbed [30,31]. The released water contents of raw lignite and FD1 result from the competition between the water–lignite bond strength and the diffusion desorption force caused by the difference between the residual water contents in these two samples and the water vapor in external environment [29]. With regard to the process of water adsorption in lignite, Shigehisa et al. [18] and Charrière et al. [37] reported that it includes three steps: (1) adsorption on active adsorption sites; (2) formation of water

clusters; and (3) pores filling by water clusters and capillary condensation in narrow pores. Raw lignite dewatered, suggesting that the partial pores of raw lignite did not fill with water under equilibrium conditions. In other words, pore volume for holding the MHC of raw lignite was higher than the requisite volume. Moreover, pore volumes and MHCs of FD2, FD3, FD4, and FD6 were larger and lower than those of raw lignite, respectively. These indicate that more pores were not filled in with water for FD2, FD3, FD4, and FD6 relative to those for raw lignite. Therefore, pore volumes of these samples were large enough to maintain MHC and the effect of pore volume on MHC was insignificant. The amounts of absorbed water in FD2, FD3, FD4, and FD6 are mainly determined by the combined effect of the water–lignite interaction strength and the diffuse adsorption force, which is a result of the different internal and external water contents between these four samples and the environment. The narrow MHC gap between FD2 and FD3, FD4, and FD6 is primarily because of the slight decrease in residual water contents of FD3, FD4, and FD6 compared to that of FD2, corresponding to a little change in the diffuse adsorption force.

6.3.4 Effects on MHC of coating treated samples with kerosene

Different amounts of kerosene were used to cover oxygen-containing functional groups on the surface of lignite. This can reduce oxygen-containing functional groups to different levels. Effects of the single factor of oxygen-containing functional groups on water re-adsorption can be investigated.

Because the MHCs of FD3, FD4, and FD6 were similar and the residual water content only changed slightly between FD4 and FD6, FD4 was selected.

Fig. 6.6 shows the water contents of FD4 and FD4 coated with different amounts of kerosene. Two coating methods, namely, direct mixing [**Fig. 6.6(a)**] and adsorption [**Fig. 6.6(b)**] methods, were used. From **Fig. 6.6**, it is clear that the water contents of all of the samples increased rapidly during the first 21 h and gradually reached equilibrium thereafter, which is also referred to as MHC.

As seen from **Fig. 6(a)**, the MHCs of all of the kerosene-coated samples clearly decreased compared with that of FD4. The MHC decreased from 0.30 (g/g-lignite, d) in FD4 to 0.21 (g/g-lignite, d) in FD4KM2.5 and 0.16 (g/g-lignite, d) in FD4KM10, the latter being the minimum value. Furthermore, when comparing changes in MHC after coating with different amounts of kerosene, the MHCs of the coated samples decreased progressively as the amount of kerosene used for coating increased. This possibly occurs because after the mixing treatment the kerosene is on the surface of lignite, which suppresses the reaction between oxygen-containing functional groups and water due to the hydrophobic nature of kerosene, and in the pores of lignite, which decreases the space available for retaining water. To reduce the amount of kerosene used in coating, the adsorption method was employed. The results are given in **Fig. 6(b)**.

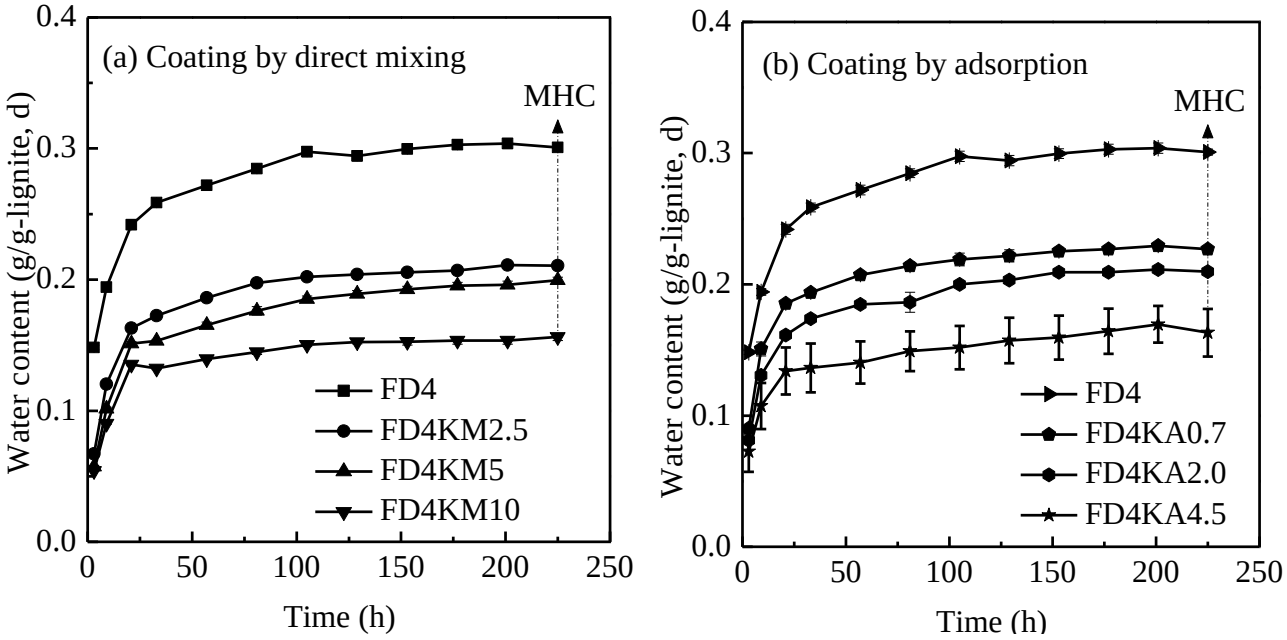

Fig. 6.6 Water contents of FD4 and FD4 coated with different amounts of kerosene using (a) direct-mixing method and (b) adsorption method. MHC: Moisture holding capacity

From **Fig. 6(b)**, it can be observed that the MHCs of samples after coating with different amounts of kerosene (i.e., 0.7, 2.0, and 4.5%) by the adsorption method remained lower than 0.23 (g/g-lignite, d) and the minimum value was 0.16 (g/g-lignite, d) when the amount of coated kerosene was 4.5%. It is interesting to note that the MHCs of FD4KM2.5, FD4KM5, and FD4KM10 changed slightly compared with those of FD4KA0.7, FD4KA2.0, and FD4KA4.5, respectively. However, the amounts of kerosene used in coating of the latter three samples were significantly lower than those of the former three samples, respectively. This phenomenon suggests that the adsorption method is better than the mixing method with regard to reducing water re-adsorption capacity. One possible explanation is that the kerosene added by the mixing method, the content of which is limited, covers the surface and fills the pores of the lignite at the same time, leading all surfaces not being covered. In the adsorption method, the first step of the

water-adsorption process in coal is water adsorption on the surface and afterwards water fills the pores [37]. Similarly, kerosene coated by the adsorption method first covers the surface of lignite and then blocks the pores if enough kerosene is adsorbed. Therefore, the adsorption method can cover more oxygen-containing functional groups, which are the primary reason for the high percentage of water in lignite [2], than can the mixing method. At the same time, the adsorption method consumes less kerosene, resulting in a better improvement in reducing water re-adsorption content.

6.4 Conclusions

In the present work, two forms of water were identified: non-interfacial and interfacial water, whose contents were 1.258 and 0.093 (g/g-lignite, d), respectively. Non-interfacial and interfacial water contents determined by FD were in good agreement with those by HT. There were three drying stages during the FD process: (1) a fast dewatering period (~2 h) controlled by non-interfacial water, (2) a reduced-drying-rate period (2~3 h) in which both non-interfacial and interfacial water are important, and (3) a substantially falling rate period (> 3 h) dominated by interfacial water.

The Midilli–Kucuk thin-layer drying model was selected as the one most suitable to describe the FD process with the highest value of R^2, the second highest value of *F-value*, and the lowest values of *RSS* and χ^2 among the nine models.

Water removal occurred in raw lignite and FD1 at a relative humidity of 97%, whereas water adsorption was dominant in the other samples. In addition, the MHCs of all of the FD treated samples were lower than that of raw lignite. These results can be attributed to that pore volumes of all of the samples being large enough and its effect on the MHC is less important than the diffusion force. The competition between the water–lignite bond

strength and the diffusion desorption force or the combined effect of the water–lignite bond strength and diffusion adsorption force determines the ultimate steady state.

After coating with kerosene using either the adsorption or direct-mixing methods, the MHCs of the corresponding samples all decreased, which can be attributed to the kerosene covering the surface and blocking the pores. The effect of coating with kerosene by the adsorption method on reducing MHC is better than that by the direct mixing method because the former can cover more surface than the latter while consuming less kerosene.

References

[1] C.Z. Li, Advances in the Science of Victorian Brown Coal, Amsterdam, Elsevier, 2004.

[2] J.L. Yu, A. Tahmasebi, Y.N. Han, F.K. Yin, X.C. Li, A review on water in low rank coals: The existence, interaction with coal structure and effects on coal utilization, Fuel Process. Technol. 106 (2013) 9–20.

[3] Y.L. Yang, X.X. Jing, Z.Q. Li, X. Liu, Y.L. Zhang, L.P. Chang, Effect of drying conditions on moisture re-adsorption performance of dewatered lignite, Dry. Technol. 31 (2013) 1430–1437.

[4] X.C. Liu, T. Hirajima, M. Nonaka, K. Sasaki, Investigation of the changes in hydrogen bonds during low-temperature pyrolysis of lignite by diffuse reflectance FT-IR combined with forms of water, Ind. Eng. Chem. Res. 54 (2015) 8971–8978.

[5] X.C. Liu, T. Hirajima, M. Nonaka, T.M. Anggoro, K. Sasaki, Use of FTIR combined with forms of water to study the changes in hydrogen bonds during low-temperature heating of lignite, Dry. Technol. 34 (2016) 185–193.

[6] K. Norinaga, H. Kumagai, J. Hayashi, T. Chiba, Classification of water sorbed in coal on the basis of congelation characteristics, Energy Fuels 12 (1998) 574–579.

[7] Y. Fe, A.L. Chaffee, M. Marshall, W.R. Jackson, Lignite–water interactions studied by phase transition–differential scanning calorimetry, Fuel 84 (2005) 1557–1562.

[8] J.I. Lombraña, M.C. Villarán, Interaction of kinetic and quality aspects during freeze drying in an adsorbent medium, Ind. Eng. Chem. Res. 35 (1996) 1967–1975.

[9] W. Wang, G.H. Chen, Freeze drying with dielectric-material assisted microwave heating, AIChE J. 53 (2007) 3077–3088.

[10] L. Rey, J.C. May, Freeze drying/lyophilization of Pharmaceutical and Biological Products, third ed., London, Informa Healthcare, 2010.

[11] L.J.J. Hansen, R. Daoussi, C. Vervaet, J.P. Remon, T.R.M. Beer, Freeze-drying of live virus vaccines: A review, Vaccine 33 (2015) 5507–5519.

[12] L.A. Segura, C.A. Oyarzún, Experimental evidence of mass transfer mechanisms during freeze-drying in a capillary porous medium, Int. J. Refrig. 35 (2012) 2102–2119.

[13] G. Broeckx, D. Vandenheuvel, I.J.J. Claes, S. Lebeer, F. Kiekensa, Drying techniques of probiotic bacteria as an important step towards the development of novel pharmabiotics, Int. J. Pharmaceut. 505 (2016) 303–318.

[14] J. Cai, S. Chen, Determination of drying kinetics for biomass by thermogravimetric analysis under nonisothermal condition, Dry. Technol. 26 (2008) 1464–1468.

[15] P.F. Zhao, L.P. Zhong, Y.M. Zhao, Z.F. Luo, Comparative studies on the effect of mineral matter on physico-chemical properties, inherent moisture and drying kinetics of Chinese lignite, Energ. Convers. Manage. 93 (2015) 197–204.

[16] C.A. Pickles, F. Gao, S. Kelebek, Microwave drying of a low-rank sub-bituminous coal, Miner. Eng. 62 (2014) 31–42.

[17] A. Tahmasebi, J. Yu, Y. Han, H. Zhao, S. Bhattacharya, A kinetic study of microwave and fluidized-bed drying of a Chinese lignite, Chem. Eng. Res. Des. 92 (2014) 54–65.

[18] T. Shigehisa, T. Inoue, H. Kumagai, Water adsorption and desorption of upgraded brown coal. Part 1: Isotherms of adsorption and desorption, Energy Fuels 28 (2014) 4986−4992.

[19] H. Choi, C. Thiruppathiraja, S. Kim, Y. Rhim, J. Lim, S. Lee, Moisture readsorption and low temperature oxidation characteristics of upgraded low rank coal, Fuel Process. Technol. 92 (2011) 2005–2010.

[20] D.M. Bruce, Exposed-layer barley drying, three models fitted to new data up to 150 ℃, J. Agric. Eng. Res. 32 (1985) 337–348.

[21] S.M. Henderson, S. Pabis, Grain drying theory. II. Temperature effects on drying coefficients, J. Agric. Eng. Res. 6 (1961) 169–174.

[22] Z.Q. Guan, X.Z. Wang, M. Li, X.Q. Jiang, Mathematical modeling on hot air drying of thin layer fresh tilapia fillets, Pol. J. Food. Nutr. Sci. 63 (2013) 25–34.

[23] O. Yaldız, C. Ertekin, Thin layer solar drying some different vegetables, Dry. Technol. 19 (2001) 583–597.

[24] S.M. Henderson, Progress in developing the thin layer drying equation, Transactions of ASAE 17 (1974) 1167–1172.

[25] L.M. Diamante, P.A. Munro, Mathematical modelling of hot air drying of sweet potato slices, Int. J. Food. Sci. Technol. 26 (1991) 99–109.

[26] A. Midilli, H. Kucuk, Z. Yapar, A new model for single-layer drying, Dry. Technol. 20 (2002) 1503–1513.

[27] C.Y. Wang, R.P. Singh, Use of variable equilibrium moisture content in modeling rice drying, Transactions of ASAE 11 (1978) 668–672.

[28] E.K. Akpinar, C. Sarsılmaz, C. Yildiz, Mathematical modelling of a thin layer drying of apricots in a sola energized rotary dryer, Int. J. Energ. Res. 28 (2004) 739–752.

[29] C.F. You, H.M. Wang, K. Zhang, Moisture adsorption properties of dried lignite, Energy Fuels 27 (2013) 177−182.

[30] D.J. Allardice, D.G. Evans, The-brown coal/water system. Part 2. Water sorption isotherms on bed-moist Yallourn brown coal, Fuel 50 (1971) 236−253.

[31] D.G. Evans, The brown-coal/water system: Part 4. Shrinkage on drying, Fuel 52 (1973) 186−190.

[32] J. Hulston, G. Favas, A.L. Chaffee, Physico-chemical properties of Loy Yang lignite dewatered by mechanical thermal expression, Fuel 84 (2005) 1940–1948.

[33] Y.L. Yang, X.X. Jing, Z.Q. Li, X. Liu, Y.L. Zhang, L.Q. Chang, Effect of drying conditions on moisture re-adsorption performance of dewatered lignite, Dry. Technol. 31 (2013) 1430–1437.

[34] K. Norinaga, J.I. Hayashi, N. Kudo, T. Chiba, Evaluation of effect of predrying on the porous structure of water-swollen coal based on the freezing property of pore condensed water, Energy Fuels 13 (1999) 1058–1066.

[35] J.Z. Liu, J.F. Zhu, J. Cheng, J.H. Zhou, K.F. Cen, Pore structure and fractal analysis of Ximeng lignite under microwave irradiation, Fuel 146 (2015) 41–50.

[36] Mahidin, Y. Ogaki, H. Usui, O. Okuma, The advantages of vacuum-treatment in the thermal upgrading of low-rank coals on the improvement of dewatering and devolatilization, Fuel Process. Technol. 84 (2003) 147–160.

[37] D. Charrière, P. Behra, Water sorption on coals, J. Colloid Interf. Sci. 344 (2010) 460–467.

CHAPTER 7

Conclusions

Word energy consumption is constantly increasing and lignite has the potential to provide a significant portion of the energy needs in the world because it has some advantages, such as abundance, easy access, and low mining cost, over high-rank coal. However, lignite contains a high percentage of water, which is the most important factor than limits its wide utilization. Consequently, a large number of drying techniques are developed for lignite dewatering. However, a major breakthrough on reducing drying cost is still the great challenge. Furthermore, systematical study on physicochemical changes during dewatering process is very important and meaningful, which can provide useful engineering design guidelines for the improvement and targeted control of lignite dewatering techniques and help to understand dewatering mechanism. In the present study, hydrothermal treatment (HT; stage 1) coupled with relatively mild mechanical expression (ME; stage 2) was employed to remove water from lignite. To examine non-interfacial and interfacial water contents, a comparison of these two types of water determined by HT and freeze drying (FD) was made. Furthermore, for HT and HT–ME, pores, residual water content, and oxygen-containing functional groups change simultaneously. As to FD, it has a slight impact on oxygen-containing functional groups and effect of FD on pore volumes is not clear. Effects of FD on water re-adsorption were also studied. Oxygen-containing functional groups covered by kerosene were used to investigate effects of oxygen-containing functional groups on water re-adsorption. We hope our studies of these two drying methods can improve and broaden lignite

dewatering techniques. Changes in physicochemical properties [e.g., hydrogen bonds (HBs), residual water content, water re-adsorption ability, pore size distribution, and combustion performance] during these two kinds of dewatering processes were also detailed investigated.

In **Chapter 1**, characteristics of lignite and a brief background of previous works regarding lignite dewatering, including dewatering techniques and the changes in lignite's physical and chemical structure during dewatering processes, were overviewed. The significances and objectives of this thesis were then presented.

In **Chapter 2**, non-interfacial and interfacial and pyrolysis water were identified. Water was linearly and relatively easily removed when temperatures were lower than 173 ℃, which was referred to as non-interfacial water. At temperatures higher than 173 ℃, dewatering slope increased, meaning the presence of another form of water, which was relatively difficult to be removed and was named as interfacial water. Furthermore, the strength of each HB from low to high was 8.74, 14.50, 20.06, 26.36, and 32.59 kJ/mol, respectively. OH–HBs changed markedly when compared with the other four types of HBs because its strength is the weakest than the other four types of HBs. The trend of OH–HBs content decreased with increasing HT temperature.

Changes in gaseous, wastewater, and solid products during HT–ME process were discussed in **Chapter 3**. The results showed that volume and TOC value of wastewater increased with increasing HT temperature. Contents of monovalent cations (Na^+ and K^+) in wastewater increased apparently in temperature range 100 to 150 ℃. As to divalent cations (Mg^{2+} and Ca^{2+}), their contents increased greatly from 150 to 200 ℃ and 150 to 250 ℃, respectively. One possible explanation of this is that divalent cations are more

strongly bound to carboxyl groups than monovalent cations. Volatile matter, fixed carbon, and acidic groups (i.e., phenolic hydroxyl and carboxyl groups) changed slightly below 150 ℃. Above 150 ℃, volatile matter and acidic groups decreased with increasing processing temperature and an opposite trend was observed for fixed carbon. These indicate that both HT and HT–ME upgrade LY lignite. Furthermore, water contents of HT treated samples decreased significantly by using the following ME treatment, indicating that the next ME treatment is useful for further dewatering. Combined with the results of Chapter 2, dewatering mechanism was proposed.

The factors that control equilibrium water contents (EWC) at various relative humiditis (RHs) were discussed in **Chapter 4**. At low RHs (RH ≤ 10%), the factor that controls EWC is water molecules–active sites interactions and each carboxyl groups is occupied by ca. one water molecule. Within RH range 10~42%, monolayer water content is important and each monolayer water molecule binds ca. two multilayer water molecules. At medium RHs (10 < RH ≤ 92%), the amount of monolayer water and mesopore volume are relatively important. At high RHs (RH > 92%), EWC is related to the comprehensive factors including total volume of macropores and cracks, the size of spaces between coal particles, the amount of carboxyl groups, and interactions between water molecules.

Previous three chapters describe fundamental knowledge about HT–ME dewatering. Effects of HT–ME on combustion performance of lignite were investigated in **Chapter 5**. Ignition temperatures for samples treated using HT and HT–ME were higher than the corresponding values for raw lignite. This is because the amounts of high-boiling-point volatile matter and char in the treated samples are higher than those in raw lignite. The

maximum combustion rates (MCRs) of the treated samples were higher than that of raw lignite. Furthermore, the average activation energy (E_a) values of the treated samples were higher than that of raw lignite. In summary, HT and HT–ME both decrease the reactivity of LY lignite, and the changes are slightly higher for HT–ME than those for HT.

In **Chapter 6**, water in lignite can be removed by FD treatment. Non-interfacial and interfacial contents determined by FD were 1.258 and 0.093 (g/g-lignite, d), which agree quite well with those by HT. The moisture holding capacity (MHC) of the FD treated samples was lower than that of raw sample. Adding kerosene to the FD treated samples using either the adsorption or direct-mixing methods can decrease MHC because kerosene is mainly coated on the surface for adsorption method and coated on the surface and in the pores for direct-mixing method. The effect of the adsorption method on reducing MHC is better than that of the direct-mixing method since the former can cover more surface than the latter while consuming less kerosene.

In **Chapter 7**, the main conclusions were summarized. As to FD, to reduce the cost, we can try to conduct some experiments at temperatures and pressures just slightly lower than the triple point. Furthermore, further reducing the amount of coated kerosene by heating treatment can be tried. If the result that just one layer kerosene covers oxygen-containing functional group and, meanwhile, a significant decrease in water re-adsorption capacity can be obtained, that is perfect. On the other hand, some low-boiling point reagents (such as pentane and hexane) can be used as a substitute for kerosene.

Acknowledgements

Remembrance of things past during my PhD period, sensei's earnest, patient, and solemn instructions are very important to me, which correct my deviation from the course and teach me how to think deeply. Sensei has made my life a turning point. Therefore, first and foremost, I am more thankful than I can express to my great supervisor Prof. Tsuyoshi Hirajima. Without my supervisor's continuous guidance, support, untiring help, and unselfish dedication I cannot complete my PhD course. What sensei has done enriches my mind and broadens my view. It is my glory to be his student.

Besides my supervisor, I would like to deeply thank Prof. Keiko Sasaki, as another member of my thesis committee, for her continuous supports for my experiments preformed in our lab and valuable discussion.

I express my sincere gratitude to Prof. Jun-ichiro Hayashi (Institute for Materials Chemistry and Engineering, Kyushu University) and Assoc. Prof. Naoko Okibe for, as well as to be members of my thesis committee. Their comments and questions are very useful.

Special thanks would like to be given to Assistant Prof. Moriyasu Nonaka. He taught me to operate many apparatuses and offered help to me in silence. In addition, his scientific research attitude deeply affects me. Furthermore, I express my gratitude to Assoc. Prof. Hajime Miki for his encouragement and broadening my view.

I am also grateful to our secretary Makiko Semba. She takes care of many works, including official procedure of PhD. Thank you Samba-san for all your help.

It is my pleasure to acknowledge all lab members in Mineral processing, Recycling and Environment Remediation laboratory. I spent many time together with them and they

made a harmonious, happy, and relaxed environment for me. I would like to list some of them: Dr. Mutia Dewi Yuniati, Dr. Widi Astuti, Dr. Wuhui Luo, Dr. Yusei Masaki, Gde Pandhe Wisnu Suyantara, Masahito Tanaka, Binglin Guo, Intan Nurul Rizki, Kojo Twum Konadu, Santisak Kitjanukit, Chitiphon Chuaicham, Osamu Ichikawa, Taichi Momoki, Mari Yoshida, Akinobu Iguchi, Hidekazu Matsuoka, Akihiro Inoue, Tsubasa Oji, Keishi Oyama, Katsutoshi Tsutsumi, Shugo Nagato, Takahiro Matsumoto, Yuta Era, Melisa Pramesti Dewi, Niko Dian Pahlevi. I learn lots form all of them. I will remember our together time forever.

I acknowledge to financial support from Japan Society for the Promotion of Science (JSPS) KAKENHI Grant Nos. 24246149 and 15H02333 and also to the scholarship provided by the China Scholarship Council. I am also appreciative the Research and Education Center of Carbon Resources, Kyushu University, which provides the lignite sample.

Last but not the least, I wish to appreciate my family for their unconditional love and supports.

Fukuoka, September 2017

Xiangchun Liu